

Developing a Breast Phantom to Test and Validate the Smart Electrosurgical Knife

By

P.G.T. van Berckel

Master Thesis in partial fulfilment of the requirements for the degree of

Master of Science
In Biomedical Engineering

At the Delft University of Technology

May 2020

Supervisors:

Prof. Dr. B.H.W. Hendriks
Prof. Dr. J. Dankelman

Philips Research/ Delft University of Technology
Delft University of Technology



Preface

This report contains my master thesis concerning the design of a breast phantom to validate the smart electrosurgical knife. I performed this project in partial fulfilment of the requirements for the degree of Master of Science in Biomedical Engineering at the Delft University of Technology. The project was performed in collaboration with the research department of Philips Healthcare in Eindhoven, the Netherlands.

During my bachelor I studied Industrial Engineering, which I really appreciated since I really liked designing and developing products for real life use. However, the reason for choosing the Master Biomedical engineering with the track “Medical Instruments and Medical Safety”, was that I could not only continue developing products, but also significantly improve people’s health and life quality with it. This same vision is reflected by my master thesis, namely developing a breast phantom that enables further validation of the smart electrosurgical knife, which subsequently improves the health and life quality of patients undergoing breast conserving surgery.

Being able to do this project at both the Delft University of Technology and Philips Healthcare was a great experience. Both institutions had great facilities available, allowing me to produce various phantoms and extensively test them. Furthermore, I enjoyed working with people from both institutions due to their great passion for the medical industry and their great expertise. Finally, Philips’s stake in the smart electrosurgical knife gave me a great sense of relevance since it might therefore be used in future breast-conserving surgery procedures.

All in all, it took me approximately one year of hard work and dedication to complete this thesis project. It was a great experience involving theoretical research, producing- and testing phantoms, and working together with a variety of people from both the TU Delft and Philips Research from which I learned a lot. I would like to thank all the people that helped me during this thesis project. Firstly, I would like to thank my daily supervisor Prof. Dr. B.H.W. Hendriks, who helped me defining my goals and refining my findings. Secondly, I would like to thank the PhD candidate S. Azizian, who greatly helped me conducting experiments and analysing its data. I would like to thank Prof. Dr. J. Dankelman for giving clarifying feedback and great support during the graduation process. Then, I would like to thank the PhD candidate S. A. Akash, for helping me processing the data with the PNSas software. Finally, I would like to thank Marco Lai from Philips Research, for helping me conducting several X-ray experiments.

Abstract

Previous studies show that the smart electrosurgical knife, which adds diffuse reflectance spectroscopy to the traditional electrosurgical knife, is a promising technique for breast-conserving surgery, namely it enables real-time tissue characterization while cutting. More specifically, based on the fat/water-ratio, it enables intraoperative healthy from malignant tissue discrimination, therefore potentially reducing the re-excision rate with breast-conserving surgery procedures. However, the smart electrosurgical knife cannot be used on patients yet since it has not been validated yet. Several studies suggest phantoms are ideal for validation of systems including imaging systems like diffuse reflectance spectroscopy. Hence, for this master thesis, the objective was to develop a breast phantom that enables validation of the smart electrosurgical knife.

Firstly, it was found that a study which enables validation of the smart electrosurgical knife, should mimic a breast-conserving surgery procedure including a breast phantom, so that the potential of the intraoperative margin assessment technique "diffuse reflectance spectroscopy", added to the traditional electrosurgical knife, could sufficiently be tested. For such a study to take place, it was found that the phantom should have a similar size and shape as human breasts containing a tumour. With regard to pre- and postoperative margin assessment, the phantom should have a contrast between the tumour and healthy phantom, which enables size, border, and location assessment of the phantom tumour upfront and residual tumour inspection after surgery. Intraoperatively, the phantom should have a significant difference in fat/water-ratio between the tumour and healthy phantom. This enables us to assess diffuse reflectance spectroscopy with its capability in discriminating healthy from malignant tissue. Furthermore, visually and mechanically, there should be a minimal difference between the tumour and healthy phantom, which eliminates the possibility of using the intraoperative margin assessment techniques, palpation and visual inspection. Finally, the phantom should have similar mechanical- electrically conductive and thermo tolerance properties as real breast tissue. This will result in realistic haptic feedback and tissue effects with electrosurgery.

To develop such a phantom, various fat/water-ratios of water and lard, in combination with various additives such as guar gum, agar, gelatin and barium sulphate, were produced and tested. It turned out that agar in combination with water, lard, and the contrast agent barium sulphate, enables breast phantom production, that meets all the aforementioned phantom requirements. More specifically, the final phantom is a breast-shaped phantom with a realistic size and shape, consisting of healthy tissue with a tumour inclusion. The healthy tissue is composed of 50% lard, 50% water and then 5% agar by weight of water, whereas the tumour is composed of 20% lard, 80% water and then 3% agar- and 5% barium sulphate by weight of water. Since this phantom meets all requirements, it enables the design of a study that subsequently enables extensive testing and further validation of the smart electrosurgical knife.

Table of Content

Preface	3
Abstract	4
Table of Content	5
List of Abbreviations	9
Introduction	11
Problem statement	11
Objective	11
Research Questions	12
Thesis outline	12

THEORY

1. Smart Electrosurgical Knife	15
1.1 Electrosurgery	15
1.2 Diffuse Reflectance Spectroscopy	18
1.3 Smart Electrosurgical Knife	19
1.4 Conclusion	19
2. Human Breast Tissue Properties	20
2.1 Breast Anatomy	20
2.2 Breast Physiology	21
2.3 Breast Cancer	21
2.4 Quantified Inter- & Intra-patient Variability	23
2.5 Conclusion	28
3. Phantom Tissue	29
3.1 Phantom tissue Requirements	29
3.2 Matrix material & Additives	30
3.3 Most Potential Matrix Material.....	30
3.4 Conclusion	31

PHANTOM REQUIREMENTS

4. Validation Study Requirements	33
---	-----------

4.1	Study Design.....	33
4.2	Status Quo BCS.....	34
4.3	Validation study Requirements.....	34
5.	Phantom Requirements	35
6.	Meeting the Requirements.....	36

RESEARCH PHASE 1 – PHANTOM PRODUCTION

7.	Process Steps and Testing.....	38
7.1	Development.....	38
7.2	Testing.....	38
7.3	Process steps and testing.....	39
8.	Mimic Relevant Studies.....	40
8.1	Guar gum.....	40
8.2	Water-lipid & Agar	41
8.3	Water-lipid, Agar & Other methods and additives	44
8.4	Water-lipid & Gelatin	46
8.5	Conclusion.....	48
9.	Producing Most Potential Phantoms.....	49
9.1	Agar	49
9.2	Gelatin.....	52
9.3	Conclusion.....	54

RESEARCH PHASE 2 – TESTING MOST POTENTIAL PHANTOMS

10.	Process Steps and Testing.....	56
11.	Compression Tests	57
11.2	Studies to compare	57
11.3	Materials and methods.....	57
11.4	Results.....	58
11.5	Conclusion & Discussion.....	60
12.	DRS Tests.....	61
12.1	Materials and methods	61
12.2	Agar and gelatin influence	64
12.3	Results.....	64
12.4	Conclusion & Discussion.....	68

13.	Electrosurgical Tests	69
13.1	Material influence	69
13.2	Materials and methods	70
13.3	Results	71
13.4	Conclusion & Discussion.....	73
14.	Conclusion – Research Phase 2	74

RESEARCH PHASE 3 – CONTRAST AGENT

15.	X-ray	77
15.1	CT-scan	77
15.2	Barium sulphate	77
16.	BaSO₄ & X-ray Contrast	78
16.1	Materials and methods	78
16.2	Production method	79
16.3	Barium sulphate & Hounsfield unit	79
16.4	Results	79
16.5	Conclusion	80
17.	BaSO₄ & IMA Requirements	81
17.1	Compression Tests	81
17.2	DRS Tests	82
17.3	Electrosurgical Tests.....	85
18.	Conclusion – Research Phase 3	87

RESEARCH PHASE 4 – FINAL PHANTOM PRODUCTION

19.	Final Phantom Production	89
19.1	Melting point.....	89
19.2	Materials & equipment	89
19.3	Production method	89
19.4	Conclusion	90
20.	General requirements	91
20.1	Requirement 1: Easy to manufacture & inexpensive.....	91
20.2	Requirement 2: Reproducible/consistent & homogeneous	91
20.3	Requirement 3: Durable & stable/long-lasting	91
20.4	Conclusion	92

21. Discussion & Recommendations	94
21.1 Discussion.....	94
21.2 Recommendations	98
22. Final Conclusion	101
Validation Study	101
Phantom Requirements	101
Final Phantom	102
References	103
APPENDIX A: Parameter Confidence intervals	113
APPENDIX B: Scientific Paper	114

List of Abbreviations

<i>a</i>	Scattering amplitude
AC	Alternating current
AP	Adipose
<i>b</i>	Scattering power or Mie slope
BCS	Breast-conserving surgery
BMI	Body Mass Index
CBCT	Cone Beam CT system
DCIS	Ductal carcinoma in situ
DRS	Diffuse reflectance spectroscopy
ECM	Extracellular Matrix
ESK	Electrosurgical knife
FAD	Fibroadenoma
[Fat/(Fat+Water)]	Fat fraction
(Fat+Water)	Total fat and water volume
<i>f_{mie}</i>	Mie-to-Rayleigh fraction
F/W	Fat/water
GL	Glandular
Hb	Hemoglobin
Hb02	Hemoglobin Oxygenation
IC	Invasive carcinoma
IDC	Invasive ductal carcinoma
IMA	Intraoperative margin assessment
MRI	Magnetic resonance imaging
N	Number of patients
NaCl	Sodium chloride
NIR	Near-infrared
NIRF	Near-infrared fluorescence
NS	Number of samples
PVA	Polyvinyl alcohol
PVC	Polyvinyl chloride
REQ	Requirement
SESK	Smart electrosurgical knife
SD	Standard deviation
<i>s800</i>	Reduced scattering amplitude
μ_a	Absorption coefficient
μ'_s	Reduced scattering coefficient
US	Ultrasonography
VIS	Visible
X-ray	Radiography

Introduction

Breast cancer is the most commonly diagnosed cancer in females worldwide and affects one in eight women during their lifetime¹. It is estimated that in 2018, worldwide 2 million new cases and 626679 deaths occurred due to breast cancer². Breast-conserving surgery (BCS) is the standard surgical treatment for early-stage breast cancer³. It involves removing the tumour with a minimal margin of healthy tissue, leaving as much normal breast tissue as possible and is used in combination with radiotherapy, which eliminates residual cancer cells in the breast. However, recognition of the tumour during BCS is very difficult. As a result, in 10-60% of the cases positive margins are found post-operatively by histopathologic evaluation and require re-excisions to obtain negative margins⁴. Re-excisions have several negative consequences, among other things delayed receipt of adjuvant therapy, impaired cosmetic outcome, worsened psychosexual function and added medical expenses^{5,6}.

Over the last decade, the In-Body Systems department of Philips Research together with the Delft University of Technology have conducted research to find a standard margin assessment technique to overcome this problem. The research studies of J. Fleischer, M. Adank, F. Mollerus and C. van Gent have shown that diffuse reflectance spectroscopy (DRS), is a promising technique for intraoperative margin assessment (IMA)^{7,8,9,10,11,12}. In their studies they used the smart electrosurgical knife (SESK), which adds DRS to the traditional electrosurgical knife (ESK) and enables real-time tissue characterization while cutting. More specifically, they showed that based on the fat/water-ratio, DRS is a promising technique for discriminating between healthy and tumour tissue intraoperatively.

Problem statement

However, their research studies were conducted under controlled experimental conditions on ex vivo animal tissue specimens that do not necessarily represent the in vivo status of human breast tissue. Substantial changes occur immediately post-mortem compared to in vivo, few samples and datasets were taken, thereby the non-uniformity of breast tissue both in an individual patient and between patients is not represented by their samples. Hence, their findings solely serve as a reference value. Further validation of the SESK is therefore still needed.

Objective

Several studies suggest that phantoms are ideal for validation of systems including imaging systems like DRS^{13,14}. Hence, developing breast phantoms that mimic the properties of healthy and malignant breast tissue will be ideal. This makes it possible to do extensive research that allows for further validation of the SESK, which brings research on the SESK one step closer to a successful launch in the medical industry¹³. At the moment there is not such a breast phantom yet, hence the objective of this master thesis is:

Develop a breast phantom that enables validation of the smart electrosurgical knife.

Research Questions

To see whether the objective is obtained, three research questions were formulated. The results of my literature study show that a breast phantom that enables SESK validation, should at least include tissue properties that are essential for the working principle of the SESK. However, dependant on how the validation study will look like, the final phantom should besides mimicking essential tissue properties, perhaps also have other requirements. Hence, the first research question is about the design of such a validation study. The second research question is about the requirements of a phantom in such a validation study. The third research question is about the production feasibility of such a phantom. The research questions are formulated as follows:

- 1) *What are the requirements of a study that enables validation of the smart-electrosurgical knife?*
- 2) *What are the requirements of a phantom that enables such a validation study?*
- 3) *Is it possible to produce a phantom that meets the phantom requirements?*

Thesis outline

To answer these questions and subsequently reach the objective, this master thesis is structured according to figure 1 on the next page. This figure shows that this thesis report is divided into seven phases, which consist of several chapters that contribute to the goal of each specific phase.

Additionally, a scientific paper is written for this thesis project and can be found in Appendix B. The paper is a concept that provides a basis to create an article with the most important results of this thesis project. The scientific paper needs to be seen as supplementary material and does not replace the thesis.



Figure 1: Schematic overview of the outline of this master thesis.

I. THEORY

The goal of this phase is to provide background information that is important for this thesis project. All theory originates from the literature study that was performed prior to this master thesis. Only the essential and relevant parts of the literature study are enclosed. For additional information, the literature study may be consulted ⁵⁹

1. Smart Electrosurgical Knife

This chapter explains the working principle of the smart electrosurgical knife and what tissue properties of human breast tissue are essential for its working principle. First, electrosurgery and diffuse reflectance spectroscopy will be discussed, followed by the combination of the electrosurgical knife and diffuse reflectance spectroscopy into the smart electrosurgical knife.

1.1 Electrosurgery

The electrosurgical knife uses high frequency alternating current (AC), which is converted to heat (up to 400 °C), to cut and coagulate (haemostasis) tissue. The amount of heat generated depends on the resistance or electrical conductivity of the tissue. Compared to the traditional surgical knife, it limits blood loss and reduces surgical time. Due to its benefits, electrosurgery is nowadays used in more than 80% of all surgical procedures ^{15,16,17,18}.

1.1.1 Electrosurgical circuit

An electrosurgical circuit is composed of a patient, electrosurgical generator and an active- and return electrode. The electrosurgical generator is the source of voltage that pushes electrons through the circuit. First, the voltage arrives at the active electrode, which conducts the electrons to the patient. The patient's tissue serves as the conductive element and acts as a resistor within this circuit. The resistance, which depends on the tissue's water content, converts electrical energy of the voltage source into thermal energy, causing heat production and tissue destruction. Finally, the electrons return to the electrosurgical generator through a patient return electrode (see figure 2) ^{16,18}.

1.1.2 Electrosurgical components influencing tissue effects

With electrosurgery, the amount of tissue effect can be altered by varying the following factors: current density, exposure time and type of current waveform ¹⁶.

Current density

The current applied per unit area is called the current density and is positively proportional to the heat generation. The generator increases the current density by increasing its power setting, whereas electrodes increase the current density by reducing the size. As a result, the active electrode is very small, resulting in a concentrated current flow and high heat at the site, whereas the return electrode is large, so that the current that returns to the electrosurgical generator is dispersed and eliminates tissue effect at the return electrode ^{16, 18,19}.

Exposure time

Tissue effects also depend on the length of time a surgeon uses an active electrode at a specific location. Wider and deeper tissue damage occurs with long activation, whereas too short activation results in an absence of the desired tissue effect ¹⁶.

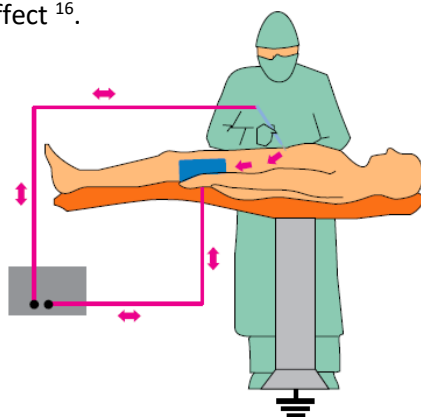


Figure 2: Monopolar electrosurgery ²⁰

Current waveforms & Tissue effects

Electrosurgical generators produce three different current waveforms: cut, coagulate and blend. These waveforms can be altered by modulation and can be used to acquire various tissue effects. The cutting waveform produces continuous sinusoidal waves involving high current and low voltage producing heat very rapidly. With temperatures exceeding 100° C, it causes vaporization of the intracellular fluid leading to the rupture of the cell membrane and cleavage of the tissue. A precise cut is created with little tissue damage and minimal homeostasis. The coagulation waveform produces intermittent sinusoidal waves involving low current and high voltage producing less heat. With temperatures starting from 60°C, it causes disruption of the cells by evaporation of the intracellular fluid, leading to protein denaturation and coagulum formation. The blend waveform is a modification of the cutting and the coagulation waveform, where the total energy output remains the same, while the ratio of voltage and current is modified. It increases haemostasis while cutting, thus providing both cutting and coagulation tissue effects ^{16,17,20,21}.

1.1.3 Tissue properties influencing tissue effects

Tissue effects also greatly depend on the properties of that specific tissue. As a matter of course, tissue identification in advance of surgery is very important to ensure the desired tissue effect.

Electrically conductivity

As earlier stated, tissue conductivity affects the amount of heating, which directly determines the amount of tissue effect. Low electrically conductive tissue, also called high resistant tissue, results in a high amount of heating with greater tissue effects than low resistant tissue. The electrical resistance of tissue depends on tissue's ion concentration and varies per tissue type. Tissues containing high ion concentrations, such as hydrated tissues like muscle and skin, are good conductors of electricity and have low resistance, whereas adipose tissue and bone have high resistance and are poor conductors of electricity (fig. 3) ¹⁶.

Thermo tolerance

Tissue effects not only depend on the amount of generated heat but also on tissue's resistance to heat, called thermo tolerance, more specifically the resistance to an applied thermal dose (temperature (T) and exposure time (t)) ²².

1.1.4 Mechanical Properties influencing haptic feedback

Another tissue property that influences the working principle of the electrosurgical knife are the mechanical properties of tissue. With electrosurgery the ESK is often in direct contact with breast tissue ¹⁶. As a result, the mechanical properties of tissue influence the haptic feedback to the surgeon (Fig. 4). Noteworthy, with BSC, haptic feedback through the ESK is not used to distinguish healthy from tumour tissue, whereas haptic feedback in the form of palpation is ²³.

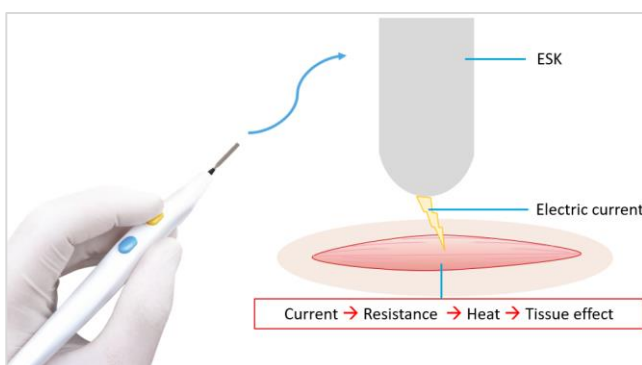


Figure 3: Tissue resistance influences tissue effect ²⁴.

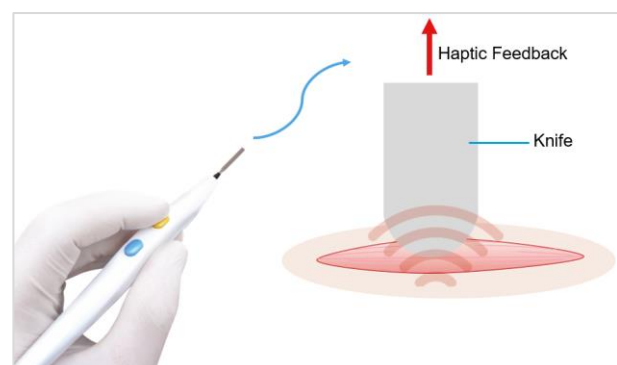


Figure 4: Mechanical properties influence haptic feedback ²⁴.

1.1.5 Clinical application electrosurgical knife

This paragraph describes the clinical application of the electrosurgical knife. More specifically its use during BCS and the accompanying challenges.

Breast-conserving surgery

Breast cancer is the most commonly diagnosed cancer in females worldwide and affects one in eight women during their lifetime ¹. It is estimated that in 2018, worldwide 2 million new cases and 626679 deaths occurred due to breast cancer ². Breast-conserving surgery (BCS) is the standard surgical treatment for early-stage breast cancer ³. It involves using an electrosurgical knife to efficiently remove the tumour with a minimal margin of healthy tissue, leaving as much normal breast as possible and is used in combination with radiotherapy, which eliminates residual cancer cells in the breast ^{3,25,26}.

Margins

A successful BCS involves a *negative margin* which is when a surgeon takes out all the breast cancer along with a minimal margin of healthy tissue around it to make sure all cancer cells are removed (fig. 5). Getting a negative margin comes with several challenges. Tumours often have irregular shapes and have extensions that go beyond the obvious palpable evident lesion. Thereby, during surgery the surgeon can only grossly estimate the margins, without precisely determining the margin width until the pathologist performs microscopic assessment days after surgery. This together with orientation differences of patients and the presence of blood, makes the evaluation of margin very difficult ^{27,28}. As a result, in 10-60% of the cases *positive margins* (cancer cells at the resection line of the removed tissue) are found post-operatively and require re-excisions to obtain negative margins ⁴. Re-excisions have several negative consequences, among other things delayed receipt of adjuvant therapy, impaired cosmetic outcome, worsened psychosexual function and added medical expenses ^{6,5}.

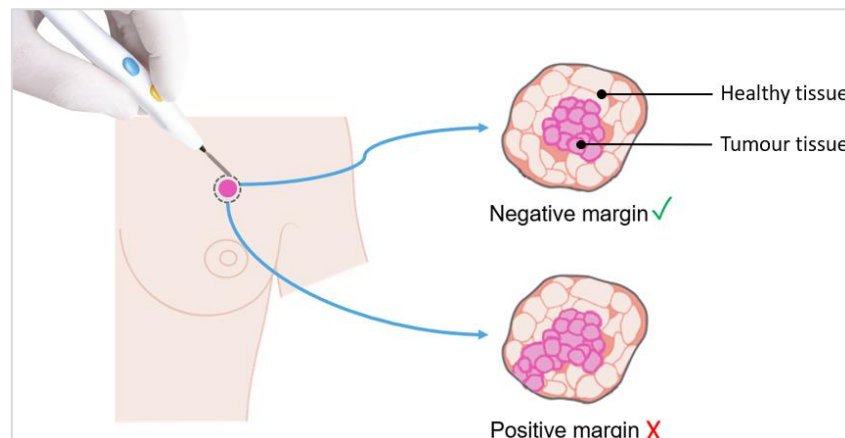


Figure 5: BCS, negative and positive margins ²⁴.

Need for IMA technique

To overcome this problem, the In-Body Systems department of Philips Research together with the Delft University of Technology have conducted research to find a standard margin assessment technique. The research studies of J. Fleischer, M. Adank, F. Mollerus and C. van Gent, have shown that diffuse reflectance spectroscopy is a promising technique for margin assessment. In their studies they used the smart electrosurgical knife, which adds DRS to the traditional ESK. Based on the optical parameter, "fat/water-ratio", this intraoperative margin assessment (IMA) technique enables accurate discrimination between healthy- and malignant breast tissue ^{7,8,9,10,11,12,29}.

1.2 Diffuse Reflectance Spectroscopy

Diffuse reflectance spectroscopy is a real-time photonic technique that measures at different wavelengths the intrinsic light absorption and scattering of tissue to obtain a DRS spectrum. By using various mathematical models, the derived DRS spectrum can be translated into the optical properties of tissue. These optical properties include the absorption and reduced scattering coefficient (μ_a and μ'_s) and present the specific composition and morphology of the examined tissue.

Absorption coefficient

The absorption coefficient (μ_a) is a linear combination of the individual absorption coefficients for each pure chromophore found (or expect to be) in the tissue. A chromophore is a part of a molecule that absorbs certain wavelengths of light, and in doing so confer colour to material. Each chromophore has its own absorption coefficient, which is defined by its extinction coefficient [$\text{cm}^{-1} \text{M}^{-1}$] multiplied by the chromophore concentration [M L^{-1}]. In the visible spectrum (400 – 700 nm) oxygenated and deoxygenated haemoglobin and β -carotene are the main chromophores, whereas in the NIR spectrum water, adipose tissue and collagen are the main chromophores. Table 1 shows the absorption peaks of the 6 main chromophores^{30,31}.

Table 1: Absorption coefficient peaks of various chromophores, table taken from³²

Chromophore	Absorption Peak (nm)
β -carotene	275, 448, 476
Collagen	911, 1030, 1200, 1510
Hb	272, 433, 556, 758
HbO ₂	274, 344, 414, 542, 576
H ₂ O	755, 972 , 1192, 1453, 1932
Lipid	760, 930 , 1042, 1211, 1393, 1414, 1720, 1760, 2142

Reduced Scattering coefficient

The scattering coefficient of a target tissue is unique, tells us something about the morphology of the tissue and depends on the underlying cellular structure, size, density and refractive index of each cellular and subcellular component. It does so by the analysis of elastic light scattering, which is the direction change of a photon while before and after the scattering occurrence the same wavelength is maintained³⁰.

Scatter amplitude and power

An increased scattering amplitude and -power respectively stand for a higher number of scattering centres (interfaces that alter the direction of propagation of photons at a microscopic level causing light diffusion) and a smaller size of scattering centres³³. Many studies report the scattering amplitude and -power instead of the reduced scattering coefficient. The reduced scattering coefficient (μ'_s) can be derived from the scattering amplitude (a) and -power (b) with formula 1, where wavelength λ is normalized by a reference wavelength λ_0 , for example, 500 nm³⁴.

$$\mu'_s(\lambda) = a \left(\frac{\lambda}{\lambda_0} \right)^{-b} \quad (1)$$

Influence cancer on DRS

With the development of cancer, the composition and morphology of tissue changes causing the absorption- and reduced scattering coefficient to change, hence also the DRS spectrum and enables discrimination of healthy from malignant breast tissue. Among other things, the amount of lipid content change, particularly in breast tumours. Malignant breast tissue contains less lipid content than healthy tissue. As a result, M. Adank and De Boer et. al. showed that the optical parameter "F/W-ratio", the ratio of chromophores of fat and water in the extended NIR region (1000-1600 nm), is the best parameter in discriminating healthy from tumour tissue^{29,35, 36,37}.

1.3 Smart Electrosurgical Knife

The smart electrosurgical knife integrates DRS into the tip of the traditional ESK and provides information regarding local margin assessment intraoperatively. This allows the surgeon to discriminate healthy from tumour tissue while dissecting the tumour, subsequently improving the accuracy of tumour localization and dissection, leading to less negative margins and better cosmetic outcomes. Two fibres are attached at the sides of the cutting blade of the electrosurgical knife. By emitting and detecting light, these fibres obtain DRS measurements of the tissue which are translated into the F/W-ratio of the measured tissue. The fibres are encapsulated in a metal sleeve to protect them from the current heat (Fig. 6).



Figure 6: The tip of the cutting blade with two fibres attached to it. Left, a microscopic picture of the prototype ⁷. Right, a schematic image of the cutting blade (C), fiber (B) and the metal sleeve (A) ¹².

1.4 Conclusion

This chapter explained the working principle of the smart electrosurgical knife and what tissue properties of human breast tissue are essential for its working principle. The electrical conductivity, thermo tolerance and mechanical properties are essential for the working principle of the ESK, whereas the optical tissue properties are essential for the working principle of DRS. In order to develop a realistic phantom, the quantified values for each of these properties need to be found. Particularly the F/W-ratio and its influence on the optical tissue properties should be mapped, because based on the F/W-ratio, DRS allows for discrimination between healthy and tumour tissue. However, due to the great variability of breast tissue intra-patient, inter-patient and as a result of cancer, we simply cannot assume the same tissue properties for everyone because this might not be representable. Therefore, in the next chapter the property variabilities intra-patient, inter-patient and as a result of cancer will be identified to see what variabilities can be ignored or have to be integrated into the final phantom tissue design to make the phantom a reliable SESK validator.

2. Human Breast Tissue Properties

This chapter describes the main properties of human breast tissue and identifies property variability inter-patient, intra-patient and as a result of cancer. This knowledge makes sure all breast types are considered when designing the phantom tissue. The following pertains exclusively to the female mature breast.

2.1 Breast Anatomy

The structure of the human breast or mammary gland reflects its function: the production of milk for lactation. It is situated on top of the pectoralis major muscle and ribcage and consists of 6 layers namely the skin, premammary layer, mammary layer, retromammary layer, pectoralis major muscle and chest wall (fig. 7). The skin covers the breast, is thickest at the base of the breast and contains the areola and nipple at the apex of the breast. The premammary layer also known as the subcutaneous fat layer, lies between the skin and the superficial fascia and is present across the whole breast except posterior to the nipple. The mammary layer is the most important layer of the breast. It contains stromal tissue and the parenchyma, which is the functional part of the organ. Stromal tissue consists of adipose tissue, fibrous connective tissues, nerves, blood vessels and lymphatics. The parenchyma consists of glandular tissue that subsequently consists of milk producing glands (lobules) and milk ducts. Milk ducts are thin tubes that carry milk from the lobules to the nipple. The retromammary layer contains fat and lies posterior to the mammary layer and allows for breast mobility relative to the underlying pectoralis major muscle ^{38,39,40,41}.

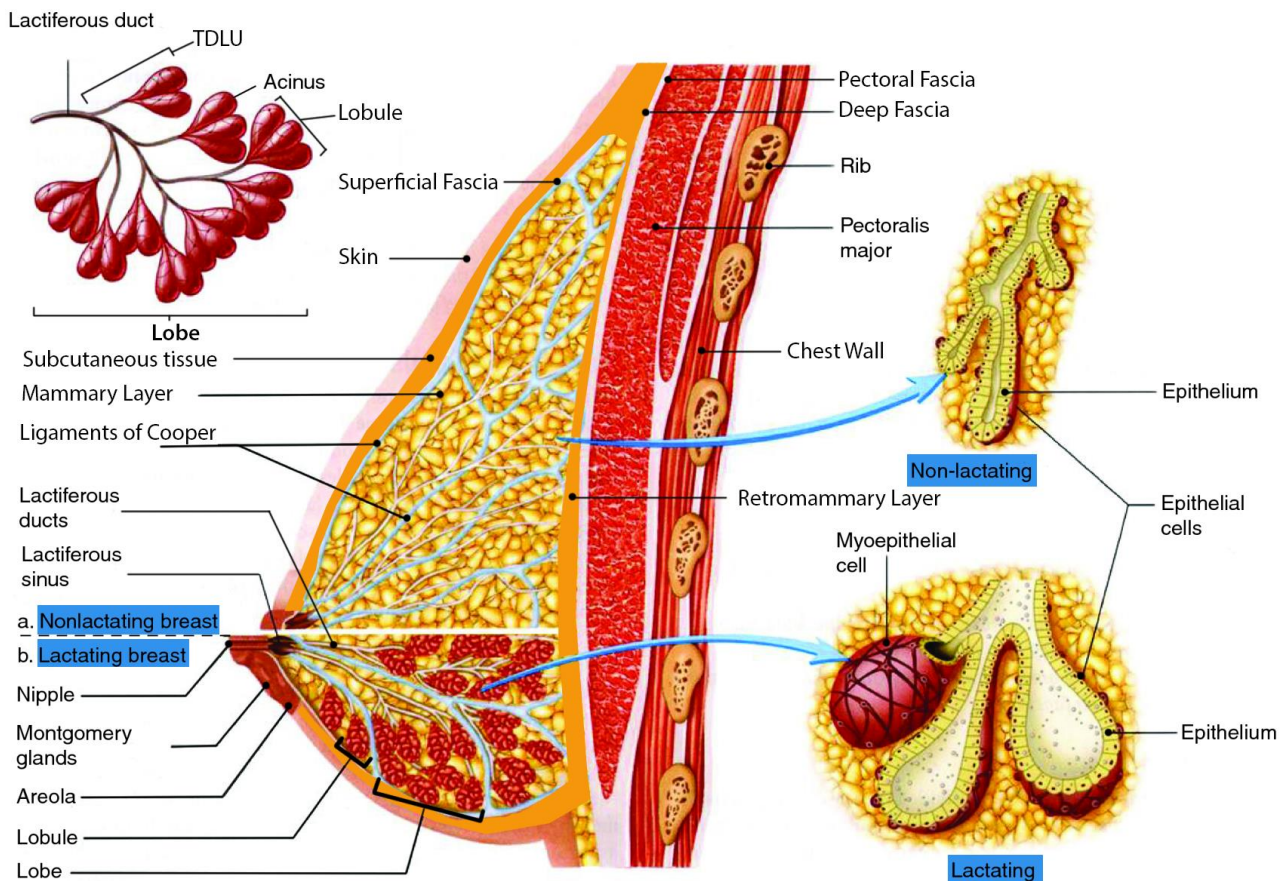


Figure 7: Anatomy Human Mammary Gland ⁴².

2.2 Breast Physiology

In the lifecycle of the female, breast tissue composition, architecture and functionality change significantly as a result of physiological changes that are aimed at allowing the breast to perform its function as a milk-producing organ with the birth of an infant.

Puberty, pregnancy & menopause

With female puberty, the initial growth of the breast is started. By the age of 18, the parenchymal structure is from a typical matured nulliparous female. Approximately until the age of 35, the process of glandular tissue differentiation continues. However, the most dramatic phase of breast development does not occur until pregnancy. During pregnancy, the breasts are being prepared for lactation. Breast enlargement takes place, with an increase in stromal vascularity, nipple size and enormous proliferation of glandular tissue at the expense of adipose tissue. By the end of pregnancy, the breast is mainly composed of highly branched glandular tissue separated by some fibrous stromal tissue. Soon after childbirth, the breast is prepared for lactation. Although the morphology of a lactating breast is very similar to a breast of a pregnant woman, the lactating breast has an increased density and glandular volume and a higher water fraction as a result of milk production. After terminating breastfeeding, overall breast volume declines with stromal and glandular tissue regression. During reproductive life, this cycle of pregnancy, parturition, lactation and post-lactation with the accompanying tissue differentiation and regression can be repeated during multiple pregnancies. The morphological changes during each pregnancy and lactation are permanent. Hence, to the onset of menopause, breasts of parous women contain more glandular tissue than breasts of nulliparous women. Between the ages of 35 and 60, the menopause occurs, which is a natural permanent cessation of the menstrual cycle. This causes regression of glandular tissue of approximately up to a third of its original volume and an increase in stromal adipose tissue^{39,43,44,45,46}.

2.3 Breast Cancer

Breast cancer, a cancer that forms in tissues of the breast, is the most commonly diagnosed cancer in females worldwide and affects one in eight women during their lifetime. Women of 50 years and older account for 81% of the diagnosed breast cancers and the median age at diagnosis for women with breast cancer is 62 years. With breast cancer the composition and morphology of tissue changes. The most common symptom of breast cancer is a lump or mass in the breast. Other symptoms include dimpling of the skin, change in size or shape of the breast, retraction of the nipple and discolouration of the skin^{1, 47,48}.

Breast Cancer Types

A tumour can be benign or malignant, from which the last is commonly referred to as breast cancer. The progression of breast cancer can be seen in figure 8. Breast cancer has many different types. The affected cell type determines the sort of breast cancer. Carcinomas account for most of the breast cancers and arise from the epithelial cells that line the lobules and ducts in the breast. Because carcinomas comprise most of the breast cancers, carcinomas will be further discussed.

A major division of carcinomas can be made between *ductal* or *lobular* and between *in situ* or *invasive* carcinomas. *Ductal carcinoma* begins in the lining of the milk ducts whereas *lobular carcinoma* begins in the lobules of the breast. *In situ carcinoma* is the earliest breast cancer and is "pre-invasive", which means the cancer cells did not invade the breast tissue yet but grow inside the pre-existing normal lobules or ducts. However, it has significant potential to become invasive cancer and must therefore be adequately treated to prevent it from becoming invasive cancer. *Invasive carcinoma* has cancer cells that disrupt the microscopic boundaries of the breast lobules and ducts and grow into the breast connective tissue. In the form of metastases, it has the potential to spread to other body sites, such as lymph nodes or other organs.

^{49,50,51,47,52,53,54}.

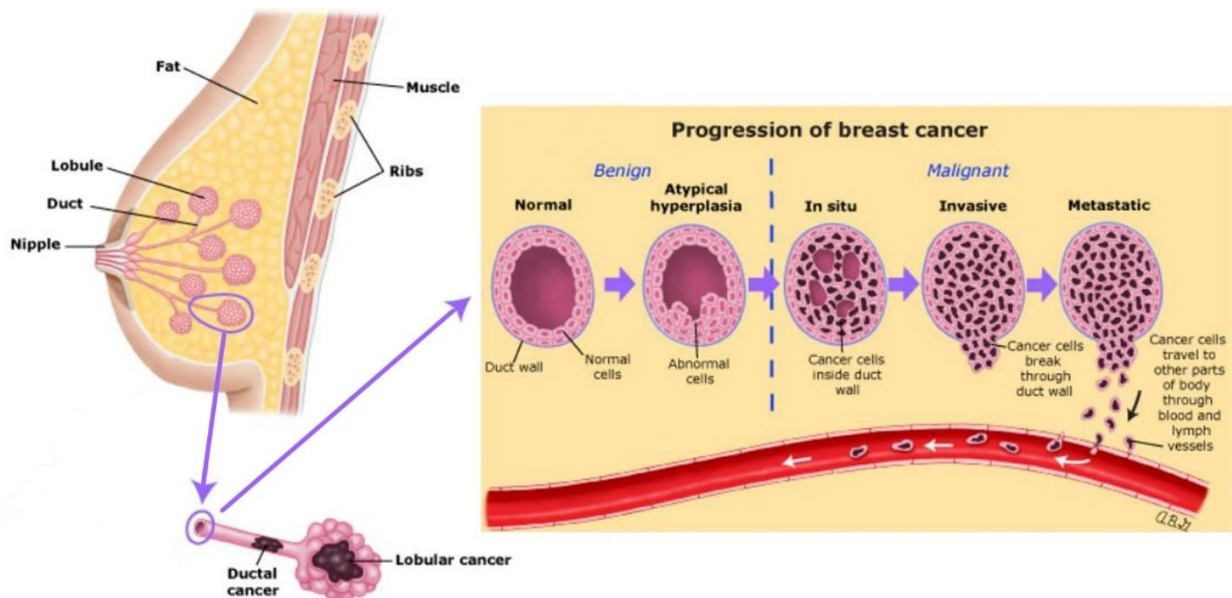


Figure 8: Progression of Breast Cancer from benign towards malignant ⁴⁷.

Compositional & Morphological Changes

With the onset and progression of cancer, significant changes in cellular and/or nuclear structure occur like differences in shape, size, crowding, chromatin organization and DNA structure. Additionally, changes in the amount of lipid content in breast tumours occur and changes in the organization and arrangement of the extracellular matrix in tumours occur. Modification of the extracellular matrix (ECM) is a result of a disruption of the balance between the synthesis and secretion in the ECM and alteration in the normal levels of matrix-remodelling enzymes. Remodelling of the ECM among other things includes an increased deposition of collagen and fibronectin. The quantified compositional and morphological changes cancer will be discussed in paragraph 2.4 ³⁶.

Treatments & Relevance BCS

The two surgical treatment options available for breast cancer are mastectomy and breast-conserving surgery (BCS), both are often used in combination with radiotherapy and chemotherapy. With BCS the tumour is removed with a minimal margin of healthy tissue, called the negative margin. BCS is preferred over mastectomy (removal of the entire breast) due to better cosmetic results, a better quality of life and similar long-term survival rates. Chapter 1.1.4 provided a more detailed description of BCS and negative margins ^{3,25,26}.

The SESK is used with BCS, which is the standard surgical treatment for early-stage breast cancer (stage I & II) with T1 or T2 breast tumours ^{3,25,26}. As seen in figure 9, BCS is the prescribed treatment for 61% of the patients with stage I or II, 21% with stage III and 7% with stage IV ⁵⁵.

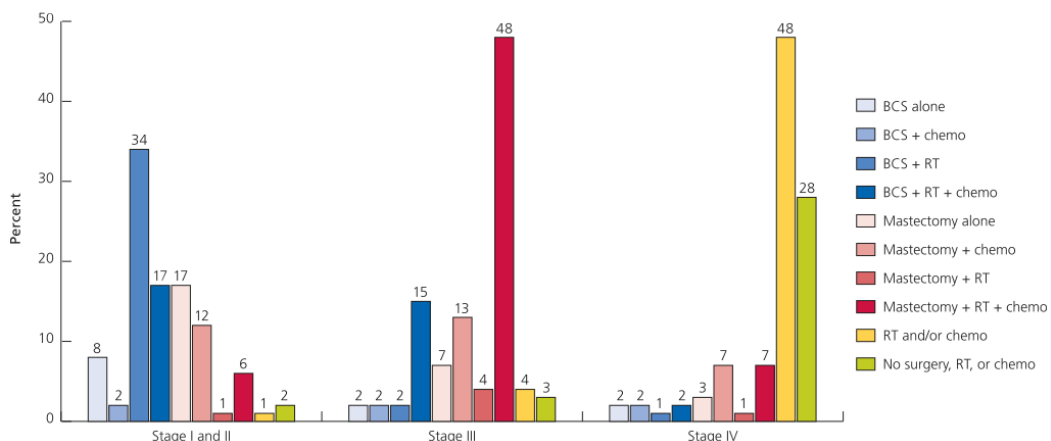


Figure 9: Percentage of prescribed treatment for different breast cancer stages ⁵⁵.

2.4 Quantified Inter- & Intra-patient Variability

A phantom that enables realistic simulation of intraoperative DRS measurements and electrosurgical cutting, includes breast properties that are relevant for the working principle of the SESK. Hence, this chapter discusses the quantified values for each of these relevant breast properties, so that realistic phantom design is made possible.

1. Similar optical properties as human breast tissue
 - *This enables further validation of DRS with its ability to discriminate healthy for tumorous tissue.*
2. Similar mechanical and surface properties as human breast tissue (Elastic modulus).
 - *This enables similar haptic feedback as real tissue when using the electrosurgical knife.*
3. Similar electrically conductive properties as human breast tissue.
 - *This enables realistic tissue effects when using the electrosurgical knife.*
4. Similar thermo tolerance properties as human breast tissue.
 - *This enables realistic tissue effects when using the electrosurgical knife.*

2.4.1 Optical Properties

The optical properties include the absorption- and reduced scattering coefficient (μ_a and $\mu's$), which are both wavelength dependent and are given by the unit reciprocal centimetre (cm^{-1}). The absorption coefficient is related to the composition or levels of chromophores in tissue (HbO_2 , Hb, β -carotene, water, fat and collagen), whereas the reduced scattering coefficient is related to the cellular structure, size, density and refractive index of each cellular and subcellular component ^{29,30}.

As earlier stated, the optical parameter "F/W-ratio", the ratio of chromophores of fat and water in the extended NIR region (1000-1600 nm), is the best parameter in discriminating between healthy and tumour tissue. Hence, the focus of this paragraph is to look at the exact fat and water concentration of human breast tissue and how that changes with cancer.

Intra-patient Heterogeneity

There is great breast heterogeneity, with Intra-patient heterogeneity ranging from 20% to 40% for the absorption coefficient (μ_a), and 5% to 20% for the reduced scattering coefficient ($\mu's$) ⁵⁶.

Table 2: Variations between left and rights breasts (%), table taken from ⁵⁷.

Parameters	Water	Lipid	Scatter amplitude	Scatter Power
$\Delta = (\text{left/right}) / \text{Average}$	12,4	13,0	11,2	23,4

Table 2 shows the study of Wang et al. regarding intra-patient variability between the left and right breasts. It clearly shows the intra-patient differences, however Shah et al. reported that no consistent intra-patient differences exist ^{57,58}. Additionally, there is also great inter-patient heterogeneity which depends greatly on demographic factors. In the following sub-paragraph, compositional changes as a result of demographic factors will be discussed ⁵⁷.

Inter-patient variability & Demographic factors

Various studies have derived quantitative in vivo information of human breast tissue properties and its dependence on the demographic parameters; age, menopausal status and BMI, see table 3. Old age, post-menopausal status and high BMI are generally accompanied by a decrease in scattering parameters and water content, and an increase in lipid content. The quantified breast tissue compositional changes that come with menopause can be found in table 4. Further quantified results of ageing and BMI can be found in my literature study ⁵⁹.

Table 3: Increased (↑), decreased(↓), non-significant (~), and not available (-) optical parameters found by different studies of human breast tissue, (1) = Diffuse optical spectroscopy, (2) = Optical Attenuation Spectroscopy, (3) = Electromagnetic imaging, (4) = Optical Imaging, (5) = Diffuse optical tomography, (6) = NIR imaging, (7) = DRS, table constructed based on references cited in this table.

Demographic Parameters	Studies	Water	Lipid	Amplitude (a)	Power (b)
Age ↑	Taroni et. al. ³³ (2015), (1), 635-1060 nm, N = 200	↓	↑	↓	↓
	Blackmore et. al. ⁶⁰ (2015), (2), 635-1060 nm, N = 202 * only significant for post-menopausal women	~	↑*	-	-
	Spinelli et al. ⁶¹ (2004), (1), 637-980, N = 113	↓	↑	-	-
	Intes ⁶² (2005), (4), 760-850 nm, N = 49	~	-	~	↓
	Cerussi et al. ⁶³ (2001), (1), 672 – 978 nm, N = 2	↓	-	-	↓
	Shah et al ⁶⁴ (2001), (1), 674-956 nm, N = 14	-	-	μ's = ↓	-
Menopausal Status (pre > post)	Taroni et. al. ³³ (2015), (1), 635-1060 nm, N = 200	↓	↑	↓	↓
	Blackmore et. al. ⁶⁰ (2015), (2), 625-1060 nm, N = 202	↓	↑	↓	~
	O'Sullivan et al. (2013), (1), 650 – 1000 nm, N = 28	↓	↑	-	-
	Cerussi et al. ⁶³ (2001), (1), 672 – 978 nm, N = 2 * only 2 subjects have been used, so no significant values can be found	↓*	↑*	-	↓*
	Shah et al ⁶⁴ (2001), (1), 674-956 nm, N = 14	↓	-	μ's = ↓	-
	De Boer et al. ⁵⁶ (2016), (7), 800 nm, (in vivo & ex vivo), N = 45	F/W-ratio = ~	-	μ's = ~	-
BMI ↑	Taroni et. al. ³³ (2015), (1), 635-1060 nm, N = 200	↓	↑	↓	~
	Blackmore et. al. ⁶⁰ (2015), (2), 635-1060 nm, N = 202	↓	↑	-	-
	Spinelli et al. ⁶¹ (2004), (1), 637-980, N = 113	↓	↑	-	-
	Poplack et al. ⁶⁵ (2004), (3), 785 nm, N = 23	-	-	μ's = ↓	-
	Intes ⁶² (2005), (4), 760-850 nm, N = 49	~	-	↓	↓
	Durduran et al. ⁶⁶ (2002), (5), 750-830 nm, N = 52	-	-	μ's = ↓	-
	Cerussi et al. ⁶⁷ (2002), (1), 672-978 nm, N = 30	-	↑	-	↓

Table 4: Tissue composition and scattering parameters of pre- and postmenopausal women, (-) not available, table constructed based on tables in references ³³, ⁶⁰, ⁶⁸, ⁶³.

Study	Menopausal Status	Water (%)	Lipid (%)	a (cm ⁻¹)	b (-)
Blackmore et al. ⁶⁰ (2015) 625-1060 nm	Pre- (N = 95)	21.3 ± 7.2	61.5 ± 10.2	14.6 ± 3.4	0.35 ± 0.31
	Post- (N = 107)	18.2 ± 5.9	68.3 ± 9.0	12.9 ± 2.9	0.38 ± 0.26
	Significant difference	YES	YES	YES	NO
O'Sullivan et al. ⁶⁸ (2013) 650 – 1000	Pre- (N = 17)	24.4 ± 1.8	67.0 ± 1.6	-	-
	Post- (N = 11)	16.6 ± 0.7	74.0 ± 1.4	-	-
	Significant difference	YES	YES	-	-
Cerussi et al. ⁶³ (2001) 672 – 978 nm	Pre- (N = 1)	45.1 ± 3.6	29.8 ± 5.6	-	0.864 ± 0.068
	Post- (N = 1)	10.3 ± 0.8	67.5 ± 3.7	-	0.555 ± 0.036
	Significant difference	-	-	-	-
	Menopausal Status	Water (mg/cm ³)	Lipid (mg/cm ³)	a (cm ⁻¹)	b (-)
Taroni et al. ³³ (2015), 635-1060 nm	Pre- (N = 93)	263.05 ± 148.36	598.29 ± 133.48	14.85 ± 2.60	0.70 ± 0.27
	Post- (N = 102)	127.92 ± 86.30	729.998 ± 111.17	12.44 ± 2.52	0.53 ± 0.24
	Significant difference	YES	YES	YES	YES

Compositional changes as a result of cancer

Several studies quantified the chromophore content and scattering parameters of healthy and diseased breast tissue. Average values per study are given in table 5, the ratio between malignant and healthy tissue is given in table 6 and an overview of the overall dependence of breast tissue composition on cancer is given in table 7⁶⁹. Almost all studies were conducted on in vivo human breast tissue. It is therefore explicitly mentioned in the tables when this is not the case.

Water & lipid Content

The tables show that the water concentration in carcinomas is larger ranging from a 7% to 100% increase, whereas the lipid concentration is smaller in carcinomas compared to healthy tissue of the same breast, and ranges from an 8% to 16% decrease. The study of De Boer et al. corresponds to these results and shows that the F/W-ratio of malignant tissue is much smaller than that of healthy tissue. The same trend can be seen for benign lesions but with smaller differences^{36,70,56}.

Scattering

Most studies show that the μ 's of carcinomas is larger than that of healthy tissue and ranges from 20% to 50%. The cause is tumour cell proliferation and infiltration of various cells into the tumour stroma which increases cell density, thus the μ 's. Apart from Spinelli et al. who measured a slight reduction in scatter power, most studies reported a higher measured scatter power coefficient b in carcinomas compared to healthy tissue. Similar results can be seen for benign lesions, however with smaller values^{70,71}.

Table 5: Optical properties of healthy, malignant and benign breast tissue (* = Median values, N = number of patients, NS = number of samples, AP = adipose, GL = glandular, FAD = fibroadenoma, IC = invasive carcinoma, DCIS = ductal carcinoma in situ), table taken from⁷⁰, further references were added and can be seen in this table.

Property	Study	λ (nm)	Healthy		Malignant		Benign		
			N	Mean \pm SD	N	Mean \pm SD	N	Mean \pm SD	
F/W ratio	De Boer et al. ⁵⁶ (2016) in & ex vivo	400 – 1600	45	7.5	45	0.8			
Water (%)	Nachabé ⁷² (2012) – Ch. 9, ex vivo	500 – 1600	47 (AP) 47 (GL)	8 55	1 (DCIS) 35 (IC)	50 65	11 (FAD)	55	
	Blackmore et al. ⁶⁰ (2015)	625 – 1060	202	19.66 \pm 6.51					
	Cerussi et al. ⁶³ (2001)	672 – 978	2	27.7 \pm 2.2					
	O'Sullivan et al. ⁶⁸ (2013)	650 – 1000	17	21.4 \pm 1.3					
	Intes ⁶² (2005)	760-850	49	28.9 \pm 11.7	11	40.8 \pm 16.6	12	49.5 \pm 20.0	
	Leproux et al. ⁷³ (2016)	650 – 1000			10	47.67 \pm 20.15	11	42.31 \pm 14.98	
	Cerussi et al. ⁷⁴ (2006)	650 – 1000	58	18.7 \pm 10.3	58	25.9 \pm 13.5			
	Wang et al. ⁷⁵ (2010)	903 – 948	3	15 \pm 4	3	26 \pm 2			
	Lipid (%)	Nachabé ⁷² (2012) – Ch. 9, ex vivo	500 – 1600	47 (AP) 47 (GL)	90 12	1 (DCIS) 35 (IC)	15 1	11 (FAD)	1
		Blackmore et al. ⁶⁰ (2015)	625 – 1060	202	65.1 \pm 9.56				
Cerussi et al. ⁶³ (2001)		672 – 978	2	48.65 \pm 4.65					
O'Sullivan et al. ⁶⁸ (2013)		650 – 1000	17	69.7 \pm 1.3					
Intes ⁶² (2005)		760-850	49	62.4 \pm 12.6					
Leproux et al. ⁷³ (2016)		650 – 1000			10	62.54 \pm 13.33	11	64.49 \pm 10.8	
Cerussi et al. ⁷⁴ (2006)		650 – 1000	58	66.1 \pm 10.3	58	58.5 \pm 14.8			
Wang et al. ⁷⁵ (2010)		903 – 948	3	69 \pm 18	3	45 \pm 7			
μ 's (cm ⁻¹)		Nachabé ⁷² (2012) – Ch. 9, ex vivo	800	47 (AP) 47 (GL)	6 cm ⁻¹ 8 cm ⁻¹	1 (DCIS) 35 (IC)	12 cm ⁻¹ 9 cm ⁻¹	11 (FAD)	8.5 cm ⁻¹
		De Boer et al. ⁵⁶ (2016) in & ex vivo	400 – 1600	45	14.5 cm ⁻¹	45	23.5 cm ⁻¹		
		Zhu et al. ⁷⁶ (2008) ex vivo	350 – 600	52	11 cm ⁻¹	54	20 cm ⁻¹	18	16 cm ⁻¹
a (cm ⁻¹)	Blackmore et al. ⁶⁰ (2015)	625 – 1060	202	13.70 \pm 3.14					
	Intes ⁶² (2005)	760-850	49	Log (a) 6.0 \pm 1.7					
	Leproux et al. ⁷³ (2016)	650 – 1000			10	Ln(a) 7.19 \pm 2.35	11	Ln(a) 6.77 \pm 1.95	
	Cerussi et al. ⁷⁴ (2006)	650 – 1000	58	Ln(a) 4.0 \pm 2.0	58	Ln(a) 5.2 \pm 2.6			
	Taroni et al. ³³ (2015)	635-1060	200	13.58 \pm 2.55					
b (-)	Blackmore et al. ⁶⁰ (2015)	625 – 1060	202	0.37 \pm 0.28					
	Cerussi et al. ⁶³ (2001)	672 – 978	2	0.710 \pm 0.052					
	Intes ⁶² (2005)	760-850	49	0.55 \pm 0.25					
	Leproux et al. ⁷³ (2016)	650 – 1000			10	1.13 \pm 0.35	11	1.06 \pm 0.29	
	Grosenick et al. ⁷⁷ (2005)	670 – 884	87	0.99 \pm 0.35	87	1.38 \pm 0.71			
	Spinelli et al. ⁷¹ (2005)	637 – 985	32	0.88 \pm 0.39 0.82 \pm 0.60 0.93 \pm 0.60	32	0.79 \pm 0.56	14 (FAD) 40 (Cyst)	0.98 \pm 0.76 1.56 \pm 0.90	
	Cerussi et al. ⁷⁴ (2006)	650 – 1000	58	0.58 \pm 0.23	58	0.72 \pm 0.32			
	Fang et al. ⁷⁸ (2011)	830	26	0.91 \pm 0.01					
	Wang et al. ⁷⁵ (2010)	903 – 948	3	1.0 \pm 2	3	1.3 \pm 2			

Table 6: Average Ratio of optical properties between malignant or benign and healthy tissue (N = number of patients, FAD = fibroadenoma), table taken from ⁷⁰, further references were added and can be seen in this table.

Property	Study	λ (nm)	Parameter	Malignant		Benign	
				N	Mean \pm SD	N	Mean \pm SD
F/W-ratio	De Boer et al. ⁵⁶ (2016) in & ex vivo	400 – 1600	Δ F/W-ratio	45	-9.11		
Water	Leproux et al. ⁷³ (2016)	650 – 1000	rH ₂ O	10	2.06 \pm 1.00	11	1.10 \pm 0.15
	Intes ⁶² (2005)	760-850	rH ₂ O	11	1.47 \pm 0.76	12	1.50 \pm 0.47
	Cerussi et al. ⁷⁴ (2006)	650 – 1000	$\Delta\%$	58	13.3%		
	Quarto et al. ⁷⁹ (2015)	635 – 1060	$\Delta\%$	45	11.12%	38	9.95%
Lipid	Anderson et al. ⁸⁰ (2015)	600 – 1000	$\Delta\%$	26	7 \pm 1%		
	Leproux et al. ⁷³ (2016)	650 – 1000	rlipid	10	0.85 \pm 0.17	11	1.00 \pm 0.09
	Cerussi et al. ⁷⁴ (2006)	650 – 1000	$\Delta\%$	58	-14.1%		
	Quarto et al. ⁷⁹ (2015)	635 – 1060	$\Delta\%$	45	-15.57%	38	-10.95%
μ' 's	Anderson et al. ⁸⁰ (2015)	600 – 1000	$\Delta\%$	26	-8 \pm 2%		
	De Boer et al. ⁵⁶ (2016) in & ex vivo	400 – 1600	$\Delta \mu'$'s	45	9.19 cm ⁻¹		
	Zhu et al. ⁷⁶ (2008) ex vivo	350 – 600	$\Delta \mu'$'s	54	9 cm ⁻¹	18	5 cm ⁻¹
	Grosenick et al. ⁷⁷ (2005)	670 – 884	r μ' 's (785 nm)	87	1.2 \pm 0.4		
a (cm ⁻¹)	Choe et al. ⁸¹ (2009)	690 – 905	r μ' 's (786 nm)	37	1.53	10	0.98
	Fang et al. ⁷⁸ (2011)	830	r μ' 's (830 nm)	26	1.18 \pm 0.34	17 (solid) 8 (cyst)	1.07 \pm 0.14 1.03 \pm 0.04
	Leproux et al. ⁷³ (2016)	650 – 1000	rln(a)	10	1.45 \pm 0.39	11	1.03 \pm 0.2
b (-)	Leproux et al. ⁷³ (2016)	650 – 1000	rb	10	1.42 \pm 0.36	11	1.03 \pm 0.19

Table 7: Increased (\uparrow), decreased (\downarrow), non-significant (\sim), and not available (-) optical parameters found by different studies when comparing malignant to non-malignant tissue. (1) = DRS, (2) = Optical Imaging, (3) = Diffuse optical spectroscopy, (4) = NIR/Optical tomography, (5) = Optical mammography, (6) = Optical and digital breast tomosynthesis, (7) = fluorescence spectroscopy, (8) = VIS-NIR spectroscopy, table constructed based on references cited in this table.

Studies	Water	Lipid	Amplitude (a)	Power (b)
Zhang et al. ⁸² (2013), (8), 400-2200 nm, N = 28, in vitro	\uparrow	\downarrow	-	-
Nachabé ⁷² (2012) – Ch. 9, (1), 500-1600 nm, N = 47, ex vivo	-	\downarrow	\uparrow	-
De Boer et al. (2016), (1), 400-1600 nm in & ex vivo	F/W-ratio = \downarrow		μ''s = \uparrow	
Zhu et al. ⁷⁶ (2008), (1)(2), 350-600 nm, ex vivo	-	-	μ''s = \uparrow	
Intes ⁶² (2005), (4), 760-850 nm, N = 49	\uparrow	-	-	-
Leproux et al. ⁷³ (2016), (3), 650-1000 nm, N = 19	\uparrow	\sim	\uparrow	\uparrow
Cerussi et al. ⁷⁴ (2006), (3), 650-1000 nm, N = 58	\uparrow	\downarrow	\uparrow	\uparrow
Wang et al. ⁷⁵ (2010), (4), 903-948 nm, N = 3	\uparrow	\downarrow	\sim	\sim
Grosenick et al. ⁷⁷ (2005), (5), 670-884 nm, N = 87	-	-	μ''s = \uparrow	
Spinelli et al. ⁷¹ (2005), (5), 637-985 nm, N = 32	-	-	-	\downarrow
Fang et al. ⁷⁸ (2011), (6), 830 nm, N = 26	-	-	μ''s = \uparrow	
Zhu et al. ⁸³ (2010), (4), 780-830 nm, N = 178	-	-	-	
Quarto et al. ⁷⁹ (2015), (5), 635-1060 nm, N = 45	\uparrow	\downarrow	-	-
Anderson et al. ⁸⁰ (2015), (5), 600-1000 nm, N = 26	\uparrow	\downarrow	-	-
Choe et al. ⁸¹ (2009), (4), 690-905 nm, N = 37	-	-	μ''s = \uparrow	

2.4.2 Other Properties

In order to make a phantom tissue that sufficiently mimics human breast tissue, not only the optical properties should be mimicked, but also the mechanical-, electrically conductive and thermo tolerance properties. This enables realistic simulation of a BCS procedure. However, precise optical mimicking is a requisite for validation of the DRS, whereas mechanical-, electrically conductive and thermo tolerance properties should only roughly be mimicked to allow for a realistic breast tumour resection. Hence, these properties have less priority and are therefore discussed in less detail than the optical properties.

Mechanical Properties

Mechanical properties characterize a material's response to an applied load. The most important mechanical property is elasticity. Elasticity is often characterized using the elastic modulus (E), which is the ratio of stress (σ), the force per unit area, to strain (ϵ_0), the fractional change in length of a sample (formula 2) ⁸⁴. It provides a convenient measure for comparison of tissue types, namely the elasticity of tissue changes in pathological processes ⁸⁵.

$$E = \frac{\sigma}{\varepsilon_0} = \frac{F/A}{\Delta l/l_0} \quad (2)$$

For a linearly elastic material, the elastic modulus is defined as the slope of the stress-strain curve. However, biological tissues such as breast tissue exhibit nonlinear elastic behaviour at strains higher than 10% and are therefore usually calculated in the regime of low strain. The elastic modulus of a material can be measured in various directions resulting in many types of elastic moduli. The main type describes the uniaxial tensile and compressive elasticity and is called the Young's modulus. It measures the stiffness of a material and is given by the unit Pa (N/m²). A stiffer material has a higher the Young's modulus^{85,84,86}.

Table 8: Summary of the results from mechanical testing of ex vivo breast tissue, Young's Modulus (kPa) and SD, table taken from⁸⁷.

Studies	Young's Modulus (kPa) and SD				
	Pre-strain compression	Normal fat tissue	Normal Glandular tissue	DCIS	IDC
Krouskop et al. ⁸⁸ (1998) (Loading frequency of 0.1 to 4 Hz)	5% preload compression	18 ± 7 – 22 ± 12	28 ± 14 – 35 ± 14	22 ± 8 – 26 ± 5	106 ± 32 – 112 ± 43
	20% preload compression	20 ± 8 – 24 ± 6	48 ± 15 – 66 ± 17	291 ± 67 – 307 ± 78	558 ± 180 – 460 ± 178
Wellman et al. ⁸⁹ (1999)	1% strain	4.8 ± 2.5	17.5 ± 8.6 Fibroglandular sample	71.2 ± 0.0	47.1 ± 19.8
	15% strain	17.4 ± 8.4	271.8 ± 67.7 Fibroglandular sample	2162 ± 0.0	1366 ± 348.2
Samani et al. ⁹⁰ (2001) Samani et al. ^{91,92} (2007)	5% preload compression	3.25 ± 0.9	3.24 ± 0.61 Fibroglandular sample	16.38 ± 1.55	Low grade: 10.4 ± 2.6 Medium grade: 19.99 ± 4.2 High grade: 42.5 ± 12.47
Sarvazyan et al. ⁹³ (1995)	-	5 ± 0.0	50 ± 0.0	100 ± 0.0 – 5000 ± 0.0	-
Matsumura et al. ⁹⁴ (2009)	0-0.2 stress	0.7 ± 0.2	0.8 ± 0.2	3.4 ± 1.3	11.5 ± 8.4
	1.0-1.2 stress	17.3 ± 4.8	15.4 ± 3.9	15.6 ± 2.0	27.0 ± 9.2
Umemoto et al. ⁹⁵ (2014)	0-0.2 stress	0.69 ± 0.19	0.73 ± 0.18	5.25 ± 0.46	13.82 ± 9.60
	1.0-1.2 stress	19.08 ± 4.99	16.99 ± 4.92	16.15 ± 4.24	30.5 ± 11.46

Ramião et al reviewed several studies that determined the mechanical properties of women breasts by ex vivo mechanical testing (table 8). Human breast tissue is very heterogeneous ranging from fatty to extremely dense tissue. Subsequently all studies show a variety of mechanical behaviours dependent on its tissue type. Furthermore, Ramião et al. found for each tissue type a wide variability in results. This variability highly depends on the preload compression, namely with increasing compression the Young's modulus of breast tissue increases. Nevertheless, a general increase in elastic modulus can be seen with invasive carcinoma and is accompanied by higher variations compared to healthy tissue. As for DCIS, with increasing compression, the elastic modulus becomes close to that of normal breast tissue. Hence, each tissue type in the breast exhibits different nonlinear characteristics⁸⁷.

Electrical Conductivity Properties

As stated in paragraph 1.1, electrosurgery uses heat to create the tissue effects cutting and coagulation. As shown in formula 3, the amount of generated heat (Q) depends on the current (I), exposure time (t) and tissue resistance (R). The current and exposure time can be regulated by the surgeon, whereas the tissue resistance is still unknown. Hence, to ensure similar tissue effects with the phantom, identification of human breast tissue resistance is necessary¹⁹.

$$Q = I^2 \times t \times R \quad (3)$$

The resistance of tissue depends on its resistivity (ρ) and its shape. Resistivity is the intrinsic resistance of a material and is given by the unit Ohm-metre ($\Omega \cdot m$), see formula 4. R stands for the electrical resistance of uniform material and the shape is a combination of its length (L) and cross-sectional area (A). Conductivity (σ) is the inverse of resistivity and is a measure of a material's tendency to allow the flow of electrical current (formula 5). Conductivity is given by the unit siemens per meter (S/m)^{96,97}.

$$\rho = R \frac{A}{\ell} \quad (4)$$

$$\sigma = \frac{1}{\rho} \quad (5)$$

Tissue's ion concentration is the main factor for tissue's conductivity and varies per tissue type. Tissues containing high ion concentrations, such as hydrated tissues like muscle and skin, are good conductors of electricity and have low resistivity, whereas adipose tissue and bone have high resistivity and are poor conductors of electricity ¹⁶. Table 9 and figure 10 show the dependence of tissue conductivity on the applied frequency. Both show similar results, with conductivity increasing drastically with the increase of frequency. Furthermore, it is clear tumours have the highest conductivity followed by skin, glandular and finally fatty breast tissue ^{98,99}.

Table 9: Relative conductivity of breast tissues at frequency range from 200 MHz to 5GHz, table taken from ⁹⁸.

Tissue	Conductivity (S/m)
Fat	0.1 – 0.2
Skin	0.15 – 3.8
Glandular	0.1 – 3.0
Tumour	0.15 – 5.0

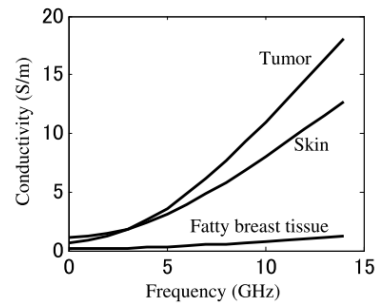


Figure 10: Conductivity of breast tissues at various frequencies ⁹⁹.

Thermo Tolerance Properties

As earlier discussed in paragraph 1.1.3, thermal tissue effects not only depend on the amount of applied heat (Q) but also on tissue's resistance or durability to a certain applied heat called thermo tolerance ²². Until 40°C, no reversible damage occurs, at 50°C approximately after 6 minutes cell death occurs, from 60°C onwards coagulation and desiccation occur, at 100°C cellular vaporization occurs and at 200°C carbonization occurs ^{21,100}. Figure 11 illustrates the thermal damage processes as a function of temperature.

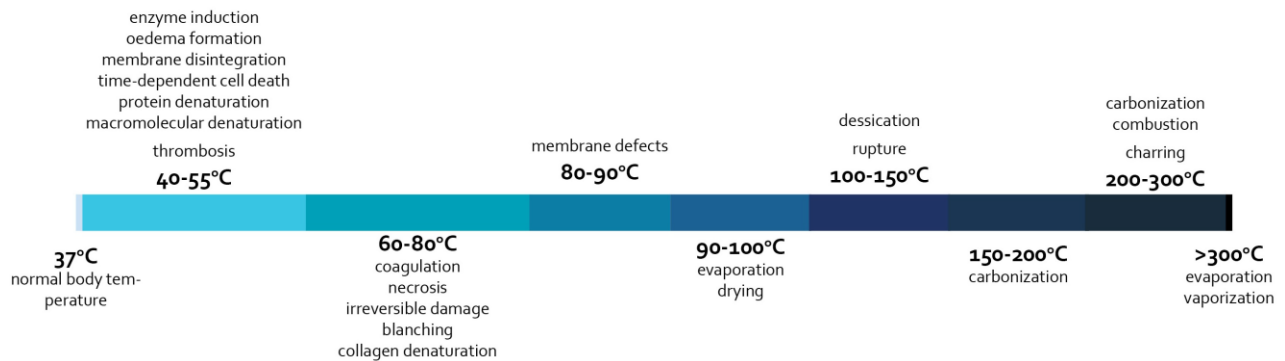


Figure 11: Tissue processes as a function of temperature ⁸.

2.5 Conclusion

This chapter discussed the optical properties of human breast tissue extensively, whereas the mechanical-, electrically conductive- and thermo tolerance properties were discussed in less detail, due to its lower priority for phantom tissue design. Due to the many different imaging modalities, methods and formulas used, the optical results varied a lot. Nevertheless, clear trends can be seen for different demographics and with the transition from healthy to malignant tissue. Similarly, the mechanical- and electrical conductivity properties also change significantly with cancer. Finally, with the thermo tolerance properties, no distinction was made between tissue types, due to its lower priority in phantom tissue design. Now it is known what the quantified tissue properties of healthy and malignant tissue are, the possibilities and requirements of phantom tissue design should be mapped. More specifically, phantom tissue which has the most potential to mimic human breast tissue should be mapped.

3. Phantom Tissue

This chapter discusses the phantom requirements based on literature. Furthermore, the various types of phantoms and what phantom has the most potential to mimic human breast tissue will also be discussed. Consult my literature study for a more elaborate explanation ⁵⁹.

3.1 Phantom tissue Requirements

Phantoms are tissue simulating objects that mimic the properties of human tissue. They play a vital role in the development, validation, and quality control of systems ¹³. An ideal phantom mimics all tissue properties. However, developing an ideal phantom is not realistic but also not necessary. Therefore, in real applications, only some of these properties are implemented while others can be neglected or given a lower priority ¹⁰¹. A phantom that enables SESK validation should include tissue properties that are essential for the working principle of the SESK. Hence, arranged according to relevance the following tissue requirements should be met:

Main tissue requirements

1. Similar optical properties as human breast tissue
 - *This enables further validation of DRS with its ability to discriminate healthy for tumorous tissue.*
2. Similar mechanical and surface properties as human breast tissue (Elastic modulus).
 - *This enables similar haptic feedback as real tissue when using the electro-surgical knife.*
3. Similar electrically conductive properties as human breast tissue.
 - *This enables realistic tissue effects when using the electro-surgical knife.*
4. Similar thermo tolerance properties as human breast tissue.
 - *This enables realistic tissue effects when using the electro-surgical knife.*

Additional requirements

Further phantom properties that are preferable for breast tissue design include ¹⁰¹:

5. Non-solid/ destroyable for electro-surgical cutting.
6. Ease of manufacturing (reproducible/ repeatable).
7. Properties are stable over time and environmental conditions.
8. Inexpensive to produce.

3.2 Matrix material & Additives

Phantoms consist of a base material called the matrix. The choice of matrix material has the largest impact on how the phantom can be used. However, to get properties closer to the desired values, the concentration of matrix material can also be altered, a change in production can be done and additives can be added ^{13,101}.

Matrix materials

The main matrix materials used nowadays are gelatin, agar, fibrin, polyvinyl alcohol (PVA), water-based, polyvinyl chloride (PVC), polyester, polyurethane and silicon. Biopolymers such as agar, gelatin, fibrin and water/lipid-based, provide a soft medium that is biologically and biochemically compatible. They allow for the addition of organic molecules for optical scattering and absorption, which are optimal for scientific laboratory studies. Synthetic polymers such as PVA, PVC, polyester, polyurethane and silicone, are permanent matrix compositions and are optimal for routine calibration and testing of established systems, among other things as a result of its durability ^{84,101,102}.

3.3 Most Potential Matrix Material

No phantom can provide the flexibility to simulate all relevant properties of human breast tissue simultaneously. Each matrix material has its respective strengths and weaknesses from which an overview is given in table 10. All stated matrix materials enable adjustable optical characteristics. However, phantoms that should validate the SESK, should contain well-calibrated and known optical properties for a chosen region of the spectrum. For this project the concentration of molecular features, more specifically the F/W-ratio in the extended NIR is important. Hence, to develop a reliable phantom that accurately mimics the F/W-ratio of tissue, the phantom should be biological compatibility in terms of the inclusion of biologically relevant chromophores such as lipid, so that realistic spectra in the extended NIR region can be ensured.

Synthetic polymers are therefore not appropriate, whereas biopolymers are. They allow easy inclusion of organic molecules and cellular constituents such as fat and blood that provide realistic spectra ¹⁰¹. Furthermore, biopolymers are similar in many respects to soft biological tissue, due to their high mass fraction of water (>80%). Gelatin and agar for example, have similar elastic, electrically conductive and thermal properties as human tissue. However, water/lipid-based biopolymers resemble the fat/water-ratio of healthy and malignant breast tissue more closely. Michaelsen et al. and Quarto et al., developed water/lipid-based biopolymer phantoms and showed these phantoms simulated the F/W-ratios of healthy and malignant breast tissue successfully. Contrary to agar and gelatin, these phantoms do not break and are mouldable into different shapes. Furthermore, these phantoms are very durable, stable, repeatable, easy to make and inexpensive ^{13,101,102,103}.

Hence, biopolymers in general are a good option, with water/lipid-based phantoms being the most promising due to its excellent optical properties. It can be assumed that the electrically conductive- and thermo tolerance properties of water/lipid-based phantoms are pretty similar to human tissue because the main constituents are lipid and water, which is prominently present in breast tissue. Thereby, combining the water/lipid-based with the gelatin and agar biopolymers, the positive characteristics of both can be used to create a phantom that has great optical, mechanical, thermal and electrically conductive properties.

Harris Profile

Table 10 uses Harris profiles to assess each matrix material on the predefined tissue requirements. Elaborate information regarding each matrix material can be found in my literature study ⁵⁹.

Table 10: Harris profile, assessing the strengths and weaknesses of matrix materials, (-) no information could be found.

Property	Gelatin				Agar				Fibrin				PVA				Water/lipid-based			
	--	-	+	++	--	-	+	++	--	-	+	++	--	-	+	++	--	-	+	++
Optical			■	■			■	■			■	■			■	■			■	■
Mechanical			■	■			■	■		■	■				■	■	-	-	-	-
Electrically Conductive			■	■			■	■	-	-	-	-	-	-	-	-	-	-	-	-
Thermo tolerance			■	■			■	■	-	-	-	-	■	■					■	■
Non-solid			■	■			■	■			■	■			■	■			■	■
Ease of Manufacturing			■	■			■	■			■	■	■	■					■	■
Stable over time	■	■					■	■			■	■			■	■			■	■
Inexpensive			■	■			■	■			■	■			■	■			■	■

Property	PVC				Polyester/ Epoxy				Polyurethane				Silicone			
	--	-	+	++	--	-	+	++	--	-	+	++	--	-	+	++
Optical		■				■				■					■	
Mechanical			■	■			■	■		■	■				■	■
Electrically Conductive	-	-	-	-	-	-	-	-	-	-	-	-	-	-	-	-
Thermo tolerance		■				■				■			■	■		
Non-solid	■	■			■	■			■	■					■	■
Ease of Manufacturing			■	■			■	■			■	■			■	■
Stable over time			■	■			■	■			■	■			■	■
Inexpensive			■	■	-	-	-	-	-	-	-	-	■	■		

It is clear that the biopolymers gelatin, agar and water/lipid-based phantoms have the highest scores, with water/lipid-based being the most promising as a result of its great optical properties. Although no exact information could be found regarding the mechanical and electrically conductive properties of water/lipid-based phantoms, it can be assumed these properties are pretty similar to human breast tissue, because the main constituents are lipid and water, which is prominently present in breast tissue. Hence, the focus will be on developing a water/lipid-based phantom with perhaps, agar or gelatin added to improve the mechanical-, thermo tolerance- and electrically conductive properties of the phantom.

3.4 Conclusion

The results of my literature study show that tissue properties that need to be included into the phantom, are tissue properties that are essential for the working principle of the SESK, with water-lipid based phantoms having the most potential to mimic these tissue properties. Nevertheless, it is not clear yet how the SESK validation study will exactly look like. Hence, dependant on how the validation study will look like, the final phantom should besides healthy and malignant tissue properties, perhaps also have other properties. Hence, the next phase will map the validation study design and the accompanying phantom requirements.

II. PHANTOM REQUIREMENTS

The goal of this phase is to map the requirements of a study that enables validation of the smart electrosurgical knife. Once it is clear what role the phantom plays in the validation study, the exact phantom requirements could be mapped. Finally, the process to meet these requirements will be briefly discussed.

4. Validation Study Requirements

The objective of the validation study is to test the potential of the intra-operative margin assessment technique “DRS”, in BCS. More specifically DRS added to the traditional ESK, namely the SESK and its capability in discriminating healthy from malignant tissue intraoperatively.

Test the potential of the SESK in BCS, with its capability of discriminating healthy from malignant tissue intraoperatively.

4.1 Study Design

To test this, surgeons have to conduct BCS with both the SESK and the traditional ESK on tissue-simulating phantoms including a tumour, and see whether surgeons who use a SESK, consistently obtain a higher percentage of negative margins than when using the traditional ESK. Only then the SESK is more promising than the traditional ESK, therefore validating its purpose.

Previous study

This idea was based on the study of Pleijhuis et al., who preclinically assessed the applicability of an IMA technique called near-infrared fluorescence (NIRF-imaging) in BCS on tissue-simulating phantoms. They showed that NIRF-guided intraoperative tumour localization and margin assessment showed feasible. However, NIRF-imaging requires the administration of an exogenous contrast agent, whereas DRS does not. Therefore, to distinguish between tumour and healthy tissue, their phantom design included a contrast agent that deviates from what is required in this thesis project, namely a contrast in F/W-ratio^{104,105}.

Figure 12 illustrates how their study was conducted. Fluorescent tumour-like agarose inclusions differing in size and shape (A) were integrated into breast-shaped phantoms (CI) prior to surgery. Preoperatively, the location of the tumour-like inclusion was assessed non-invasively using a NIRF camera system (B). Intraoperatively, the inclusion was excised under real-time NIRF guidance or guided solely by visual and tactile information (CII). At the end of the surgical procedure, the NIRF camera system was applied to inspect for residual disease and evaluate the extent of surgery (CIII).

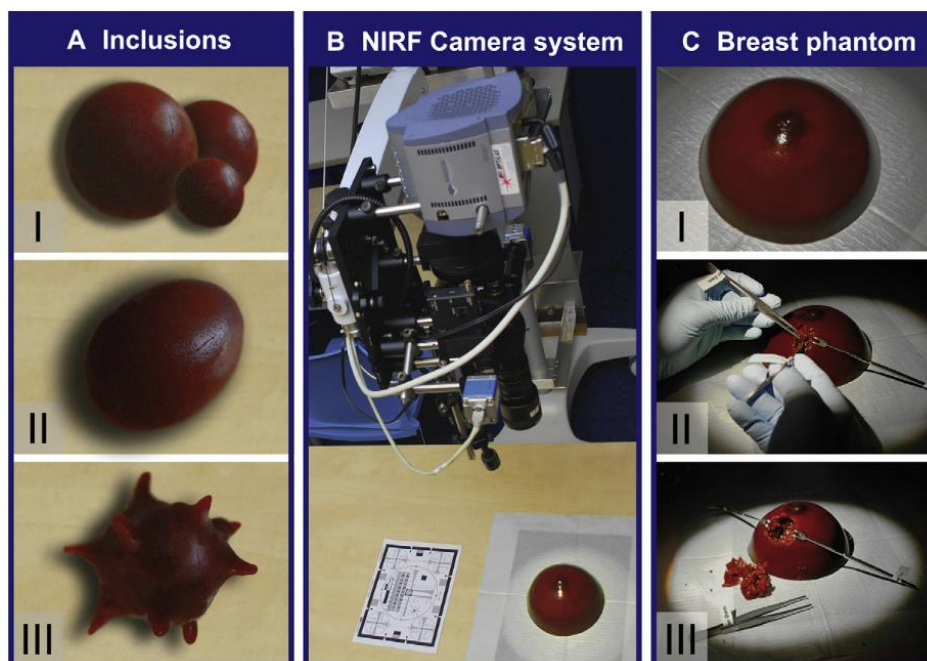


Figure 12: Tumour-like agarose inclusions differing in size and shape (A), NIRF camera system (B), breast-shaped phantom (CI), breast-conserving surgery (CII), postoperative margin assessment (CIII).

4.2 Status Quo BCS

Since the validation study needs to simulate a BCS procedure, and since a BCS procedure consists of three margin assessment phases, the status quo of each phase will be briefly discussed.

4.2.1 Margin assessment

The first step in BCS procedures is preoperative margin assessment also called preoperative planning. This includes non-invasive imaging modalities that determine the location, size and border of the tumour and enable location-dependent incisions. Commonly used preoperative imaging modalities are radiography (X-ray), ultrasonography (US) and magnetic resonance imaging (MRI) ¹⁰⁶. Although these preoperative methods accurately determine the tumour location and size, they are difficult to use intraoperatively due to altered body position and tissue manipulation. With regard to IMA, currently, the only available methods to guide resection are palpation and visual inspection combined with the surgeon's experience and judgment ²³. However, surgeons can only identify the boundaries of easily identifiable solid masses. When there is no clear boundary between healthy and malignant tissue, for example in dense breasts, palpation and visual inspection are insufficient to obtain negative margins ¹⁰⁷. Finally, postoperative margin assessment includes a histologic examination to inspect for residual disease and typically takes place for 1-2 weeks ¹⁰⁸.

4.3 Validation study Requirements

In order to simulate a realistic BCS procedure, the validation study should include all three margin assessment phases. However, during the validation study, the SESK should be tested, hence certain elements of a traditional BCS should be modified to make sure the SESK gets properly tested. The validation study should meet the following requirements:

1. Include preoperative margin assessment
 - *This enables the surgeon to assess the size, border and location of the tumour phantom upfront.*
2. Include tumour resection with the help of DRS, namely the SESK, but without any other IMA technique.
 - *This enables assessment of DRS with its capability in discriminating healthy from malignant tissue.*
 - *The experimental group will solely use DRS, whereas the control group cannot use any other IMA technique (palpation and visual inspection). This is to make sure solely DRS and its capability in discriminating healthy from malignant tissue is tested.*
3. Include postoperative margin assessment
 - *This enables us to inspect for residual tumour phantom and compare the results of the experimental group to the results of the control group.*

5. Phantom Requirements

Since we know now how the validation study will look like, we can determine what role the phantom will play in this study, hence determine the phantom requirements. Only if these phantom requirements are met, the validation study can take place. The phantom should be or include:

General requirements

1. Easy to manufacture & inexpensive
 - *This enables extensive phantom production, hence extensive testing.*
2. Reproducible/consistent & homogeneous
 - *Changes in derived data can then only be attributed to the test setup or tested system ¹³.*
3. Durable & stable/long-lasting
 - *So that the phantom remains usable for longer periods of time.*

Preoperative margin assessment

4. A contrast between tumour and healthy phantom tissue which is assessable preoperatively.
 - *This enables the surgeon to assess the size, border and location of the phantom tumour upfront.*

Intraoperative margin assessment

5. A significant difference in F/W-ratio that simulates tumour and healthy breast tissue content.
 - *This parameter difference enables us to assess DRS with its capability in discriminating healthy from malignant tissue.*
6. Similar mechanical properties as real breast tissue (at room temperature)
 - *This enables similar haptic feedback as real breast tissue when using the electrosurgical knife.*
7. Minimal mechanical differences between tumour and healthy tissue
 - *This eliminates the possibility of using palpation, so that solely DRS and its capability in discriminating healthy from malignant tissue can be tested.*
8. Minimal visible differences between tumour and healthy tissue
 - *This eliminates the possibility of using visual inspection, so that solely DRS and its capability in discriminating healthy from malignant tissue can be tested.*
9. Similar electrically conductive properties as human breast tissue, at room temperature
 - *This enables realistic tissue effects when using the electrosurgical knife.*
10. Similar thermo tolerance properties as human breast tissue, at room temperature
 - *This enables realistic tissue effects when using the electrosurgical knife.*

Postoperative margin assessment

11. A contrast between tumour and healthy phantom tissue which is assessable postoperatively.
 - *This enables us to inspect for residual tumour phantom and compare the results of the experimental group to the results of the control group.*

Shape and size

12. Similar shape and size as human breasts containing a tumour.
 - *So that the validation study is as close to a BCS procedure as possible.*

6. Meeting the Requirements

The goal is now to see whether it is possible to produce a phantom that meets all phantom requirements. In order to do so, an incremental process will be used, namely the production process will be split into four research phases where each successive phase builds upon previous phases adding more functionality¹⁰⁹.

1. With the first research phase, various phantoms will be produced that potentially meet the F/W-ratio-, mechanical- and visual requirements (5-8). The produced phantoms will efficiently be tested, from which the most potential phantoms will be used for further research.
2. With the second research phase, the most potential phantoms will be tested extensively on all IMA requirements (5-10). The best phantoms will be used for further research.
3. This phantom will be further developed concerning the pre- and postoperative margin assessment requirements (4 and 11), without interfering with the IMA requirements.
4. In the last research phase, the final phantom will be made, which will have a similar size and shape as a real breast (REQ 12). Furthermore, this phantom will be evaluated with regard to the general requirements.

**During each research phase, the general requirements will be taken into account (1-3).*

III. RESEARCH PHASE 1

PHANTOM PRODUCTION

The goal of this phase is to see whether it is possible to produce a phantom that potentially meets the F/W-ratio-, mechanical- and visual requirements. In chapter 7,8 and 9, an overview of research phase 1 will be given, relevant phantom studies will be mimicked and finally, the most potential phantoms will be produced.

7. Process Steps and Testing

Requirements 5 till 8 state that the tumour and healthy tissue in the final phantom, should have a significant difference in F/W-ratio, realistic mechanical properties and minimal differences in mechanical- and visual properties. My literature study showed that various studies were capable of producing phantoms that sufficiently mimic one of these properties, but none of them developed a phantom combining all these properties together ⁵⁹. Hence, this chapter gives an overview of research phase 1, namely the iterative production process towards a phantom that combines all these properties together and potentially meets requirements 5 till 8.

The iterative process consists of a development and test stage ¹¹⁰. With the development stage, phantoms will be produced that should come as close to requirements 5 till 8 as possible, whereas with the test stage, these phantoms will be evaluated with regard to these requirements. The results will be used to select the most potential phantoms for further research.

7.1 Development

With the development stage, phantoms will be produced that should come as close to requirements 5 till 8 as possible. My literature study shows that the biopolymers such agar-, gelatin- and water/lipid-based phantoms, showed promising results with regard to mimicking breast properties. Each of these biopolymers has its own advantages ⁵⁹. Water/lipid-based phantoms enable realistic F/W-ratios, whereas agar and gelatin have excellent mechanical properties. Since mimicking the F/W-ratio has the highest priority, the focus will be on developing a water/lipid-based phantom with perhaps, agar or gelatin added to improve the mechanical properties of the phantom.

7.2 Testing

With the test stage, the produced phantoms will be tested on the F/W-ratio, visual- and mechanical properties, which can easily be done by visual- and haptic inspection, therefore enable time-efficient phantom production. The F/W-ratio will be tested by visual inspection on its homogeneity, more specifically its F/W-ratio uniformity. The mechanical and visual properties will respectively be tested by haptic and visual inspection, on its mechanical feel and colour (Table 11).

Table 11: Qualitative testing the produced phantoms.

Requirement	Property	Qualitative testing method
5	F/W-ratio	Visual inspection: Is the phantom homogeneous?
6 & 7	Mechanical	Haptic inspection: How does the phantom feel?
8	Visual	Visual inspection: What colour does the phantom have?

7.3 Process steps and testing

This paragraph gives a structured overview of the whole iteration process with regard to developing a phantom that potentially meets the F/W-ratio, mechanical- and visual requirements.

Mimic fat and water spectrum

The first step in this process is to find materials that can sufficiently mimic the fat and water spectra of tumour and healthy breast tissue. Michaelsen et al. tested various fat types namely: butter, margarine, olive oil, canola oil, vegetable oil, and lard. They concluded that lard in combination with water resembles the optical properties of human breast tissue the best. This is because animal fat is more similar to human adipose content than the other fat types. Additionally, Quarto et al. also used lard and similarly showed promising results with regard to the fat/water spectra. Hence, as a starting point, lard and water will be used to mimic the fat and water content of human breast tissue ^{13,103}.

Mimic relevant studies - Chapter 8

Step two is to find a combination of materials and production methods that enable lard and water to be mixed into different F/W-ratios. Table 12 gives an overview of studies who all used water/lipid-based biopolymers to mimic the F/W-ratio of breast tissue. The table shows all these studies used water/lipid as a matrix material and agar or other materials, such as guar gum as an additive to emulsify fat and water or to alter the mechanical properties.

In chapter 8 I will mimic and test these studies if feasible. Feasibility depends on material purchase time, -costs and -availability, and on production time, -costs and equipment availability. In case these studies are reproduced, the phantoms will be tested qualitatively on its F/W-ratio- and mechanical properties.

Table 12: Studies producing F/W-ratios similar to human breasts, table constructed based on references cited in this table.

Study	Matrix Material	Additives		F/W-ratio range
		Emulsifiers	Coagulants/ Solidification agent	
Michaelsen et al. ¹³ (2014)	<u>Water/lipid-based</u> Water: Regular water Fat: Lard	Guar gum	-	15:85 – 85:15
Quarto et al. ¹⁰³ (2013)	<u>Water/lipid-based</u> Water: Distilled Water Fat: Lard	Agar	-	30:70 – 70:30
Ohmae et al. ¹¹¹ (2018)	<u>Water/lipid-based</u> Water: Distilled Water Fat: Soybean oil, Intralipos	Soybean Lecithin	Agar Oil-solidifying agent	95:5 – 1:99
Bush et al. ¹⁴ (2018)	<u>Water/lipid-based</u> Water: Distilled Water Fat: Peanut Oil	Water soluble surfactant Oil soluble surfactant	Agar	0:100 – 100:0

Producing most potential phantoms – Chapter 9

In chapter 8 many different studies were replicated and evaluated. From the results, a lot of information was extracted which enables goal-oriented phantom development. Hence, in chapter 9 combinations of materials and production methods will be used to produce phantoms that have a lot of potential to meet the F/W-ratio, mechanical- and visual requirements. The produced phantoms will be tested qualitatively on its F/W-ratio, mechanical- and visual properties, from which the most potential phantoms will be selected and used for further research, namely research phase 2.

8. Mimic Relevant Studies

In this chapter, many different studies that successfully mimicked the F/W-ratio of breast tissue will be replicated. The produced phantoms will be tested qualitatively on its F/W-ratio and mechanical properties. From these tests, a lot of useful information can be extracted, like what materials in combination with what production methods, work best to produce phantoms with different F/W-ratios and good mechanical properties.

8.1 Guar gum

Michaelsen et al. tested various emulsifiers (guar gum, soy lecithin and borax) in combination with lard and water and concluded that guar gum was the most viable option. They showed that guar gum enabled the production of homogeneous phantoms with different F/W-ratios ranging from 15:85 to 85:15. These phantoms were durable for several weeks, were semisolid like breasts and compared to other emulsifiers, had the lowest signal attenuation in optical measurements. Finally, the absorption spectra of the guar gum/water/lipid-based phantoms show discernible peaks for their lipid (930) and water constituents (970 nm), see figure 13¹³. In this study, I tried to make guar gum/water/lipid-based phantoms with a wide range of F/W-ratios. In order to do so, the study of Michaelsen et al. was replicated. I strived to use the same production method and materials.

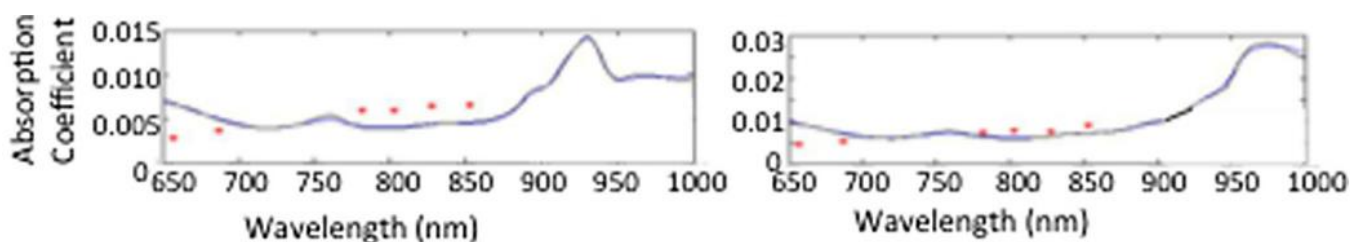


Figure 13: Spectra for mostly lipid (left) and mostly water (right) phantom, with its specific lipid (930 nm) and water peak (970 nm) ¹³.

8.1.1 Materials and methods

Materials & equipment

The phantoms consisted of lard, water and guar gum. Michaelsen et al. did not specify what type of lard, guar gum and water were used. Hence, regular lard from the local butcher (Alain Bernard, Amsterdam), low-cost guar gum (Original Superfoods Guar Gum Powder¹¹²) and tap water were used. Michaelsen et al. used a handheld automated mixer but did not specify where from. Hence, a regular handheld mixer (Tefal Quickchef) was used. Furthermore, to heat up the lard, the “IKA C-MAG HS7 control” heater was used¹³.

Setup and methods

The phantoms consisted of 200 mL fat and water, with F/W-ratios ranging from 30/70 to 70/30. For each phantom type a total of three samples was produced, to make sure the results were consistent. The lard was heated until melted (40 °C). 3% guar gum by weight of water was added to the water (20 °C) and mixed for 3 minutes at low and then medium speed. The melted lard was added to the guar gum/water mixture and mixed for 3 minutes at low and then medium speed. This mixture was then poured into glass cups, covered by plastic foil and refrigerated (4°C) overnight to solidify. The following day these phantoms were taken out of the refrigerator and cups to get to room temperature (3 hours waiting).

8.1.2 Results & Conclusion

Three phantom types made of guar gum, water and lard were produced with F/W-ratios ranging from 30/70 to 70/30, see table 13 and figure 14 and 15. Guar gum only showed good emulsification for a F/W-ratio of 30F/70W. Furthermore, guar gum in combination with water made a slushy composition. Possible explanations might be that the used guar gum and mixer, were not exactly the same as the ones used by Michaelsen et al. Since the qualitative results were far from promising, guar gum was not used for further phantom production.

Table 13: Results table guar gum phantoms.

Phantom type	Visual inspection: Homogeneous?	Haptic inspection: Realistic Feel?
1. 100mL Fat/100mL Water + 3 gr guar gum.	No	No: Lower 50% slushy, upper 50% buttery.
2. 60mL Fat/140mL Water + 4,2 gr guar gum.	Yes	No: Very slushy
3. 140mL Fat /60mL Water + 1,8 gr guar gum.	No	No: Lower 30% is very slushy, upper 70% sticky



Figure 14: Guar gum phantoms: 1 left, 2 middle, 3 right



Figure 15: Guar gum phantoms: 1 left, 2 middle, 3 right

8.2 Water-lipid & Agar

Quarto et al., Ohmae et al. and Bush et al. all showed promising results when using water/lipid-based phantoms in combination with agar as an emulsifier or coagulant. They showed that agar enabled the production of homogeneous semi-solid phantoms, with a wide range of F/W-ratios, having great durability ranging from one week to several months. Each study was conducted slightly different with different materials and production methods. Quarto et al. was the only one using solely agar to mix fat and water^{103,14,111}. In this study, I tried to make agar phantoms with a wide range of F/W-ratios, by using Quarto et al. as a guideline. Production methods from the other two studies were also used and tested.

8.2.1 Materials and methods

Materials & equipment

Quarto et al. was the only one who specified where they got their agar from, namely from Sigma-Aldrich. However, Sigma-Aldrich has many different types of agar, thereby agar from Sigma-Aldrich is very expensive. As a result, regular cheap Agar (Terrasana¹¹³) was used. Quarto et al. mixed water with 1% of agar by weight of water, whereas Bush et al. and Ohmae et al. respectively mixed 3% and 5% of agar by weight of water. Therefore, phantoms with various amounts of agar concentrations were produced. Quarto et al. did not specify where they got their lard from. Hence, regular lard from the local butcher (Alain Bernard, Amsterdam) was used. Quarto et al. used lard at room temperature, whereas Michael et al. used lard at melting temperature (40 °C), hence both temperatures were tested. Quarto et al., Ohmae et al. and Bush et al., all used distilled water but did not specify from what company. Hence, regular distilled water (HORBACH 5L) was used. Additionally, regular tap water was also used, to see whether distilled water was a requisite for making agar phantoms. Quarto et al. used a professional disperser (OV5, VELP Scientifica), Ohmae et al. used a handheld blender (unspecified) and Bush et al. used a Stir bar (unspecified). Since no professional dispenser was available a handheld mixer (Tefal Quickchef) was used. Additionally, a stir bar (IKA C-MAG HS7 control) was used to see what mixer enabled the most homogeneous phantoms. Quarto et al. mixed water with agar at 90°C, whereas Ohmae et al. and Bush et al. respectively at 100°C and 350°C. Since, the used heater (IKA C-MAG HS7 control) did not enable temperatures higher than 110°C, only 90°C and 100°C agar mixtures were tested^{103,14,111}.

Setup and methods

The phantoms consisted of 200 mL fat and water, with F/W-ratios ranging from 30/70 to 70/30. For each phantom type a total of three samples was produced, to make sure the results were consistent. The lard was used at room temperature (20 °C) or heated until melted (40 °C). Distilled water or tap water was heated to 90°C or 100°C. Various concentrations (1-5%) of agar by weight of water were added to the water and mixed. Either the mixture was mixed by the stir bar for 3 minutes at 800 rpm, or for 3 minutes by the handheld mixer at low and then high-speed. The lard was added to the agar/water mixture and mixed for several minutes. Again, either the mixture was mixed by the stir bar for 3 minutes at 800 rpm, or for 3 minutes by the handheld mixer at low and then high-speed. The mixture was then poured into glass cups and refrigerated (4°C) overnight to solidify. The following day these phantoms were taken out of the refrigerator and cups, to get to room temperature (3 hours). Initial work involved mixtures with a F/W-ratio of 50F/50W. After satisfactory results were obtained, phantoms of 30F/70W and 70F/30W were tested.

8.2.2 Results

Lard temperature: Mixing lard at room temperature with agar/water was not possible with the stir bar nor the handheld mixer. The lard was too stiff for both mixers, namely the mixers did not have enough torque. However, both mixers easily mixed melted lard with agar/water. As a result, solely melted lard will be used for further phantom production (40°C).

Mixer: When mixing melted lard (40°C) and agar/water at 90°C or 100°C, both the stir bar and the handheld mixer enabled homogeneous mixtures. Since the stir bar is also used for heating, solely the stir bar will be used for further phantom production.

Water temperature: Two phantom types of 5% agar by weight of water were produced. One phantom type was produced with 90 °C of tap water and the other one with 100 °C of tap water. Table 14 shows agar dissolved better in 100 °C of tap water than in 90 °C tap water. Hence, with further phantom production, agar will be dissolved in water with a temperature of 100 °C.

Table 14: Results table - agar absorbed in different temperatures.

Phantom type	Visual inspection: <i>Homogeneous?</i>
1. 100mL tap water + 5gr agar at 90 °C.	Homogeneous: Yes
2. 100mL tap water + 5gr agar at 100 °C.	Homogeneous: Yes: But finer than with 90 °C.

Agar concentrations: Early tests indicated that small percentages of agar (1 and 2%) was not enough to emulsify lard and water sufficiently for F/W-ratios of 50F/50W. As a result, three phantom types of 200 mL fat and water with a F/W-ratio of 50F/50W were produced, with agar concentrations of respectively 3,5 and 6% by weight of water. Table 15 and figure 16 show 5% of agar by weight of water, resulted in the most homogeneous phantom with the best mechanical properties. As a result, further phantom production involves 5% of agar by weight of water.

Noteworthy, adding lard to fast to the agar/water mixture, resulted in a bad emulsified mixture, whereas adding lard slowly to the agar/water mixture, allowed lard to slowly react with the agar/water mixture, leading to a good emulsification. Hence, for further phantom production, lard will slowly be added to the agar/water mixture. Furthermore, similarly to Quarto et al., during the whole process water got evaporated¹⁰³. Hence, to keep the desired F/W-ratio with further phantom production, from now on, the weight deviation will be corrected for by adding the right amount of water (100 °C) to the mixture.

Table 15: Results table - different concentrations of agar solved in water.

Phantom type	Visual inspection: <i>Homogeneous?</i>	Haptic inspection: <i>Realistic Feel?</i>
1. 100mL Fat/100mL tap water + 4 gr agar at 100 °C.	A little bit: Some fat clumps.	No: Buttery and brittle.
2. 100mL Fat/100mL tap water + 5 gr agar at 100 °C.	Yes	Yes: Quite bouncy but stiff.
3. 100mL Fat/100mL tap water + 6 gr agar at 100 °C.	A little bit: Some fat clumps.	No: Too stiff and a little bit brittle.

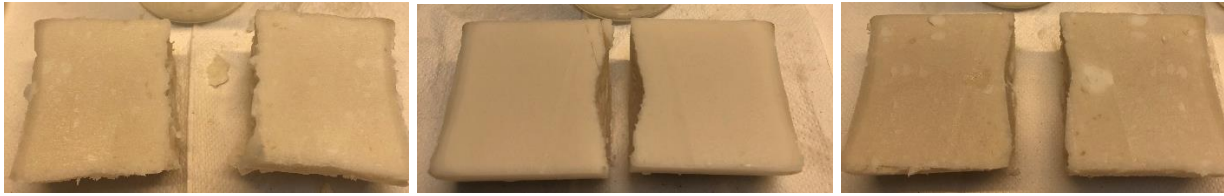


Figure 16: Different concentrations of agar phantoms: 1 left, 2 middle, 3 right

Water: Since a F/W-ratio of 50/50 was successfully obtained, further F/W-ratios were tested. Six phantom types of 200 mL fat and water, with different F/W-ratios and 5% of agar by weight of water were produced (table 16 & 17, figure 17 & 18). Three phantom types were made with tap water and three phantom types were made with distilled water. The results show that with distilled water, solely homogeneity was obtained for the 30F/70W phantom, whereas with tap water, homogeneity was obtained for the 50F/50W- and the 30F/70W phantom while having realistic mechanical properties. Hence, agar works better in combination with tap water than with distilled water. However, even with tap water, not all F/W-ratios were successfully obtained. Hence, in the following experiments, we aim to obtain homogeneity for 70F/30W phantoms while using tap water.

Table 16: Results table - distilled water-based phantoms.

Phantom type	Visual inspection: <i>Homogeneous?</i>	Haptic inspection: <i>Realistic Feel?</i>
1. 140mL Fat/60mL distilled water + 3 gr agar at 100 °C.	No: Fat and water/agar mixture totally separated.	No
2. 100mL Fat/100mL distilled water + 5 gr agar at 100 °C.	No: Fat and water/agar mixture totally separated.	No
3. 60mL Fat/140mL distilled water + 7 gr agar at 100 °C.	Yes	Yes: Quite bouncy but stiff.



Figure 17: Phantoms with different F/W-ratios and produced with distilled water: 1 left, 2 middle, 3 right.

Table 17: Results table - tap water-based phantoms.

Phantom type	Visual inspection: <i>Homogeneous?</i>	Haptic inspection: <i>Realistic Feel?</i>
4. 140mL Fat/60mL tap water + 3 gr agar at 100°C.	No: Fat and water/agar mixture totally separated.	No: Very buttery at the fat part and stiff at the agar part.
5. 100mL Fat/100mL tap water + 5 gr agar at 100°C.	Yes.	Yes: Quite bouncy but a little bit stiff.
6. 60mL Fat/140mL tap water + 7 gr agar at 100°C.	Yes.	Yes: Quite bouncy but stiff.



Figure 18: Phantoms with different F/W-ratios and produced with tap water: 4 left, 5 middle, 6 right.

8.2.3 Conclusion

In this study various agar/water/lipid-based phantoms were produced. Homogeneity was obtained for phantoms with a F/W-ratios of 1 (50F/50W) and 0.43 (30F/70W), while having a realistic mechanical feel. To produce these phantoms successfully, among other things the following production steps were taken: correct for water evaporation, melt lard at 40°C, solve 5% agar in 100 °C tap water, slowly add the melted lard to the agar/water mixture and mix these together with a stir bar.

However, even if all these production steps were done right, a F/W-ratio of 2.33 (70F/30W) could not be obtained. Hence, in the next paragraph other production methods and additives will be tested, to see whether phantom production with a F/W-ratio of 70/30 is possible.

8.3 Water-lipid, Agar & Other methods and additives

In this paragraph, other production methods and additives will be tested to produce water/lipid-based phantoms in combination with agar, with a F/W-ratio of 70/30. This paragraph is divided into two studies, study one tests other production methods and study two tests various additives.

Study 1: Temperature decrease

In this study, inspiration was taken from Pleijhuis et al., who produced breast phantoms made of gelatin ¹⁰⁴. To make sure the mixture stayed homogeneous, the gelatin mixture was cooled down to 35 °C, while mixing continued. Hence, in this study the same technique will be used but with an agar/water/lard mixture of 70F/30W and 5% agar by weight of water.

8.3.1 Materials and methods

Materials & equipment

Tap water, agar (Terrasana ¹¹³) and lard from the local butcher (Alain Bernard, Amsterdam) were used. The IKA C-MAG HS7 control was used to heat up the water and lard and mix all the materials together.

Setup and methods

The phantom consisted of 200 mL fat and water with a F/W-ratio of 30/70. In total, three samples were produced to make sure the results were consistent. Lard was heated until melted (40 °C) and tap water was heated to 100°C. 5% of agar by weight of water was added to the water and mixed for 3 minutes at 800 rpm. The lard was slowly added to the agar/water mixture and mixed for 3 minutes at 800 rpm. In case the total mixture seemed homogeneous, the mixture was weighted. If due to water evaporation, the total weight was still too low, it was corrected for by adding the right amount of water (100 °C) and mixed for 3 minutes at 800 rpm. The heater was turned off and the mixture was put into an ice bath. Mixing was continued until the mixture had a temperature of 35 °C. The mixture was then poured into glass cups and refrigerated (4°C) overnight to solidify. The following day these phantoms were taken out of the refrigerator and cups, to get to room temperature (3 hours).

8.3.2 Results

The results show that the 70F/30W phantom obtained sufficient homogeneity, however insufficient mechanical properties, namely very buttery (table 18 and figure 19). Perhaps the phantom could become more homogeneous and less buttery by adding an extra emulsifier or coagulant.

Table 18: Results table – agar/water/lipid-based phantoms with a temperature decrease to 40 °C.

Phantom type	Visual inspection: Homogeneous?	Haptic inspection: Realistic Feel?
1. 140mL Fat + 60mL tap water + 3 gr agar	A little bit: Still some fat clumps.	No: Good stiffness but very buttery.
2. 140mL Fat + 60mL tap water + 3 gr agar	A little bit: Still some fat clumps.	No: Good stiffness but very buttery.



Figure 19: Agar/water/lipid-based phantom with a temperature decrease to 35 °C: 1 left, 2 right.

Study 2: Emulsifiers and coagulants

Study two is about Ohmae et al. and Bush et al. who used next to agar other emulsifiers and coagulants to mix fat and water to produce phantoms with F/W-ratios up to 95F/5W ^{14,111}. Hence, in this study the emulsifiers and coagulants they used in combination with agar, water and lard will be tested.

8.3.3 Materials and methods

Materials & equipment

The main used materials were tap water, agar (Terrasana ¹¹³) and lard from the local butcher (Alain Bernard, Amsterdam). Additionally, the following materials were considered; As an emulsifier, Ohmae et al. used soybean lecithin (FUJIFILM Wako Pure Chemical Corporation ¹¹⁴) to mix fat and water. As a result, the same material was ordered, however according to the company the product was not available anymore. Hence, soybean lecithin was not used eventually. Additionally, Ohmae et al. used an oil solidifying agent but did not specify what type ¹¹¹. As a result, the company “Chempri Oleochemicals” was contacted, who are specialized in oleochemistry, and recommended to use ethoxylated PEG-based castor oil (EL 11 & EL 33 with CAS nr.: 61791-12-6 ^{115,116}). According to them, EL 11 and EL 33 are both emulsifiers and oil-coagulants. More specifically, they are solvable in lard, mix water and lard very well, and will give lard more body. Hence, these exact materials were ordered and used. Since Bush et al. did not specify what emulsifiers were used, solely EL 11 and EL 33 were tested. To mix all the materials together, the IKA C-MAG HS7 control was used, which was also used to heat up the water and lard to the desired temperatures ¹⁴.

Setup and methods

The phantom consisted of 200 mL fat and water with a F/W-ratio of 30/70. In total, three samples per phantom type were produced to make sure the results were consistent. Lard was heated until melted (40 °C) and tap water was heated to 100°C. 10% of EL 11 or EL 33 by weight of lard was added to the melted lard and mixed for 3 minutes at 800 rpm. 5% of agar by weight of water was added to the water and mixed for 3 minutes at 800 rpm. The lard/EL mixture was slowly added to the agar/water mixture and mixed for 3 minutes at 800 rpm. In case the total mixture seemed homogeneous, the mixture was weighted. If due to water evaporation, the total weight was still too low, it was corrected for by adding the right amount of water (100 °C) and mixed for 3 minutes at 800 rpm. The mixture was then poured into glass cups and refrigerated (4°C) overnight to solidify. The following day these phantoms were taken out of the refrigerator and cups, to get to room temperature (3 hours).

8.3.4 Results

Both EL11 and EL33 emulsified water and lard excellently, however the mechanical feel of both phantoms was very bad, namely very buttery (table 19 and figure 20).

Table 19: Results table – agar/water/lipid-based phantoms in combination with EL 11 or EL 33.

Phantom type	Visual inspection: <i>Homogeneous?</i>	Haptic inspection: <i>Realistic Feel?</i>
3. 140mL Fat + 14gr EL 11 /60mL water + 3 gr agar	Yes	No: Very buttery and stiff
4. 140mL Fat + 14gr EL 33 /60mL water + 3 gr agar	Yes	Yes: Very buttery and soft.



Figure 20: Agar/water/lipid-based phantoms in combination with EL 11 or EL 33: 1 left, 2 right.

8.3.5 Conclusion Study 1 & 2

Both studies showed an improvement in the emulsification of lard and water with study 2 showing the best homogeneity. Hence, it is possible to produce phantoms with a F/W-ratio of 2.33 (70F/30W), however it is clear that it is very hard to obtain realistic mechanical properties with such a F/W-ratio. Even though Chempri Oleochemicals stated that EL 11 and EL 33 should've increased the stiffness of lard, the mixture turned out to be even more buttery. Hence, these two studies showed that producing homogeneous agar/water/lipid phantoms with good mechanical properties, does not work for a F/W-ratio of 70F/30W.

8.4 Water-lipid & Gelatin

Until now, I showed that water/lipid-based phantoms in combination with agar solely enable F/W-ratios equal to and smaller than 50/50, while having good homogeneity and realistic mechanical properties. However, as suggested in my literature study, not only agar but also gelatin in combination with water/lipid showed promising results. More specifically, gelatin works as a great emulsifying agent and has mechanical properties similar to human tissue, see references ^{117,118,119,120}.

Hence, the goal of this study is to produce water/lipid-based phantoms in combination with gelatin and see whether larger F/W-ratios can be obtained than 50/50, while at the same time having sufficient mechanical properties. Pleijhuis et al. produced gelatin-based breast phantoms with good optical homogeneity and mechanical properties. Hence, the study of Pleijhuis et al. will be used as a guideline ¹⁰⁴.

8.4.1 Materials and methods

Materials & equipment

Tap water and lard from the local butcher (Alain Bernard, Amsterdam) were used. Just like Pleijhuis et al., 250 bloom, beef-based gelatin from Natural Spices (Watergang, the Netherlands ¹²¹) was used. Pleijhuis et al. solved TBS (50 mmol Tris-HCl, 150 mmol NaCl, pH 7.4) into the water and subsequently solved 10% gelatin in the TBS/water mixture. However, they did not specify from what company. Since I couldn't find TBS with the same pH value, TBS of sigma Aldrich (50 mmol Tris-HCl, 150 mmol NaCl, Ph 7.6, product nr.: 94158 ¹²²) was used. Additionally, water without TBS was also used, to see whether TBS was a requisite for making successful gelatin phantoms. The IKA C-MAG HS7 control was used to heat up the water and lard and mix all the materials together ¹⁰⁴.

Setup and methods

The phantom consisted of 200 mL fat and water with F/W-ratios ranging from 30/70 to 70/30. In total, three samples per phantom type were produced to make sure the results were consistent. Lard was heated until melted (40 °C) and tap water was heated to 50°C. 10% of gelatin by weight of water was added to either solely water or a water/TBS mixture, and mixed for 3 minutes at 800 rpm. Lard was slowly added to the gelatin/water mixture and mixed for 3 minutes at 800 rpm. In case the total mixture seemed homogeneous, the mixture was weighted. If due to water evaporation, the total weight was still too low, it was corrected for by adding the right amount of water (50 °C) and mixed for 3 minutes at 800 rpm. The heater was turned off and the mixture was put into an ice bath. Mixing was continued until the mixture had a temperature of 35 °C. The mixture was then poured into glass cups and refrigerated (4°C) overnight to solidify. The following day these phantoms were taken out of the refrigerator and cups, to get to room temperature (3 hours).

8.4.2 Results & Conclusion

Six phantom types with different F/W-ratios and 10% of gelatin by weight of water were produced (table 20 & 21, figure 21 & 22). Three phantom types were made with a TBS/water mixture and three phantom types were made with solely water. Homogeneity was obtained for all phantoms that used solely water, whereas the TBS phantoms showed homogeneity for solely two phantom types. Concerning the mechanical properties, all phantoms showed too low stiffness and the 70F/30W phantoms were additionally too buttery. All in all, the results are promising for phantoms without TBS, since homogeneity was reached for all tested F/W-ratios. However, the mechanical properties should be improved, perhaps increasing the stiffness by increasing the gelatin concentration.

Table 20: Results table – TBS/water-based phantoms.

Phantom type	Visual inspection: <i>Homogeneous?</i>	Haptic inspection: <i>Realistic Feel?</i>
1. 140mL Fat/60 mL water + TBS + 6 gr gelatin	Yes	No: Not stiff very squashy and buttery
2. 100mL Fat/100 mL water + TBS + 10 gr gelatin	Yes	A little bit: Very squashy, not stiff
3. 60mL Fat/140 mL water + TBS + 14 gr gelatin	Little bit, many fat and gelatin clumps	No: Low stiffness and squashy



Figure 21: Gelatin/TBS/water phantoms: 1 left, 2 middle, 3 right.

Table 21: Results table - water-based phantoms.

Phantom type	Visual inspection: <i>Homogeneous?</i>	Haptic inspection: <i>Realistic Feel?</i>
4. 140mL Fat/60 mL water + 6 gr gelatin	Yes	No: Not stiff very squashy and buttery
5. 100mL Fat/100 mL water + 10 gr gelatin	Yes	Al little bit: Little bit buttery, squashy, not stiff
6. 60mL Fat/140 mL water + 14 gr gelatin	Yes	No: Low stiffness and very squashy.



Figure 22: Gelatin/water phantoms: 4 left, 5 middle, 6 right.

8.5 Conclusion

In this chapter, many different studies that mimicked the F/W-ratio of breast tissue were replicated. The produced phantoms were tested qualitatively on its F/W-ratio and mechanical properties. From these tests, a lot of useful information was extracted, like what materials in combination with what production methods work best. The results show that water/lipid-based phantoms in combination with agar or gelatin, enable phantom production with F/W-ratios and mechanical properties similar to breast tissue. Table 22 gives an overview of the most promising production method for agar and gelatin in combination with water and lard, whereas table 23 gives an overview of the results for each of these materials.

Table 22: Most promising production method for agar/water/lipid-based and gelatin/water/lipid-based phantoms.

Agar	Gelatin
Materials	Materials
Agar: Regular agar (Terrasana) ¹¹³ . Lard: Regular lard from (Alain Bernard, Amsterdam). Water: Regular tap water.	Gelatin: Regular beef-based gelatin 250 (Natural Spices, Watergang, the Netherlands) ¹²¹ . Lard: Regular lard from (Alain Bernard, Amsterdam). Water: Regular tap water.
Equipment	Equipment
Mixer: Stir bar (IKA C-MAG HS7 control). Heater: IKA C-MAG HS7 control	Mixer: Stir bar (IKA C-MAG HS7 control). Heater: IKA C-MAG HS7 control
Setup and methods	Setup and methods
<ol style="list-style-type: none"> The phantoms will have a total fat and water volume of 200 mL Lard is heated until melted (40 °C) and water is heated to 100°C. Various concentrations of agar by weight of water are added to the water and mixed for 3 minutes at 800 rpm. The melted lard is slowly added to the agar/water mixture and mixed for 3 minutes at 800 rpm. In case the total mixture seems homogeneous, weight the phantom. If due to water evaporation, the total weight is still too low, correct for this by adding the right amount of water (100 °C) and mixed for 3 minutes at 800 rpm. Turn off the heater and put the mixture into an ice bath. Continue to mix at 800 rpm while the mixture cools down to 35 °C. The mixture is then poured into glass cups and refrigerated (4°C) overnight to solidify. The following day these phantoms are taken out of the refrigerator and cups to get to room temperature (3 hours) 	<ol style="list-style-type: none"> The phantoms will have a total fat and water volume of 200 mL. Lard is heated until melted (40 °C) and water is heated to 50°C. Various concentrations of gelatin by weight of water are added to the water and mixed for 3 minutes at 800 rpm. The melted lard is slowly added to the gelatin/water mixture and mixed for 3 minutes at 800 rpm. In case the total mixture seems homogeneous, weight the phantom. If due to water evaporation, the total weight is still too low, correct for this by adding the right amount of water (50 °C) and mixed for 3 minutes at 800 rpm. Turn off the heater and put the mixture into an ice bath. Continue to mix at 800 rpm while the mixture cools down to 35 °C. The mixture is then poured into glass cups and refrigerated (4°C) overnight to solidify. The following day these phantoms are taken out of the refrigerator and cups to get to room temperature (3 hours)

Table 23: Results table – Water/lipid in combination with agar- or gelatin-based phantoms.

Phantom type Property	Agar – 5% by weight of water			Gelatin – 10% by weight of water		
	70F/30W	50F/50W	30F/70W	70F/30W	50F/50W	30F/70W
F/W-ratio:	A little bit: still some fat clumps.	Yes	Yes	Yes	Yes	Yes
Visual inspection: <i>Homogeneous?</i>						
Mechanical properties	No: Good stiffness but very buttery.	Yes: Bouncy but a little bit stiff.	Yes: Bouncy but stiff.	No: Very buttery, low stiffness	Al little bit: Little bit buttery, squashy, not stiff	No: Low stiffness and squashy
Haptic inspection: <i>Realistic feel?</i>						

As can be seen in table 23, agar-based phantoms enable homogeneous F/W-ratios of 1 and 0.43, whereas gelatin-based phantoms enable all F/W-ratios (2.33, 1 & 0.43). Hence, gelatin is a better emulsifier than agar. However, compared to agar-, gelatin-based phantoms showed worse results with regard to mechanical properties.

Nevertheless, this chapter solely tested three F/W-ratios with only a limited amount of material concentrations. Hence, there is still a lot of potential with regard to optimizing the homogeneity and mechanical properties of each these materials. Therefore, in the next chapter for both agar and gelatin, the F/W-ratios and accompanying material concentration will be optimized.

9. Producing Most Potential Phantoms

Requirements 5,6,7 and 8 respectively state that the tumour and healthy tissue in the final phantom should have a significant difference in F/W-ratio, realistic mechanical properties and minimal mechanical- and visual differences. Chapter 8 showed both agar and gelatin in combination with water and lard have a lot of potential to produce different F/W-ratios, while having sufficient mechanical properties. However, until now solely three F/W-ratios were tested, with only a limited amount of material concentrations.

Hence in this chapter for both agar and gelatin, more F/W-ratios and material concentrations will be tested, so that the highest and lowest possible F/W-ratio with good visual- and mechanical properties can be found. Tables 5,6 and 7, show that healthy breast tissue has a higher F/W-ratio than tumour tissue⁵⁹. Hence, the highest F/W-ratio will simulate healthy breast tissue whereas the lowest F/W-ratio will simulate tumour breast tissue. The goal of this chapter with the accompanying test methods will be:

Find the highest and lowest possible F/W-ratio for both agar and gelatin, with the best accompanying material concentrations. The phantoms should be homogeneous and mechanically realistic. Furthermore, the mechanical- and visual properties of these phantoms should be as close to each other as possible.

- Homogeneity will be tested by visual inspection.
- Mechanical testing will be done by haptic inspection. To compare the phantoms sufficiently a scale will be used for the mechanical properties, ranging from 1 (very squashy) to 5 (very stiff), with 3 being realistic like real breast tissue. Furthermore, just like real breasts, the phantoms cannot be buttery/sticky, brittle and watery.
- The colour of the phantoms will be tested by visual inspection.

9.1 Agar

In chapter 8, solely phantoms with F/W-ratios of 70F/30W, 50F/50W and 30F/70W and a limited amount of material concentrations were tested. In this paragraph, the highest and lowest possible F/W-ratio with the accompanying material concentration will be found for agar/water/lipid-based phantoms. The most promising production method will be used to produce the phantoms, see table 22.

9.1.1 Results

Agar/water/lipid-based phantoms were produced with F/W-ratios ranging from 70F/30W to 10F/90W, and agar concentrations ranging from 2 to 6% by weight of water. The phantoms consisted of 200 mL fat and water. Furthermore, three samples per phantom type were made to make sure the results were consistent. An overview of the qualitative results is given in table 24. The results show that for a constant agar concentration by weight of water, a decrease in F/W-ratio, hence an increase in the agar/water amount and a decrease in the lard amount, the phantom stiffness increased, which is a result of agar's stiff nature¹²³. Hence, it can be concluded that at room temperature, even low agar concentrations of 2% by weight of water, have a higher stiffness than solely lard. Furthermore, the results show that it is easier to produce homogeneous phantoms when the F/W-ratio is low compared to when the F/W-ratio is high. This is because, for a constant agar concentration by weight of water, a low F/W-ratio means there is less fat to be emulsified and more agar which works as an emulsifier, whereas with a high F/W-ratio, there might be too much fat and too little agar to emulsify the fat and water. In line with literature, simply increasing the agar concentrations does not always work, since it could result in a brittle phantom, see the 6% agar phantoms for example¹²³. However, with regard to the 50F/50W phantoms, an increase in agar concentration did reduce the butteriness of the phantoms. Finally, with the 10F/90W phantoms, the F/W-ratio was too low, namely too little lard was present, resulting in too stiff and watery phantoms.

Table 24: Results– Agar/water/lipid phantoms with different F/W-ratios and agar concentrations, phantoms marked in green are sufficiently homogeneous and mechanically realistic.

Agar Concentration ↓	Samples 70F/30W	Samples 60F/40W	Samples 50F/50W	Samples 30F/70W	Samples 20F/80W	Samples 10F/90W
2%						 <p>Homogeneous: Yes Realistic feel: No, too watery, slippery and bouncy like a ball. Stiffness</p>
3%			 <p>Homogeneous: A little bit, some fat clumps. Realistic feel: No, buttery and brittle. Stiffness</p>	 <p>Homogeneous: Yes Realistic feel: Yes, bouncy but stiff. Stiffness</p>	 <p>Homogeneous: Yes Realistic feel: Yes, bouncy but stiff. Stiffness</p>	
4%	 <p>Homogeneous: A little bit, still some fat clumps. Realistic feel: No, very buttery more than with 3%. Stiffness</p>	 <p>Homogeneous: Yes Realistic feel: No, good stiffness but buttery and brittle. Stiffness</p>	 <p>Homogeneous: Yes Realistic feel: Yes, bouncy and a little bit stiff. Stiffness</p>	 <p>Homogeneous: Yes Realistic feel: Yes, bouncy but a little bit stiff. Stiffness</p>		
5%	 <p>Homogeneous: A little bit, still some fat clumps. Realistic Feel: No, good stiffness, but very buttery. Stiffness</p>	 <p>Homogeneous: A little bit, some fat clumps. Realistic Feel: No, quite buttery. Stiffness</p>	 <p>Homogeneous: Yes Realistic feel: Yes, bouncy but a little bit stiff. Stiffness</p>	 <p>Homogeneous: Yes Realistic feel: Yes, bouncy but a little bit stiff. Stiffness</p>		
6%	 <p>Homogeneous: No, still agar particles visible. Realistic feel: No good stiffness, but very buttery and brittle. Stiffness</p>	 <p>Homogeneous: No, fat particles visible Realistic feel: No buttery, brittle and stiff. Stiffness</p>	 <p>Homogeneous: A little bit, some fat clumps. Realistic Feel: No, a bit brittle and too stiff. Stiffness</p>			

9.1.2 Most potential phantoms

As can be seen in table 24, the phantom with the highest F/W-ratio while having sufficient homogeneity and mechanical properties, was the phantom with a F/W-ratio of 50/50 and an agar concentration of 5%. Although this phantom was stiffer than real breasts, all other phantoms with either the same or higher F/W-ratio, were not suitable as they were buttery, not perfectly homogeneous and in some cases even brittle. Furthermore, the table shows that phantoms with the lowest F/W-ratio, while having sufficient homogeneity and mechanical properties, were the 20F/80W phantoms with an agar concentration of 3 or 4% by weight of water. All phantoms with lower F/W-ratios (10F/90W), were either too watery or too stiff. The 20F/80W phantoms had similarly to the 50F/50W/5% agar phantom, a slightly higher stiffness than real breasts. Additionally, the three phantoms were visually nearly identical, namely all three had an off-white colour. This is ideal since there should be a minimal difference in mechanical- and visual properties between the highest and lowest F/W-ratio phantom. Table 25 displays pictures taken from these phantoms, all taken in the same room at the same time.

Figure 23 shows that pure lard has an off-white colour and 5% agar/water has a brownish colour. When adding even the slightest amount of lard to an agar/water mixture, the phantom colour turned off-white, see the 10F/90W phantom in table 24 for example. As a matter of course, the three most promising phantoms also turned out off-white.

Table 25: Most potential agar/water/lipid-based phantoms.

50F/50W + 5% agar	20F/80W + 3% agar	50F/50W + 4% agar
		
Stiffness	Stiffness	Stiffness
		



Figure 23: Pure lard sample and 5% agar/water sample.

9.2 Gelatin

In chapter 8, solely F/W-ratios of 70F/30W, 50F/50W and 30F/70W were tested with only a limited amount of material concentrations. In this paragraph, the highest and lowest possible F/W-ratio with the accompanying material concentration will be found for gelatin/water/lipid-based phantoms. The most promising production method will be used to produce the phantoms, see table 22.

9.2.1 Results

Gelatin/water/lipid-based phantoms were produced with F/W-ratios ranging from 70F/30W to 10F/90W, and gelatin concentrations ranging from 10 to 35% by weight of water. The phantoms consisted of 200 mL fat and water. Furthermore, three samples per phantom type were made to make sure the results were consistent. An overview of the qualitative results is given in table 26. The results show that for constant gelatin concentrations of 10%, 20% and 30%, a decrease in F/W-ratio, hence an increase in the gelatin/water amount and a decrease in the lard amount, respectively resulted in a lower, slightly higher and much higher stiffness. Hence, 10%, 20% and 30% gelatin solved in water respectively have a lower, slightly higher and much higher stiffness compared to lard at room temperature. Furthermore, the results show that for various gelatin concentrations, it was very easy to produce homogeneous phantoms for both low- and high F/W-ratios, which is due to the fact that gelatin is a great emulsifying agent^{117,118,120}. Furthermore, the 60F/40W and 50F/50W phantoms show that an increase in gelatin concentration reduced the butteriness of the phantoms. However, adding too much gelatin, degradation of homogeneity and -mechanical properties occurred (e.g. the 35% phantom, table 26). The cause for this is unknown, maybe due to water/gelatin saturation and therefore its incapacity to further mix with lard. Finally, with the 10F/90W phantoms, the F/W-ratio was too low, namely too little lard was present, resulting in either too stiff or too watery phantoms.

9.2.2 Most potential phantoms

As can be seen in table 26, the phantom with the highest F/W-ratio while having sufficient homogeneity and mechanical properties, was the phantom with a F/W-ratio of 60/40 and a gelatin concentration of 30%. Although this phantom was stiffer than real breasts, all other phantoms with either the same or higher F/W-ratios were not suitable, as they were too buttery or inhomogeneous. The table shows that the phantoms with the lowest F/W-ratio while having sufficient homogeneity and mechanical properties, were the 20F/80W phantoms with a gelatin concentration of 20% and 25% by weight of water. All phantoms with lower F/W-ratios (10F/90W), were either too watery or too stiff.

The 20F/80W phantoms had similarly to the 60F/40W/30% gelatin phantom, a slightly higher stiffness than real breasts. However, the 20F/80W/20% gelatin phantom was visually more identical to the 60F/40W/30% gelatin phantom, than the 20F/80W/25% gelatin phantom. This might be due to the lower concentration of gelatine used in the 20F/80W/20% gelatin phantom, since the used gelatin had an intrinsic light brown colour. Hence, since there should be a minimal difference in the mechanical- and visual properties between the highest and lowest F/W-ratio phantom, the 20F/80W/20%gelatin and 60F/40W/30% gelatin phantoms are the most promising. However, the results are based on qualitative tests, therefore quantitative tests have to be performed to be sure. Table 27 displays pictures taken from these phantoms, all taken in the same room at the same time.

Table 26: Results table – Gelatin/water/lipid phantoms with different F/W-ratios and gelatin concentrations, phantoms marked in green are sufficiently homogeneous and mechanically realistic.









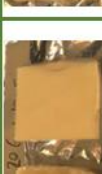











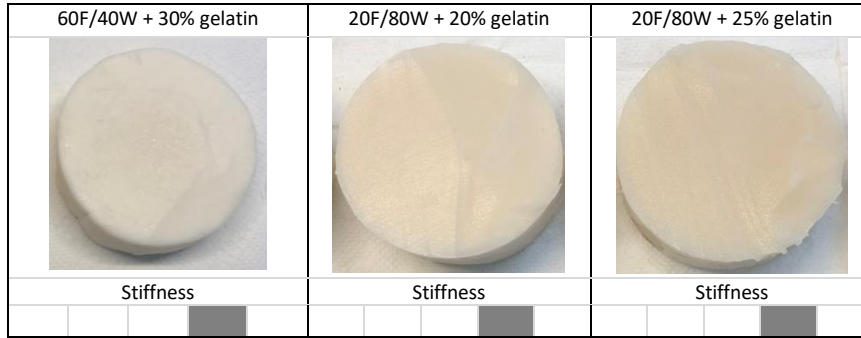
Gelatin Concentration ↓	Samples 70F/30W	Samples 60F/40W	Samples 50F/50W	Samples 30F/70W	Samples 20F/80W	Samples 10F/90W
10%	 <p>Homogeneous: Yes Realistic feel: No, very buttery</p> <p>Stiffness</p>	 <p>Homogeneous: Yes Realistic feel: A little bit, a bit buttery, quite squashy and not stiff</p> <p>Stiffness</p>	 <p>Homogeneous: Yes Realistic feel: No, very squashy.</p> <p>Stiffness</p>	 <p>Homogeneous: Yes Realistic feel: No, very squashy.</p> <p>Stiffness</p>	 <p>Homogeneous: Yes Realistic feel: No, very squashy.</p> <p>Stiffness</p>	 <p>Homogeneous: Yes Realistic feel: No, very squashy, too watery.</p> <p>Stiffness</p>
20%	 <p>Homogeneous: Yes Realistic feel: No, very buttery</p> <p>Stiffness</p>	 <p>Homogeneous: Yes Realistic feel: No, squashy like breasts, but buttery still.</p> <p>Stiffness</p>	 <p>Homogeneous: Yes Realistic feel: Yes, squashy like breasts.</p> <p>Stiffness</p>	 <p>Homogeneous: Yes Realistic feel: Yes, very squashy like real breasts.</p> <p>Stiffness</p>	 <p>Homogeneous: Yes Realistic feel: Yes, squashy, but a little bit stiff.</p> <p>Stiffness</p>	 <p>Homogeneous: Yes Realistic feel: No, squashy like breasts, but too watery.</p> <p>Stiffness</p>
25%	 <p>Homogeneous: Yes Realistic feel: No, squashy like breasts, but buttery still.</p> <p>Stiffness</p>	 <p>Homogeneous: Yes Realistic feel: No, squashy like breasts, but buttery still.</p> <p>Stiffness</p>			 <p>Homogeneous: Yes Realistic feel: Yes, squashy, but a little bit stiff.</p> <p>Stiffness</p>	
30%	 <p>Homogeneous: Yes Realistic feel: No, still a bit buttery.</p> <p>Stiffness</p>	 <p>Homogeneous: Yes Realistic feel: Yes, squashy, not buttery, but a little bit stiff.</p> <p>Stiffness</p>			 <p>Homogeneous: Yes Realistic feel: No, far too stiff</p> <p>Stiffness</p>	 <p>Homogeneous: Yes Realistic feel: No, too stiff and watery.</p> <p>Stiffness</p>
35%		 <p>Homogeneous: No, separated Realistic feel: No, separated</p> <p>Stiffness</p>				

Table 27: Most potential gelatin/water/lipid-based phantoms.



9.3 Conclusion

The goal of this study was to find gelatin and agar phantoms with the highest and lowest possible F/W-ratio, while having good mechanical properties and a minimal difference in visual- and mechanical properties. To do so, various F/W-ratios and material concentrations of agar and gelatin were tested. The highest F/W-ratio simulated healthy breast tissue whereas the lowest F/W-ratio simulated tumour tissue.

With regard to gelatin, the highest and lowest possible F/W-ratio while having sufficient mechanical and visual properties, was respectively the 60F/40W phantom with 30% of gelatin by weight of water, and the 20F/80W phantom with 20% of gelatin by weight of water. With regard to agar, the highest and lowest possible F/W-ratio while having sufficient mechanical and visual properties, was respectively the 50F/50W phantom with 5% of agar by weight of water, and the 20F/80W phantoms with 3 or 4% of agar by weight of water. Although both phantoms had a slightly higher stiffness than usual breasts, they were still sufficiently similar to real breasts. Furthermore, for both gelatin and agar, the mechanical- and visual properties between the healthy and tumour phantoms were nearly identical and therefore ideal.

To determine whether the acquired F/W-ratios are realistic, they have to be compared to F/W-ratios of real breast tissue. Table 28 gives an overview of the F/W-ratios of the produced phantoms and that of healthy and tumour breast tissue measured *in vivo*. Although the studies showed varying results, it can be concluded that the acquired F/W-ratios, namely 1 and 0.25 for the agar- and 1.5 and 0.25 for the gelatin phantoms, are realistic since they fall within the range of the F/W-ratios acquired by breast studies (0.22 – 11.25).

Although these results are promising, they are solely based on qualitative tests. Hence, in the next research phase, quantitative tests will be performed with regard to the F/W-ratio and mechanical properties. Furthermore, a statistical test will be performed to see whether the acquired healthy and tumour phantom F/W-ratios actually differ significantly. Finally, the electrical conductivity and thermo tolerance properties will also be tested to see whether the most potential phantoms meet all IMA requirements. However, the visual properties are already sufficient enough to meet requirement 8, therefore there is no need to further test this property in the next research phase.

Table 28: F/W-ratio of healthy and tumour tissue & F/W-ratios of most potential phantoms, AP = adipose, GL = glandular, IC = invasive carcinoma, DCIS = ductal carcinoma *in situ*, table constructed based on references cited in this table and based on the conducted experiments.

Study	Healthy tissue			Tumour tissue		
	Lipid (%)	Water (%)	F/W-ratio	Lipid (%)	Water (%)	F/W-ratio
	Mean	Mean	Mean	Mean	Mean	Mean
De Boer et al. ⁵⁶ (2016) in & ex vivo	-	-	7.5	-	-	0.8
Nachabé ⁷² (2012) – Ch. 9, ex vivo	90 (AP)	8 (AP)	11.25	15 (DCIS)	50 (DCIS)	0.3
	12 (GL)	55 (GL)	0.22			
Blackmore et al. ⁶⁰ (2015)	65.1	19.66	3.31	-	-	-
Cerussi et al. ⁶³ (2001)	48.65	27.7	1.76	-	-	-
O'Sullivan et al. ⁶⁸ (2013)	69.7	21.4	3.26	-	-	-
Intes ⁶² (2005)	62.4	28.9	2.16	-	40.8	-
Leproux et al. ⁷³ (2016)	-	-	-	62.54	47.67	1.31
Cerussi et al. ⁷⁴ (2006)	66.1	18.7	3.53	58.5	25.9	2.26
Wang et al. ⁷⁵ (2010)	69	15	4.6	45	26	1.73
Agar	50	50	1	20	80	0.25
Gelatin	60	40	1.5	20	80	0.25

IV. RESEARCH PHASE 2

TESTING MOST POTENTIAL PHANTOMS

The goal of this phase is to test the most potential phantoms with regard to the F/W-ratio, mechanical, electrically conductive- and thermo tolerance requirements and chose the best phantom for further research. In chapter 10,11,12 and 13, respectively an overview of research phase 2 will be given, the mechanical properties will be tested quantitatively, the F/W-ratio will be tested quantitatively, and the electrical conductivity and thermo tolerance properties will be tested qualitatively.

10. Process Steps and Testing

This chapter gives an overview of research phase 2, namely extensively testing the most potential phantoms, with regard to the F/W-ratio, mechanical-, electrically conductive- and thermo tolerance requirements, so that the best phantom can be chosen for further research. Table 29 gives an overview of how these requirements will be tested.

Table 29: Testing methods for the most potential phantoms.

Requirement	Property	Testing methods
5	F/W-ratio	Quantitative testing: With the help of DRS. Does the phantom show homogeneity, consistency and accuracy with regard to the F/W-ratio? Furthermore, is there a significant difference in F/W-ratio between the healthy and tumour phantom?
6 & 7	Mechanical properties	Quantitative testing: With the help of a compression test. Are the mechanical properties realistic and is there a minimal difference in mechanical properties between the healthy and tumour phantom?
9	Electrically conductive properties	Qualitative testing: With the help of electrosurgical testing: Are the thermal tissue effects realistic?
10	Thermo tolerance properties	Qualitative testing: With the help of electrosurgical testing: Are the thermal tissue effects realistic?

Mechanical tests – Chapter 11

In chapter 9, phantoms were produced that had the potential to meet the mechanical requirements (6 & 7). To make sure these phantoms actually meet these requirements, quantitative tests will be performed. Hence, chapter 11 quantitatively tests the most potential phantom on its mechanical properties, by doing compression tests.

DRS test – Chapter 12

In chapter 9, phantoms were produced that potentially meet the F/W-ratio requirement (5). In order to make sure these phantoms actually meet this requirement; quantitative tests will be performed. Hence, chapter 12 quantitatively tests the most potential phantoms on its F/W-ratio, by doing DRS tests.

Electrosurgical tests – Chapter 13

In case these phantoms meet the F/W-ratio, visual- and mechanical property requirements, the electrical conductivity- and thermo tolerance properties of these phantoms will be tested. Since tissue effects in electrosurgery are directly related to the electrical conductivity and thermo tolerance properties of a specific material, qualitative tests will be performed by looking at the phantom tissue effects with electrosurgery.

11. Compression Tests

In order to meet the mechanical requirements, the agar and gelatin phantoms should be mechanically realistic and should have a minimal difference in mechanical properties between the healthy and tumour phantom (req. 6 & 7). Hence, in this study, the mechanical properties of the most potential agar and gelatin phantoms will be tested and compared to studies that measured Young's Moduli of real breast tissue, agar and gelatin phantoms by doing compression tests. Literature shows that Young's modulus greatly depends on the used pre-strain compression and strain-rate, namely how higher the pre-strain compression or strain rate, how higher the measured Young's Modulus^{87,119}. Hence, in order to sufficiently compare the acquired results to literature, I strive to use the same pre-strain compression and strain-rate.

11.2 Studies to compare

The studies of Matsumura et al. and Umemoto et al. determined Young's Modulus of women breasts ex vivo (table 8). They showed consistent results with the same test setup, namely a pre-strain compression of 0% and a low strain rate of 1 mm/min. Similarly, to Matsumura et al. and Umemoto et al., Chen et al. measured Young's modulus of agar and gelatin phantoms with a similar low strain-rate of 6mm/min and zero pre-strain compression. Hence, I strived to use the same pre-strain compression and strain rate to sufficiently compare my results to these studies.

11.3 Materials and methods

Equipment

The equipment used in this study was all located at the Minimally Invasive Surgery and Interventional Techniques (MISIT) lab at 3mE. A uniaxial compression test was used to measure the Young's Modulus of the most potential phantoms. A linear stage was used PRO-115 (Aerotech, USA/UK) to exert force on the phantoms via a square object with a surface area of 1600 mm². Between the square surface and the linear stage, a 22N Force Sensor, LSB200 (FUTEK, USA) was mounted to measure the force.

Phantoms

The most potential agar and gelatin phantoms were made according to the production methods stated in table 22. Two samples per phantom type were made. All samples had a thickness of 18 mm and a square surface of 1444mm², which is smaller than the compression surface, and therefore accounts for geometrical changes as the samples are compressed. Figure 24 shows a picture of each phantom type.

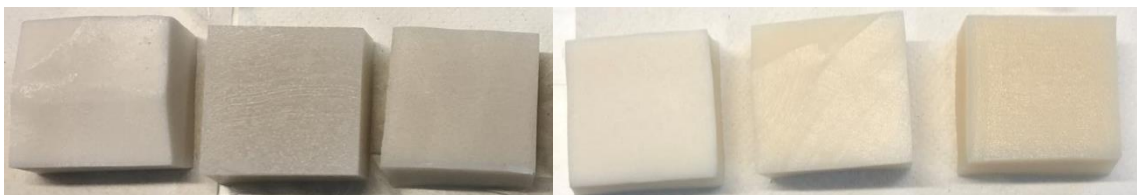


Figure 24: Sample of each phantom type, from left to right: 50F/50W/5%agar, 20F/80W/3%agar, 20F/80W/4%agar, 60F/40W/30%gelatin, 20F/80W/20%gelatin, 20F/80W/25%gelatin.

Setup and methods

A zero-pre-strain compression and a low strain rate of 6mm/min were used. Manickam et al. stated that agar has a brittle nature and has a yield point that could be reached above 15% strain. Hence, to enable several measurements per agar sample, a maximum strain of around 15% was applied¹²³. With regard to the gelatin samples, similarly to Matsumura et al. and Umemoto et al., a maximum strain of 30% was applied. On each

sample, two measurements were performed resulting in a total of 4 measurements per phantom type. All tests were carried out at room temperature. Figure 25 shows the experiment setup.

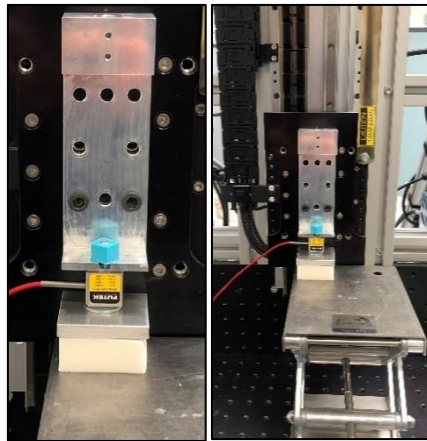


Figure 25: Experiment setup with linear stage, force sensor and sample.

Data Analysis

The raw data from these tests consisted of a measured output voltage and position of the linear stage. By calibrating the force sensor, the measured output voltage was converted to a measured force. The position and measured force were used to calculate the stress and strain from these phantoms. To eliminate the effect of noise, a moving average was used from which subsequently, a stress-strain curve with a clear line was derived. To compare the phantoms to literature studies, the Young's Modulus was derived from the slope of the stress-strain curve using Excel.

11.4 Results

The average stress-strain response of the agar and gelatin phantoms and the derived Young's Moduli are respectively given in figure 26, 27 and table 30.

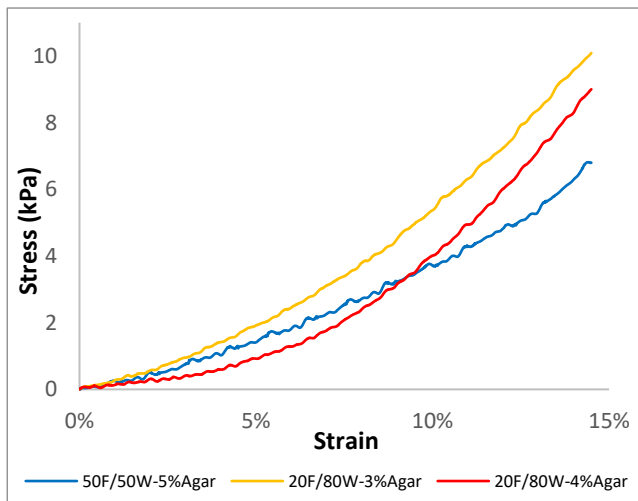


Figure 26: Average stress-strain response of agar phantoms.

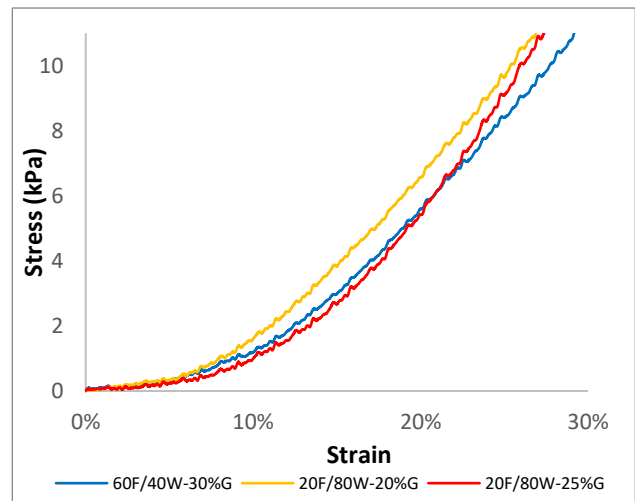


Figure 27: Average stress-strain response of gelatin phantoms.

General

Literature shows that an increase in agar or gelatin concentration increases the stiffness^{123,119}. However, as can be seen in table 30, figure 26 and figure 27, for low stress and strains the results are not always in line with literature, whereas for high stress and strains (marked in green), it is clear that a higher material

concentration results in a higher stiffness. The reason for that is that the measurements at low stress and strains are more susceptible to shape irregularities than measurements performed at high stress and strains. Thus, since the produced samples were not perfectly identical in shape, the results for low stress and strains are less reliable than the results for high stress and strains.

Table 30: Young's Moduli of relevant studies and produced agar and gelatine phantoms. Phantoms marked in orange are mechanically realistic and have a sufficiently small difference in mechanical properties.

Young's Modulus (kPa) and SD					
Studies	Phantom- or tissue type	Strain rate:	Slope 1 – 1.2 stress (kPa)	Slope <20% strain	
<u>Agar & Gelatin</u> Chen et al. ¹¹⁹ (2016) Data derived from fig. 2	Agar 1% w/w	6mm/min	-	80	
	Agar 2% w/w		-	450	
	Gelatin 20% w/w		-	44	
	Gelatin 24% w/w		-	60	
<u>Breast tissue</u> Matsumura et al. ⁹⁴ (2009) (zero pre-strain)	Normal fat tissue	1mm/min	17.3 ± 4.8	-	
	Normal glandular tissue		15.4 ± 3.9	-	
	DCIS		15.6 ± 2.0	-	
	IDC		27.0 ± 9.2	-	
<u>Breast tissue</u> Umemoto et al. ⁹⁵ (2014) (zero pre-strain)	Normal fat tissue	1mm/min	19.08 ± 4.99	-	
	Normal glandular tissue		16.99 ± 4.92	-	
	DCIS		16.15 ± 4.24	-	
	IDC		30.5 ± 11.46	-	
Results	Phantom type	Strain rate:	Slope 1 – 1.2 stress (kPa)	Slope 14 - 15% strain	Slope 19 - 20% strain
<u>Agar</u>	50F/50W+5% agar by weight of water	6mm/min	38 ± 2	90 ± 19	-
	20F/80W+3% agar by weight of water		41 ± 5	100 ± 26	-
	20F/80W+4% agar by weight of water		51 ± 3	138 ± 27	-
<u>Gelatin</u>	60F/40W+30% gelatin by weight of water		23 ± 8	36 ± 15	56 ± 10
	20F/80W+20% gelatin by weight of water		30 ± 12	45 ± 9	58 ± 5
	20F/80W+25% gelatin by weight of water		22 ± 5	30 ± 5	64 ± 5

Comparing the phantoms with gelatin and agar studies - Chen et al.

The acquired Young's Moduli were first compared to the study of Chen et al., who measured the Young's Moduli of pure gelatin and agar phantoms at a similar strain rate of 6mm/min. However, they did not clearly define at what strain range exactly, namely somewhere under 20%. Therefore, the Young's Moduli of the gelatin phantoms were measured for two strain ranges under 20%, namely between 19-20% and 14-15%, to see whether the strain range makes a big difference. The results show that, compared to the 14-15% strain range, the 19-20% strain range shows a significant increase in Young's Moduli, ranging from 50 to 100%. Nevertheless, for both strain ranges, the Young's Moduli of the gelatin phantoms are very similar to the gelatin phantoms tested by Chen et al.

Since the maximum applied strain on the agar phantoms was 15%, the Young's Moduli were measured between the strain range of 14-15%. The results show the measured Young's Moduli of the agar phantoms are somewhat lower than reported by Chen et al. This is because the phantoms are mixed with a decent amount of lard which has a lower stiffness than agar. Furthermore, the used strain range of 14-15% might be a little low, resulting in a suboptimal comparison of Young's Moduli. Nevertheless, even with these limitations, the Young's Moduli of the agar phantoms are sufficiently similar to those in the study of Chen et al. ¹¹⁹.

Comparing the phantoms with breast tissue studies - Matsumura et al. and Umemoto et al.

The phantoms were compared to the studies of Matsumura et al. and Umemoto et al., who used zero-strain compression, -a strain rate of 1mm/min and measured the Young's Moduli of breast tissue locally between 1 – 1.2 kPa. In this study, also zero-strain compression and a stress range of 1 – 1.2 kPa was used. However, due to equipment limitations, the phantoms were compressed over the whole surface and a strain rate of 6mm/min was used, which according to Chen et al. leads to an increase in the measured Young's Moduli.

Nevertheless, even with these limitations, both agar and gelatin phantoms show promising results, namely both have Young's Moduli similar to breast tissue, with the gelatin phantoms being the most similar^{119,124,95}.

Comparing the most potential phantoms

As can be seen in table 30, for different F/W-ratios, the produced agar and gelatin phantoms, have very similar mechanical properties, which is in line with the qualitative mechanical results of chapter 9. The two agar phantoms with the most similar Young's Moduli are the healthy- and tumour phantom made of 50F/50W/5%agar and 20F/80W/3%agar. The two gelatin phantoms with the most similar Young's Moduli are the healthy- and tumour phantom made of 40F/60W/30%gelatin- and 20F/80W/20%gelatin (see the boxed marked in orange).

11.5 Conclusion & Discussion

In this chapter, the mechanical properties of the most potential agar and gelatin phantoms were tested and compared to studies that measured the Young's Modulus of real breast tissue. Both the produced agar and gelatin phantoms have good mechanical properties. They show Young's Moduli in line with agar and gelatin studies and are sufficiently similar to breast tissue, with the gelatin phantoms being the most similar to breast tissue. Furthermore, for both agar and gelatin, a sufficiently small difference in mechanical properties was found between healthy and tumour phantoms. Namely between the 50F/50W/5%agar- and 20F/80W/3%agar phantom and between the 40F/60W/30%gelatin- and 20F/80W/20%gelatin phantom.

However, these results are solely based on two samples and a total of four measurements per phantom type. Furthermore, when comparing them to literature, slightly different strain rates and strain ranges were used. Thereby, Matsumura et al. and Umemoto et al. compressed their breast samples locally, whereas I compressed the samples over the whole surface. Despite these limitations, the results are promising enough, since the mechanical requirements, do not require high mechanical accuracy. Therefore, both phantom types meet requirements 6 and 7.

12. DRS Tests

In this chapter, the optical properties and subsequently the F/W-ratio of the most potential gelatin and agar phantoms will be acquired by doing DRS measurements. The optical homogeneity, accuracy and consistency of each phantom type will be tested and evaluated. Furthermore, for both the agar and gelatin phantoms, a statistical analysis will be performed, to see whether they meet requirement 5, namely whether there is a significant difference in F/W-ratio between the healthy- (highest F/W-ratio) and tumour (lowest F/W-ratio) phantom.

12.1 Materials and methods

Equipment

An optical system, which consists of a spectroscopic system and a fibre-optic-probe, was used to obtain DRS spectra of the most potential phantoms (figure 28). A white tungsten broadband light (Avantes, Apeldoorn, the Netherlands) was emitted by the spectroscopic system, through the illuminating fibre of the probe and onto the measured phantom. Within the phantom, the light undergoes multiple scattering and absorption and is diffusely reflected back onto the collecting fibres of the probe. The penetration depth of the light, depends on the absorption and reduced scattering coefficient of the phantom and is approximately half the distance between the illuminating- and collecting fibres ⁷². The fibre distance between the illuminating fibre and collecting fibres (VIS & NIR) was 1.8 mm, hence the penetration depth was approximately 0.9mm. The collecting fibres transmit the light to the fibre splitter which divides the light into two wavelength components, namely the visual- and the NIR range. The spectroscopic system consists of two spectrometers that process the light in the visual-(400-1000 nm, Mayapro 2000, Ocean Optics, Dunedin, USA) and the NIR range (900-1650 nm, NIRQUEST 512, Ocean Optics, Dunedin, USA). The whole system was controlled by a custom-made, Labview Software user interface (National Instruments, Austin, Texas, USA). With the help of the PNSas software, which is a program developed by Philips, the measured spectra were fit and the optical characteristics were derived ¹¹.

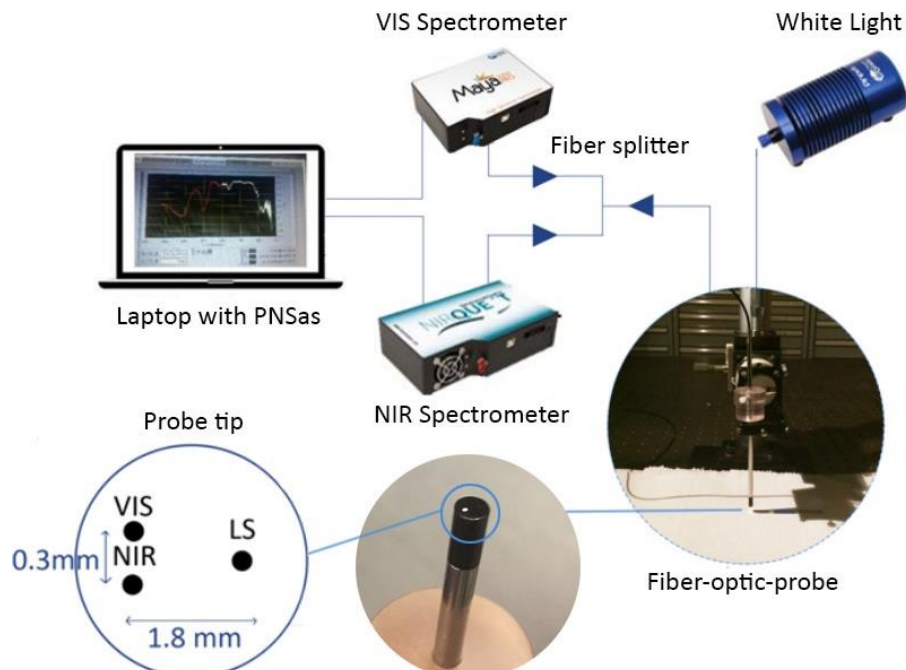


Figure 28: Overview of optical system ¹¹.

Phantom measurements

The most potential agar and gelatin phantoms were made according to the production methods stated in table 22, namely the 60F/40W-30%gelatin, 20F/80W-20%gelatin, 50F/50W-5%agar and 20F/80W-3%agar phantoms. DRS measurements were performed while the probe was in full contact with the phantom (figure 29). All measurements were performed at room temperature. For each measurement an integration time of 0.5 seconds was used. Per phantom type, 3 samples were created, and each sample was measured at five different measurements locations. On each measurement location three DRS measurements were performed, amounting up to a total of 15 measurements per sample and 45 measurements per phantom type (fig. 30).

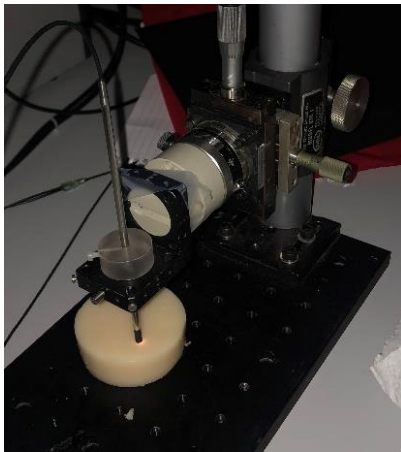


Figure 29: Measurements in full contact between the probe and sample.



Figure 30: 15 DRS measurements spread over 5 measurements locations.

Data analysis

The measurements were analysed by using PNSas software, which is a program based on Farrell's model, to fit and stitch the measured spectra together and translate the measured spectra into optical parameter estimates. Farrell et al.'s model is based on the diffusion theory, which assumes scattering events are isotropic and are big compared to the absorption events ($\mu'_s \gg \mu_a$). Furthermore, the mean free path length is small compared to the source-detector distance, so that the light diffuses before it reaches the detector. In prior publications, this model has been discussed in detail, including a validation of the performance ^{31,125,126,127}.

Spectral Shape

The fitted spectra have a range of 400 to 1600 nm, with a spectral resolution of 1 nm. The spectra of the different phantoms were compared to each other by looking at the signal shape. Figure 31 gives the absorption spectra of fat and water between 900 and 1600nm. The higher the absorption coefficient, the more light is absorbed. Since the phantoms contain mainly fat and water, it is expected to find valleys in the measured DRS spectra, at wavelengths where the fat and water chromophores have high absorption coefficients. Figure 31 shows that the absorption peaks for fat are 930, 1042, 1211, 1393, and 1414 nm and for water are 977, 1192 and 1453 nm ^{32, 126,127}.

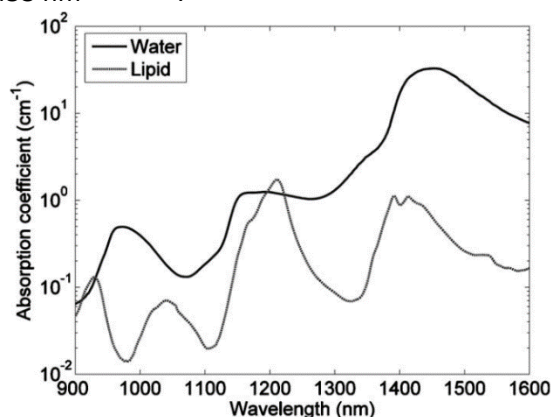


Figure 31: The absorption coefficients of fat (dotted line) and water (solid line) between 900 and 1600 nm ³⁶.

Nachabé et al. noticed that both fat and water have an absorption peak around 1200-nm, but that the widths of these peaks are different, namely the lipid peak is much narrower than the water peak. Hence, in line with Nachabé's findings, it is expected to find narrow valleys in the vicinity of 1200 nm for high F/W-ratio phantoms¹²⁷.

Optical Parameters

The known absorption- and scattering coefficients present in the phantoms, were used by the PNSas software, to translate the spectra into relevant parameters. These parameters included the fat fraction [$Fat/(Fat+Water)$], the total volume of fat and water ($Fat+Water$) and scattering media. Scattering media included the reduced scattering amplitude at 800 nm (s_{800}), the Mie slope (b) and the Mie-to-Rayleigh fraction of scattering (f_{mie}). Confidence intervals of each parameter were calculated to determine the significance of the fitted values⁴.

From these optical parameters, the fat percentage was derived by multiplying the fat fraction with the total volume of fat and water. Subsequently, the water percentage was derived by subtracting the fat fraction from the total volume of fat and water. Thereafter, the F/W-ratio was calculated by dividing the fat by the water concentration. In this way, any over-estimation of the individual parameters due to being at the boundary of the diffusion approximation was minimized⁴.

The reduced scattering coefficient (μ'_s) can be derived from the scattering amplitude (s_{800}), Mie-slope (b) and Mie-to-Rayleigh fraction with formula 6, where wavelength λ is normalized by a reference wavelength λ_0 at 800 nm. As can be seen, the reduced scattering coefficient increases with an increase in the scattering amplitude and a decrease in Mie slope³¹.

$$\mu'_s(\lambda) = s_{800} \left[f_{mie} \left(\frac{\lambda}{\lambda_0} \right)^{-b} + (1 - f_{mie}) \left(\frac{\lambda}{\lambda_0} \right)^{-4} \right] \quad (6)$$

The scattering amplitude and Mie slope are respectively a measure for the quantity and size of scatterers. How higher the scattering amplitude and -Mie slope, how higher the number of scatterers and smaller the average scattering particles are. With regard to the Mie-to-Rayleigh fraction, Mie scattering is caused by particles that are of the same size or bigger than the wavelength of incident radiation, whereas Rayleigh scattering occurs when the particles are much smaller than the wavelength of incident radiation^{31,126}.

To test the parameter accuracy, consistency and homogeneity of each phantom, the following was done; the accuracy per phantom type was tested by comparing its measured- to its reference values, the consistency was tested by looking at the inter-sample variations and the homogeneity by looking at the intra-sample variations.

Statistics

For both agar and gelatin phantoms, an independent one-tailed two-sampled t-test was performed to see whether the phantoms with a high F/W-ratio, had a significant higher F/W-ratio than the phantoms with a low F/W-ratio. It was assumed that the measured F/W-ratios were normally distributed. H_0 states the highest and lowest F/W-ratio are equal. The significance level is $\alpha = 0.05$, hence H_0 can be rejected if $p < 0.05$. In case $p = 0.05$, we wrongfully reject H_0 in 5% of the cases. With regard to the scattering media, an independent two-tailed two-sampled t-test was performed, to see whether there was a significant difference between the highest and lowest F/W-ratio phantom types. It was assumed that the measured scattering media were normally distributed. H_0 states the scattering media are equal and the significance level is $\alpha = 0.05$. Hence, H_0 can be rejected if $p < 0.05$. In case $p = 0.05$, we wrongfully reject H_0 in 5% of the cases.

12.2 Agar and gelatin influence

This sub-paragraph discusses the expected influence of gelatin and agar on the fat and water peaks in the NIR region. Cook et al. determined the absorption of gelatin phantoms between 400 to 1300nm and concluded that gelatin solely increases the optical absorption between 400 and 950 nm, however does not have any influence on the fat and water peaks between 900 and 1300 nm (see figure 32) ¹²⁸. With regard to agar, no studies were found that determined the absorption properties in the NIR region. Nevertheless, Quarto et al. compared the absorption of water/lipid/agar phantoms, to pure water/lipid-based phantoms and concluded that agar does not have any influence on the fat and water peaks of 930 and 970 nm (see figure 33) ¹⁰³. Additionally, Ohmae et al. and Bush et al. both developed water/lipid/agar phantoms and recovered F/W-ratios almost identical to the theoretical value ^{111, 14}. Finally, Dabbagh et al. and Cubeddu et al. both found that agar-based phantoms have negligible absorption and can therefore be very well used for optical studies ^{129,130}. Based on these studies, the recovered F/W-ratios of the most-potential phantoms are expected to be very close to the theoretical value.

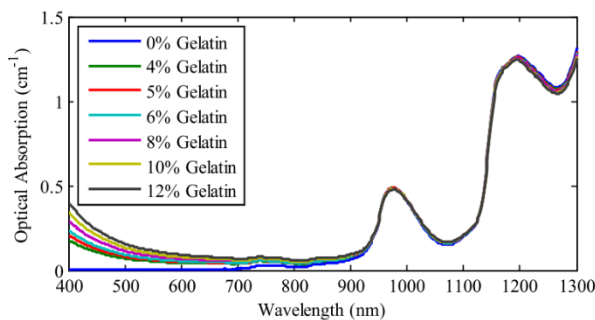


Figure 32: Optical absorption spectra of gelatin phantoms with different concentrations of gelatin. Spectral range of 400 to 1300 nm ¹²⁸.

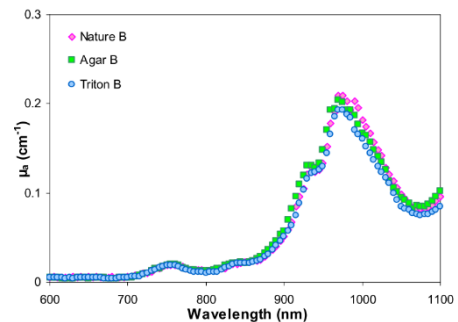


Figure 33: Optical absorption spectrum of 50F/50W phantoms: without additive "Nature B", with 1% agar weight by water "Agar B" and with 0.3% TritonX-100 weight by fat "Triton B" ¹⁰³.

12.3 Results

Spectral shape

Figure 34 and 35 show the normalized average spectra of the most potential gelatin and agar phantoms. Nachabé et al. developed water/lipid-based phantoms and acquired diffuse optical spectra of phantoms with varying F/W-ratios ¹²⁷. In line with Nachabé's results, the most potential phantoms with a big F/W-ratio, have a sharp valley at 1211 nm and a small valley at 930 nm, which is a result of high fat absorption. Furthermore, the most potential phantoms with a small F/W-ratio, have a small valley at 970 nm and an overall low DRS intensity above 1400 nm, which is due to high water absorption.

M. Adank found an easier way to discern F/W-ratios with the help of DRS spectra. She concluded that the DRS intensity between 1200 and 1400 nm, represents the F/W-ratio the best. An increase in this range is accompanied with an increase in F/W-ratio ^{1,7}. As expected, and in line with M. Adank's findings, both figures show that the phantoms with a high F/W-ratio, have a higher DRS intensity between 1200 and 1400 nm, than the phantoms with a low F/W-ratio.

However, figure 34 and 35 show it is clear that these spectral characteristics are much more obvious with the gelatin phantoms than with the agar phantoms. Obviously, the 50F/50W-5%agar phantom has a lower F/W-ratio than the 60F/40W-30%gelatin phantom. However, not that much smaller, therefore it was expected that the spectral differences between the 50F/50W-5%agar and 20F/80W-3%agar phantom, would have been bigger. Perhaps the used agar influenced the absorption peaks of fat and water.

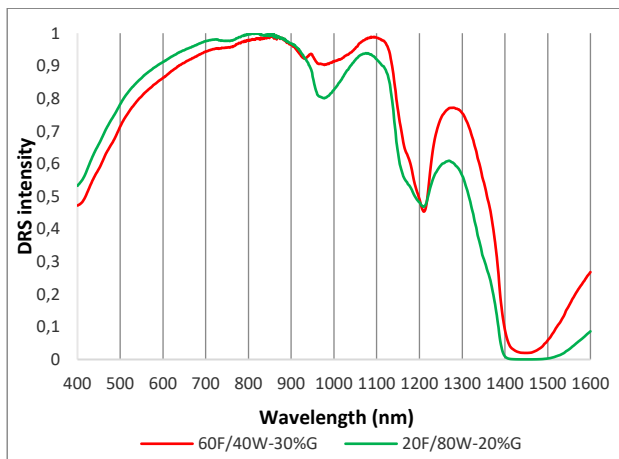


Figure 34: Average DRS spectrum of most potential gelatin phantoms

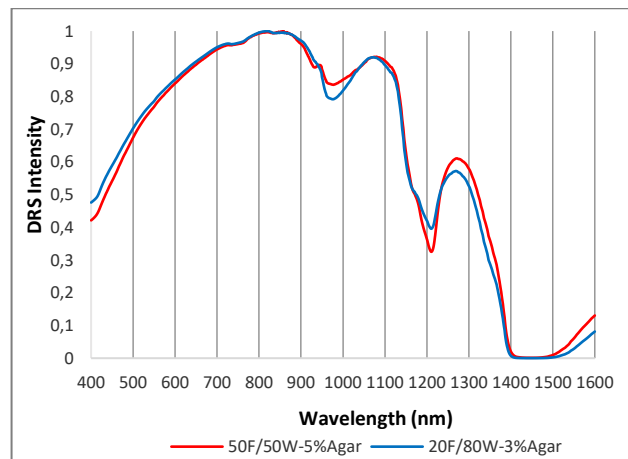


Figure 35: Average DRS spectrum of most potential agar phantoms

Optical Parameters

In order to determine the significance of the fitted values, confidence intervals for each parameter were calculated by the PNSas software and given in Appendix A. All confidence intervals are very small; hence the estimated fitted parameter values are reliable and can therefore be used.

F/W-ratio

In table 31, the average estimated fat and water parameters and its standard deviations are given. With standard deviations smaller than 15% of the average value, both gelatin and agar show great intra-sample homogeneity and within a phantom type, great inter-sample consistency. However, both gelatin and agar show inaccurate results concerning the estimations of the fat and water concentration.

With the gelatin phantoms, the water concentrations were slightly underestimated, namely with 13.1% (26.9% - 40%) for the 60F/40W phantom and 9.8% (70.2% - 80%) for the 20F/80W phantom. This subsequently led to an overestimation of the F/W-ratio, and an underestimation of the total chromophore concentration.

On the other hand, with the agar phantoms, the fat concentrations were significantly overestimated with 37.6% (87.6% - 50%) for the 50F/50W phantom and 27% (47% - 20%) for the 20F/80W phantom. This led to a significant underestimation of the F/W-ratio and a significant overestimation of the total chromophore concentration.

Figure 36 shows the average DRS spectra of the gelatin and agar phantoms with the same F/W-ratio. As can be seen, the agar phantom has a deeper valley at the fat absorption peak (1211 nm) than the gelatin phantom. Hence, agar might have influenced the fat absorption peak at 1211 nm, which might have led to the overestimation of fat.

The agar results are somewhat unexpected since literature shows agar does not have any influence on F/W-ratio estimates of water/lipid-based phantoms^{103,111,14}. However, solely Quarto et al. and Cubeddu et al. specified where they got their agar from, namely expensive purified agar from Sigma Aldrich, whereas I used cheap impurified agar from the local food store, which might be the cause for the unexpected results.

Nevertheless, table 32 shows the obtained F/W-ratios, namely 2.0 and 0.35 for the gelatin- and 1.61 and 0.62 for the agar phantoms, are still realistic since they fall within the range of F/W-ratios (0.22 – 11.25) reported by breast studies in table 32. The highest F/W-ratio simulates healthy breast tissue whereas the lowest F/W-ratio simulates tumour breast tissue.

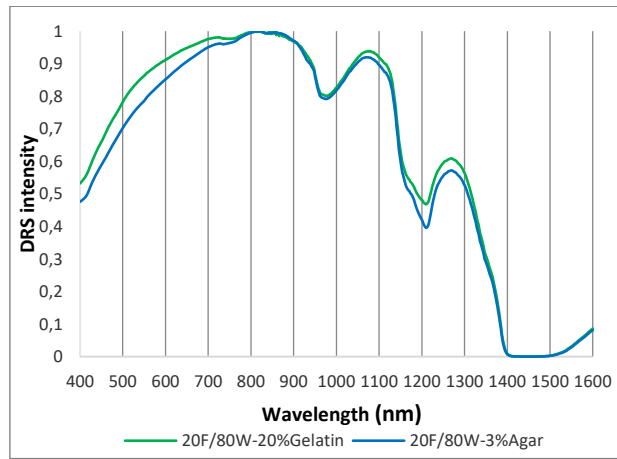


Figure 36: Average DRS spectrum of 20F/80W gelatin and agar phantom.

Table 31: Average estimated parameters with its standard deviations (SD)

Phantom type	Sample	Fat %	Water %	F/W-ratio	s800	b	fmie
60F/40W + 30%Gelatin	Reference value	60%	40%	1.5	-	-	-
	Intra-sample average \pm SD (Homogeneity)	1 57.3 \pm 2.9	23.8 \pm 0.9	2.40 \pm 0.07	18.1 \pm 2.2	0.47 \pm 0.04	0.96 \pm 0.01
		2 50.5 \pm 3.3	28.3 \pm 0.9	1.78 \pm 0.07	22.7 \pm 2.1	0.52 \pm 0.10	0.97 \pm 0.02
		3 51.9 \pm 2.2	28.6 \pm 1.1	1.82 \pm 0.02	18.9 \pm 1.2	0.34 \pm 0.06	0.95 \pm 0.01
	Inter-sample average \pm SD (Consistency)	53.2 \pm 4.1	26.9 \pm 2.4	2.00 \pm 0.29	19.9 \pm 2.8	0.44 \pm 0.10	0.96 \pm 0.01
Δ with reference value (Accuracy)		-6.8%	-13.1%	0.5	-	-	-
20F/80W + 20%Gelatin	Reference value	20%	80%	0.25	-	-	-
	Intra-sample average \pm SD (Homogeneity)	1 24.8 \pm 3.1	70.1 \pm 7.6	0.35 \pm 0.02	14.4 \pm 1.5	0.65 \pm 0.12	0.96 \pm 0.02
		2 24.9 \pm 2.3	74.0 \pm 4.0	0.34 \pm 0.02	13.5 \pm 0.6	0.55 \pm 0.08	0.94 \pm 0.01
		3 21.9 \pm 1.3	66.2 \pm 2.1	0.33 \pm 0.02	15.1 \pm 1.2	0.44 \pm 0.14	0.87 \pm 0.01
	Inter-sample average \pm SD (Consistency)	23.9 \pm 2.7	70.2 \pm 6.1	0.34 \pm 0.02	14.6 \pm 1.6	0.56 \pm 0.14	0.94 \pm 0.02
Δ with reference value (Accuracy)		3.9%	-9.8%	0.09	-	-	-
50F/50W + 5%Agar	Reference value	50%	50%	1.0	-	-	-
	Intra-sample average \pm SD (Homogeneity)	1 85.4 \pm 2.3	52.9 \pm 0.8	1.61 \pm 0.03	15.5 \pm 0.2	1.42 \pm 0.02	1.00 \pm 0.00
		2 86.5 \pm 2.4	54.1 \pm 2.6	1.60 \pm 0.06	15.7 \pm 0.2	1.42 \pm 0.03	1.00 \pm 0.00
		3 91.0 \pm 3.7	56.9 \pm 2.0	1.60 \pm 0.07	16.0 \pm 0.4	1.45 \pm 0.04	0.99 \pm 0.01
	Inter-sample average \pm SD (Consistency)	87.6 \pm 2.8	54.6 \pm 2.6	1.61 \pm 0.05	15.8 \pm 0.3	1.43 \pm 0.03	1.00 \pm 0.01
Δ with reference value (Accuracy)		37.6%	4.6%	0.61	-	-	-
20F/80W + 3%Agar	Reference value	20%	80%	0.25	-	-	-
	Intra-sample average \pm SD (Homogeneity)	1 44.6 \pm 3.3	81.0 \pm 4.0	0.55 \pm 0.06	15.2 \pm 0.2	1.42 \pm 0.03	1.00 \pm 0.00
		2 49.3 \pm 2.2	74.9 \pm 3.6	0.66 \pm 0.05	16.2 \pm 0.5	1.47 \pm 0.03	1.00 \pm 0.00
		3 47.2 \pm 2.7	72.8 \pm 5.7	0.65 \pm 0.06	16.1 \pm 0.4	1.40 \pm 0.02	0.98 \pm 0.02
	Inter-sample average \pm SD (Consistency)	47.0 \pm 3.4	76.3 \pm 5.7	0.62 \pm 0.08	15.8 \pm 0.6	1.43 \pm 0.04	0.99 \pm 0.01
Δ with reference value (Accuracy)		27.0%	-3.7%	0.37	-	-	-

Table 32: F/W-ratio of healthy and tumour tissue & F/W-ratios of most potential phantoms, table constructed based on references cited in this table and based on the conducted DRS tests.

Study	Healthy tissue			Tumour tissue			
	Lipid (%)	Water (%)	F/W-ratio	Lipid (%)	Water (%)	F/W-ratio	
	Mean	Mean	Mean	Mean	Mean	Mean	
De Boer et al. ⁵⁶ (2016) in & ex vivo	-	-	7.5	-	-	0.8	
Nachabé ⁷² (2012) – Ch. 9, ex vivo	90 (AP)	8 (AP)	11.25	15 (DCIS)	50 (DCIS)	0.3	
	12 (GL)	55 (GL)	0.22				
Blackmore et al. ⁶⁰ (2015)	65.1	19.66	3.31	-	-	-	
Cerussi et al. ⁶³ (2001)	48.65	27.7	1.76	-	-	-	
O'Sullivan et al. ⁶⁸ (2013)	69.7	21.4	3.26	-	-	-	
Intes ⁶² (2005)	62.4	28.9	2.16	-	40.8	-	
Leproux et al. ⁷³ (2016)	-	-	-	62.54	47.67	1.31	
Cerussi et al. ⁷⁴ (2006)	66.1	18.7	3.53	58.5	25.9	2.26	
Wang et al. ⁷⁵ (2010)	69	15	4.6	45	26	1.73	
Gelatin	Reference values	60	40	1.5	20	80	0.25
	Obtained DRS values	53.2	26.9	2.0	23.9	70.2	0.34
Agar	Reference values	50	50	1	20	80	0.25
	Obtained DRS values	87.6	54.6	1.61	47.0	76.3	0.62

Figure 37 and 38 display the boxplots of the obtained F/W-ratios of the gelatin and agar phantoms. In both cases the null-hypothesis is rejected, hence there is a significant difference in F/W-ratio between healthy and tumour phantom tissue. More specifically, the 60F/40W gelatin phantom has a significant higher F/W-ratio ($M = 2.00$, $SD = 0.29$) than the 20F/80W gelatin phantom ($M = 0.34$, $SD = 0.02$), $t(45) = 37.70$, $p = 2.0 \cdot 10^{-35}$, and the 50F/50W agar phantom has a significant higher F/W-ratio ($M = 1.61$, $SD = 0.05$) than the 20F/80W agar phantom ($M = 0.62$, $SD = 0.08$), $t(45) = 68.10$, $p = 7.3 \cdot 10^{-71}$.

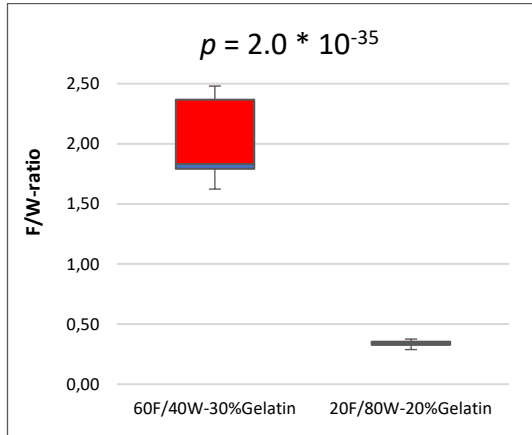


Figure 37: Boxplot of F/W-ratios of most potential gelatin phantoms.

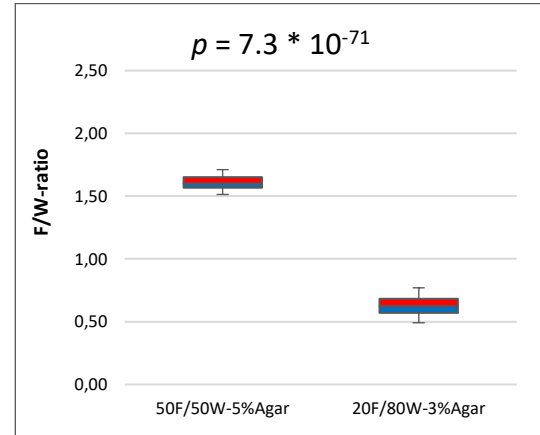


Figure 38: Boxplot of F/W-ratios of most potential agar phantoms.

Scattering Media

Both phantoms show scattering parameter values similar to that of breast tissue^{56,70,76,72}. Nachabé et al. developed water/lipid-based phantoms and acquired scattering media of phantoms with varying F/W-ratios. In line with Nachabé's findings, the gelatin phantom with a high F/W-ratio has a significantly higher scattering amplitude than the gelatin phantom with a low F/W-ratio, which is expected since lipid is the only scatterer in the phantom¹²⁷. Furthermore, the Mie-slope and Mie-to-Rayleigh fraction of the gelatin phantoms, significantly decrease and increase with a higher F/W-ratio. A rationale would be that the used fat particles are bigger than the gelatin particles, therefore decreasing the Mie-slope. Additionally, the gelatin particles are small enough to cause Rayleigh scattering, therefore increasing the Mie-to-Rayleigh fraction with an increase in F/W-ratio. However, no literature was found to substantiate these findings. Hence, further research is needed to find out what gelatine's in combination with lard's exact influence is on the scattering parameters. Nevertheless, according to formula 6, the overall reduced scattering coefficient of the gelatin phantom with a high F/W-ratio, is higher than of the gelatin phantom with a low F/W-ratio.

The agar phantoms on the other hand, show different results, namely no significant differences in scattering amplitude, Mie-slope and Mie-to-Rayleigh fraction when increasing the F/W-ratio. This could be because increasing the amount of fat-particles increases the scattering, whereas increasing the amount of agar concentration decreases the scattering^{127,130}. Hence, further research is needed to find out what agar's in combination with lard's exact influence is on the scattering parameters. The p -values concerning whether or not the phantoms significantly differ in scattering parameters, can be found in table 33.

Table 33: Average estimated parameters with its standard deviations (SD) and its p -value.

Parameter	20F/80W + 20%Gelatin	60F/40W + 30%Gelatin	20F/80W + 3%Agar	50F/50W + 5%Agar
s800	14.6 ± 1.6	19.9 ± 2.8	15.8 ± 0.6	15.8 ± 0.3
p value	5.4 * 10 ⁻¹⁷		0.48	
b	0.56 ± 0.14	0.44 ± 0.10	1.43 ± 0.04	1.43 ± 0.03
p value	2 * 10 ⁻⁵		0.66	
fmie	0.94 ± 0.02	0.96 ± 0.01	0.99 ± 0.01	1.00 ± 0.01
p value	4.7 * 10 ⁻⁶		0.62	

12.4 Conclusion & Discussion

The goal of this chapter was to see what the optical properties of the most potential gelatin and agar phantoms were and whether the healthy and tumour phantoms showed a significant difference in F/W-ratio. Both gelatin and agar emulsified lard and water sufficiently, showing great homogeneity and -consistency in the fat and water concentration. However, the accuracy was not optimal, the water concentration of the gelatin phantoms was slightly underestimated and the fat concentration of the agar phantoms was significantly overestimated. These inaccuracies were partially due to the estimation error of DRS and its analytical model ¹²⁷. However, agar also played a role in these inaccuracies, more specifically it presumably influenced the fat absorption peak at 1211 nm, which subsequently caused fat overestimation. Despite these inaccuracies, both the gelatin and agar phantoms still showed a significant difference in F/W-ratio between the healthy- and tumour phantom, therefore meeting requirement 5.

13. Electrosurgical Tests

Both gelatin and agar show promising results concerning the optical-, visual- and mechanical properties. In this chapter the electrical conductivity- and thermo tolerance properties of these phantoms will be tested. As explained in paragraph 1.1.3, the tissue effects as a result of electrosurgery are among other things related to the electrical conductivity and thermo tolerance properties of that specific material. Hence, qualitative tests will be performed by looking at the phantom tissue effects when conducting electrosurgery on it.

13.1 Material influence

In this sub-paragraph, the expected phantom tissue effects when applying electrosurgery on it, will be discussed by comparing the phantom material to the breast tissue properties. As earlier stated, the tissue effects are directly related to the electrical conductivity and thermo tolerance properties of that specific material. High electrical conductivity is accompanied by high heat production, whereas high thermo tolerance or resistance to heat, is accompanied by little thermal tissue effects for a given thermal dose (temperature and exposure time). Table 34 gives an overview of the electrical conductivity properties of breast tissue and the main phantom materials ²².

Table 34: Electrically conductive properties of human breasts and phantom materials.

Study	Material	T (°C)	Conductivity (S/m)									
			n.a. Hz	50 Hz	500 Hz	1 MHz	13.5 MHz	27 MHz	40 MHz	100 MHz	200 MHz	5 GHz
Tiang et al. ⁹⁸	Breast gland	-	-	-	-	-	-	-	-	-	0.1	3.0
	Breast tumour	-	-	-	-	-	-	-	-	-	0.15	5.0
	Breast fat	-	-	-	-	-	-	-	-	-	0.1	0.2
C. Gabriel ¹³¹	Breast fat	37	-	-	0.02	0.02	-	-	0.03	-	0.04	0.3
Halter et al. ¹³²	Breast tumour in vivo	37	-	-	0.05	-	-	-	-	-	-	4
	Breast tumour ex vivo	-	-	-	0.1	-	-	-	-	-	-	6
Suk et al. ¹³³	Porcine muscle	-	0.55 - 0.64	-	-	-	-	-	-	-	-	-
	Agar & gelatin	-	0.76	-	-	-	-	-	-	-	-	-
Marchal et al. ¹³⁴	Human tissue	37	-	-	-	-	0.40 - 0.60	-	-	-	-	-
	Gelatin 20% w/w	20	-	-	-	-	0.27	-	-	-	-	-
		50	-	-	-	-	-	0.47	-	-	-	-
Kandadai et al. ¹³⁵	Agar 1.5% w/w	22	-	-	0.08	-	-	-	-	-	-	-
		37	-	-	0.1	-	-	-	-	-	-	-
	Gelatin 0.6% w/w	22	-	-	0.13	-	-	-	-	-	-	-
Kato et al. ¹³⁶	Agar 4% w/w	23.5	-	-	-	0.2	0.2	-	0.2	-	-	-
Ishida et al. ¹³⁷	Agar 2% w/w	22	-	-	-	-	0.5	-	-	-	-	-
Yuan et al. ¹³⁸	95% Gelatin – 5% oil	37	-	-	-	-	-	-	-	0.84	-	-
Shirsat et al. ¹³⁹	Pork fat	20	-	0.04	-	-	-	-	-	-	-	-

Table 34 shows a big variety in the obtained conductivity values, which among other things is due to the different materials, measurement equipment, frequencies and temperatures used in the studies ¹³¹. Hence, the results of these studies are hard to compare due to the different experiment setups used. Nevertheless, in general gelatin and agar have a similar/slightly higher electrical conductivity than breast tissue, whereas pork fat has a similar low electrical conductivity as breast fat. Since the phantoms are composed of gelatin or agar in combination with lard, it is expected that the phantoms have similar electrical conductivity as breast tissue and therefore similar heat production with electrosurgery.

The amount of thermo tolerance, is directly related to the melting point, thermal conductivity and specific heat of a material. A material with a high thermo tolerance, has a high melting point or high resistance to high temperatures, a low thermal conductivity or little thermal spread, and finally, a low specific heat or low required thermal dose to reach the thermal equilibrium, therefore minimizing the height of the reached temperatures near the electrosurgical cut ^{22,140,141}.

Table 35 gives an overview of the thermo tolerance properties of breast tissue and the main phantom materials. Very similar results among various studies were found. Gelatin and agar have a similar specific heat as breast tissue and a slightly higher thermal conductivity than breast tissue, whereas pork fat has a similar thermal conductivity and specific heat as breast fat. Since the phantoms are composed of gelatin or agar in combination with lard, the expected thermal conductive and specific heat properties of the phantoms will be the same as breast tissue, and therefore will result in similar expected thermal tissue effects.

However, gelatine's and lard's melting points are way below that of where breast thermal damage occurs (50 °C), whereas agar's melting point is in the range of where breast thermal damage occurs (50-200 °C). Nevertheless, this should not make a difference since with electrosurgery temperatures can rise up to 400 °C, which is also much higher than the temperatures where breast and agar thermal damage occurs. Hence, it is expected that with electrosurgery, both the gelatin and agar phantoms show thermal tissue effects similar to that of breast tissue.

Table 35: Thermo tolerance properties of human breasts and phantom materials.

Study	Material	T (°C)	Thermal conductivity (W/m K)	Specific heat (J/Kg K)	Tissue effects
Zuluaga et al. ¹⁴²	Breast gland	37 °C	0.48	3770	- 50°C after 6 minutes cell death
	Breast tumour		0.48	3852	- 60°C coagulation and desiccation
	Breast fat		0.21	2674	- 100°C cellular vaporization - 200°C carbonization
Study	Material	T (°C)	Thermal conductivity (W/m K)	Specific heat (J/Kg K)	Melting point
Krokida et al. ¹⁴³	Gelatin-water	25 °C	0.59	-	35 °C ¹⁴⁴
	Gelatin	25 °C	0.96	-	35 °C ¹⁴⁴
Yuan et al. ¹³⁸	95% Gelatin – 5% oil	37 °C	0.49	3710	-
Krokida et al. ¹⁴³	Agar-water	30 °C	0.62	-	85 °C ¹⁴⁵
Holt et al. ¹⁴⁶	Agar	21 °C	0.65	3300	85 °C ¹⁴⁵
Huang et al. ¹⁴⁷	Agar	-	0.59	3700	85 °C ¹⁴⁵
Will et al. ¹⁴⁸	Pork fat	-1.87 °C	0.21	-	-
ASHRAE ¹⁴⁹	Pork fat	0 °C > x	0.22	2170	-
Dabbagh et al. ¹²⁹	Fat	-	0.23	-	-
Krokida et al. ¹⁴³	Lard	25 °C	0.12	-	38°C ¹³

13.2 Materials and methods

Phantoms

The most potential gelatin and agar phantoms were tested, namely the 60F/40W-30%gelatin, 20F/80W-20%gelatin, 50F/50W-5%agar, 20F/80W-3%agar phantoms. One sample per phantom type was made according to the production methods stated in table 22. They had a 12 cm diameter and a thickness of approximately 18 mm. The phantom tissue effects were compared to the tissue effects of pork tissue instead of human tissue, since pork tissue was cheap and easy to obtain and does not have ethical restrictions for experiments, whereas human tissue does. Pork belly from the Albert Heijn was used and consisted of muscle (red) and adipose (white) tissue and had a thickness of approximately 10 mm (fig. 39).



Figure 39: Left: Gelatin phantoms, Middle: Agar phantoms, Right: Pork belly.

Equipment

The electrosurgical circuit was composed of a sample, electrosurgical generator (Force FX, Valleylab, Boulder, United States), a monopolar electrosurgical knife (Weide) and a dispersive pad (fig. 40). The current flows from the electrosurgical generator through the knife to the sample. The sample serves as the conductive element and acts as a resistor within this circuit. The resistance, converts the electrical energy into thermal energy, causing heat production and tissue destruction. The current leaves the sample at the dispersive pad and returns to the electrosurgical generator.



Figure 40: Left: Electrosurgical generator, Middle: electrosurgical knife, Right: Dispersive pad ⁷.

Setup and methods

All samples were cut at room temperature. On each sample 30 seconds of pure cut, blend cut, and coagulation was performed, while the ESK was held slightly away from the sample. For all three waveforms, a power setting of 50 Watt was used, which is a commonly used setting for monopolar electro surgery ¹⁶. First, the pork samples were tested, followed by the gelatin and agar samples. The samples were compared to each other qualitatively, among other things by looking at the thermal spread and haptic feedback.

13.3 Results

Figure 41 illustrates a pork belly and phantom sample on the dispersive pad. The dispersive pad consisted of two parts, which had to be connected before it would enable current conduction. Since the phantoms were not perfectly flat, a wet tissue was needed to put the phantoms in full contact with the dispersive pad. Only then electrosurgery on the phantoms was possible.



Figure 41: Left: Pork belly on dispersive pad, Right: phantom tissue on dispersive pad.

Figure 42 displays the tissue effects of pork muscle and -fat for the three different waveforms. In line with literature, the most thermal spread occurred with coagulation, followed by blend and the least with the pure cutting mode ²⁰. Furthermore, there is a significant difference between the tissue effects on pork muscle and -fat tissue. The incisions on pork muscle are local whereas the incisions on pork fat are less delicate and wider, which corresponds to the findings of M. Adank ⁷. Finally, it seems like pork fat slightly melts, whereas pork muscle does not.

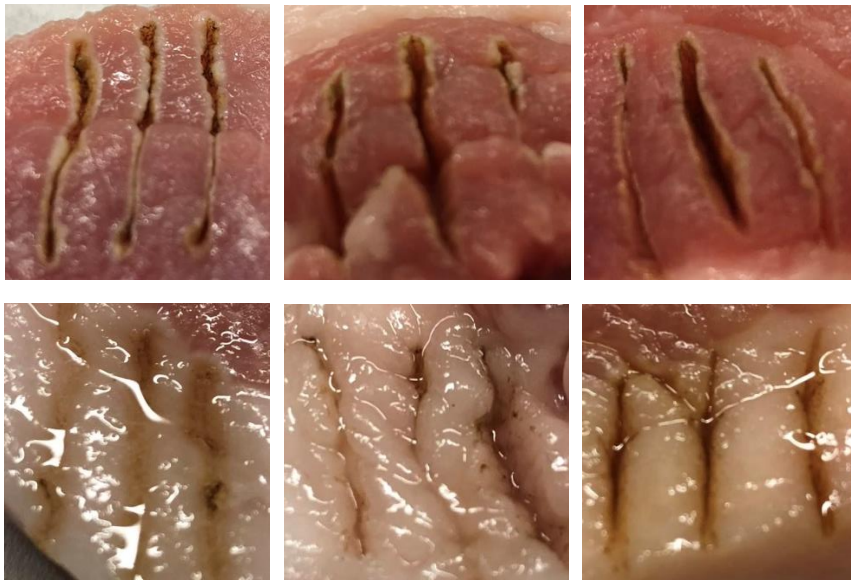


Figure 42: Upper row from left to right: coagulate, blend and cut pork muscle tissue. Bottom row form left to right: coagulate, blend and cut pork fat tissue.

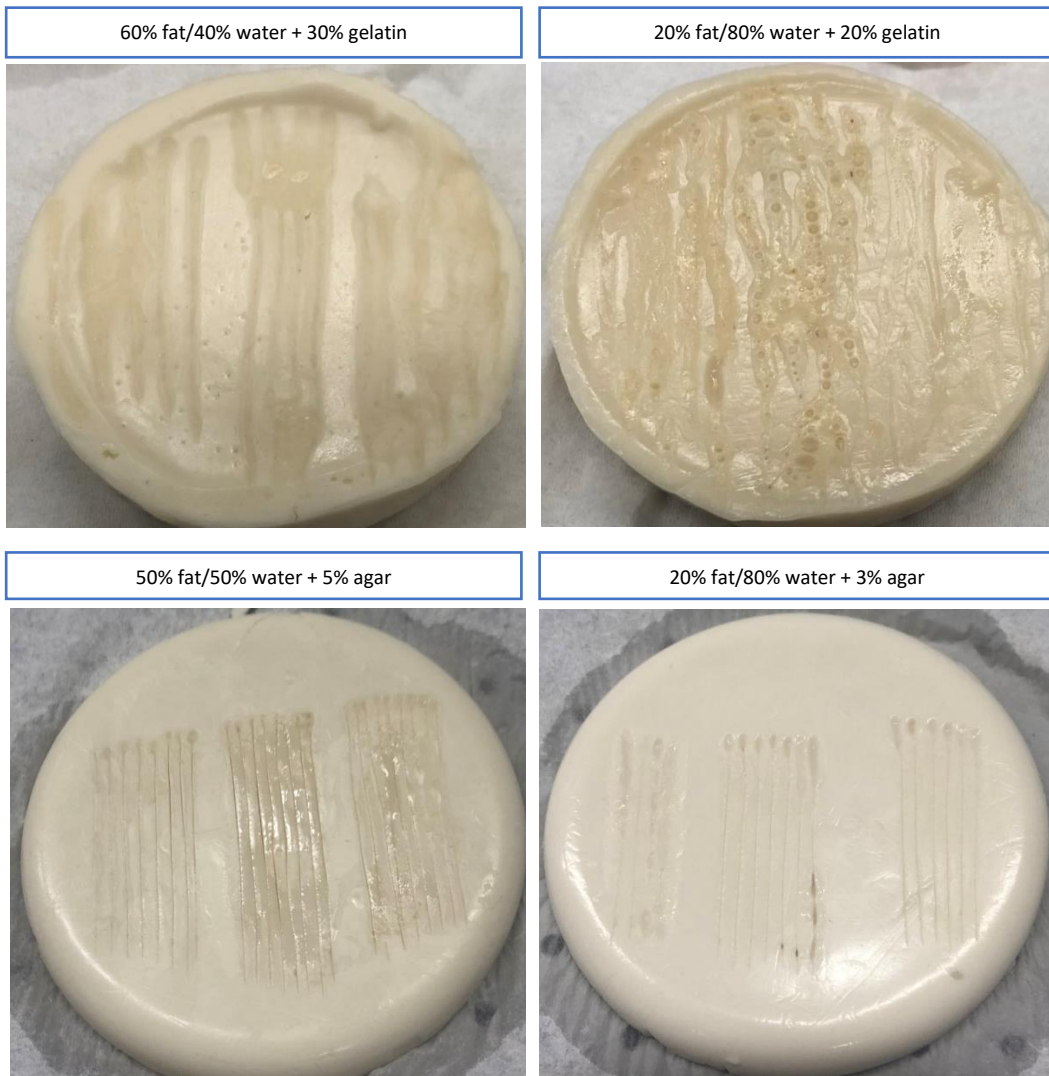


Figure 43: Upper row the most potential gelatin phantoms. Bottom row the most potential agar phantoms. From left to right, tissue effects as a result of coagulation, blend cut and pure cut.

Figure 43 displays the tissue effects of the most potential phantoms for the three different waveforms. In line with the mechanical property findings from chapter 10, all phantoms gave realistic haptic feedback, with the agar phantoms feeling slightly stiffer than the pork tissue and gelatin phantoms. Noteworthy, it was possible to cut into both phantoms without using current but solely pushing the ESK downwards, whereas it was not possible to cut with the ESK into pork belly without using current. Nevertheless, as earlier stated, the haptic feedback when using the ESK with current was realistic, which is solely relevant for meeting requirement 6.

With regard to the tissue effects, the gelatin phantoms showed widespread melting accompanied by bubbles and incisions that melted together after being cut, whereas the agar phantoms showed for all waveforms, local incisions similar to pork muscle tissue. Hence, solely the agar phantoms showed realistic tissue effects. Figure 44 displays the results of electrosurgical cutting on a pure agar and pure gelatin phantom showing similar results.

Figure 45 illustrates the thermal gradient of electrosurgery on human tissue¹⁵⁰. With this in mind and the fact that agar's and gelatine's thermal properties mostly differ in melting temperature, a rationale for the tissue effect differences would be that the temperature in the vicinity of the electrosurgical cut, mounted up above the melting temperature of the gelatin phantoms, but not above the melting temperature of the agar phantoms.



Figure 44: Left pure agar phantom with 5% of agar by weight of water. Right pure gelatin phantom with 20% gelatin by weight of water. From left to right tissue effects as a result of coagulation, blend cut and pure cut.

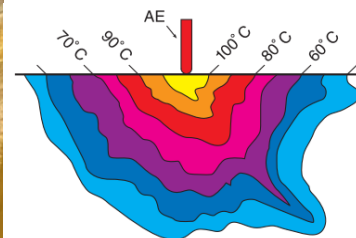


Figure 45: Thermal gradient of human tissue as a result of electrosurgery¹⁵⁰

In line with this rationale, studies suggest that due to agar's high and gelatine's low melting point, agar is and gelatin is not desirable for applications where high temperatures are achieved¹²⁹. Hence, apart from the bubbling, the tissue effect differences could among other things be explained by the differences in melting temperature.

13.4 Conclusion & Discussion

The electrosurgical tissue effects of the gelatin and agar phantoms were compared to that of pork tissue. The agar phantoms showed realistic tissue effects, namely local incisions without much thermal spread, whereas the gelatin phantoms showed unrealistic tissue effects, namely widespread melting accompanied by bubbles and incisions that melted together. The cause for this difference is probably due to the low melting point of pure gelatin (35 °C) and the high melting point of pure agar (85 °C). To make sure of this, further research should be done with regard to the exact melting temperatures and thermal distribution of the phantoms with electrosurgery. However, all in all the agar phantoms show realistic tissue effects, therefore meeting the electrically conductive- and thermo tolerance requirements (9 & 10), whereas the gelatin phantoms do not. For this thesis project, these qualitative results are promising enough to meet the concerning requirements. However, to determine the actual cause for the observed phantom tissue effects, not only on the melting point and thermal distribution, but also on the electrical conductivity and other thermo tolerance properties (specific heat and thermal conductivity) should be determined. Hence, for further research it is recommended to measure and quantify the aforementioned phantom properties, to find out what exactly caused the observed tissue effects.

14. Conclusion – Research Phase 2

In research phase 1, various F/W-ratios of water and lard, in combination with varying material concentrations of agar and gelatin were produced. In this research phase, the most potential agar and gelatin phantoms were extensively tested and evaluated with regard to all IMA requirements, namely the F/W-ratio-, mechanical-, electrically conductive- and thermo tolerance properties. The most potential gelatin phantoms that simulate healthy- and tumour breast tissue, were respectively the 40F/60W+30%gelatin- and the 20F/80W+20%gelatin phantom. The most potential agar phantoms that simulate healthy and tumour breast tissue, were respectively the 50F/50W+5%agar- and the 20F/80W+3%agar phantom. Table 36 gives an overview of how these phantoms are evaluated with regard to the IMA requirements and shows that the gelatin phantoms do not meet all IMA requirements, whereas the agar phantoms do. Therefore, in the next research phase we will continue to use the agar phantoms.

Table 36: Harris profile, assessing the most potential gelatin and agar phantoms with regard to the IMA requirements.

Requirements	Gelatin				Agar			
	--	-	+	++	--	-	+	++
5								
6								
7								
8								
9								
10								

Requirement 5: A significant difference in F/W-ratio that simulates tumour and healthy breast tissue content.

With regard to the fat and water concentration, both gelatin and agar emulsified lard and water sufficiently, with gelatin being the superior emulsifier. As a result, both materials enabled phantom production with various F/W-ratios. These phantoms showed great homogeneity and -consistency. However, the accuracy was not optimal, the water concentration of the gelatin phantoms was slightly underestimated and the fat concentration of the agar phantoms was significantly overestimated. These inaccuracies were partially due to the estimation error of DRS and its analytical model ¹²⁷. However, agar also played a role in these inaccuracies, more specifically it presumably influenced the fat absorption peak at 1211 nm, which subsequently caused fat overestimation. This is somewhat unexpected since literature showed agar does not have any influence on the fat estimates of water/lipid-based phantoms ^{103,111,14}. However, in contrast to literature, cheap impurified agar (Terrasana ¹¹³) from the local food store, instead of expensive purified agar from Sigma Aldrich was used, which most likely caused the differences in result ¹⁰³. However, due to the Corona virus, all testing facilities were closed, therefore no DRS tests and thus conclusions could be drawn with regard to the exact optical properties of the used agar and gelatin.

Nevertheless, for both phantoms the obtained F/W-ratios, namely 2.0 and 0.34 for the gelatin- and 1.61 and 0.62 for the agar phantoms, are still realistic since they fall within the range of F/W-ratios (0.22 – 11.25) reported by breast studies in table 32. The highest F/W-ratio simulates healthy breast tissue whereas the lowest F/W-ratio simulates tumour breast tissue. However, more importantly, both gelatin and agar phantoms still showed a significant difference in F/W-ratio between the healthy- and tumour phantoms. Hence, both the gelatin and agar phantoms meet requirement 5, which enables us to sufficiently assess DRS with its capability in discriminating healthy from malignant breast tissue.

Requirement 6: Similar mechanical properties as real breast tissue (at room temperature).

Requirement 7: Minimal mechanical differences between tumour and healthy tissue.

Both the gelatin and agar phantoms showed good mechanical properties. The measured Young's Moduli were sufficiently similar to breast tissue, with the gelatin phantoms being the most similar to breast tissue and the agar phantoms being slightly stiffer than breast tissue. Furthermore, both the gelatin and agar phantoms showed a sufficiently small difference in mechanical properties between the healthy- and tumour phantoms. However, these results are solely based on two samples- and a total of four measurements per phantom type. Furthermore, due to equipment limitations, a slightly different experiment setup was used than in literature. Nevertheless, in order to meet the mechanical requirements, the accuracy of mechanical properties does not have to be that high, therefore the results are promising enough. Hence, both the gelatin and agar phantoms meet requirement 6 and 7, thus respectively enable realistic haptic feedback when using the ESK and eliminate the possibility of using intraoperative palpation, so that solely DRS with its capability in discriminating healthy from malignant tissue can be tested.

Requirement 8: Minimal visual differences between tumour and healthy tissue.

In research phase 1, visual inspection showed both gelatin and agar phantoms had a sufficiently small difference in colour or visual properties between the healthy- and tumour phantoms. Hence, both agar and gelatin phantoms meet requirement 8 and therefore eliminate the possibility of using intraoperative visual inspection, so that solely DRS with its capability in discriminating healthy from malignant tissue can be tested.

Requirement 9: Similar electrically conductive properties as human breast tissue, at room temperature.

Requirement 10: Similar thermo tolerance properties as human breast tissue, at room temperature.

The tissue effects as a result of electrosurgery are among other things related to the electrical conductivity and thermo tolerance properties of that specific material. As a result, the electrosurgical tissue effects of gelatin and agar were compared to that of pork tissue. The agar phantoms showed realistic tissue effects similar to pork muscle, namely local incisions without much thermal spread, whereas the gelatin phantoms showed unrealistic tissue effects, namely widespread melting accompanied by bubbles and incisions that melted together. The cause for this difference is probably due to a difference in thermo tolerance, namely a low melting point of gelatin (35 °C) and a high melting point of agar (85 °C). As a result, the temperature in the vicinity of the electrosurgical cut, mounted up above the melting temperature of the gelatin phantoms, but not above the melting temperature of the agar phantoms. To make sure of this, further research should be done with regard to the exact melting temperatures of the phantoms and the thermal distribution of the phantoms with electrosurgery. Nevertheless, for now, solely the agar phantoms meet requirement 9 and 10, therefore enabling realistic tissue effects when using the electrosurgical knife.

For this thesis project, these qualitative results are promising enough to meet the concerning requirements. However, to determine the actual cause for the observed phantom tissue effects, not only on the melting point and thermal distribution, but also on the electrical conductivity and other thermo tolerance properties (specific heat and thermal conductivity) should be determined. Hence, for further research it is recommended to measure and quantify the aforementioned phantom properties, to find out what exactly caused the observed tissue effects.

V. RESEARCH PHASE 3

CONTRAST AGENT

The goal of this phase is to further develop the most potential agar phantoms with regard to the pre- and postoperative margin assessment requirements (requirement 4 and 11), without interfering with the IMA requirements.

15. X-ray

The goal of this research phase is to further develop the most potential agar phantoms with regard to the pre- and postoperative margin assessment requirements (requirement 4 and 11), without interfering with the IMA requirements. The pre- and postoperative margin assessment requirements state that preoperatively, the tumour phantom location, size and border should be assessable, whereas postoperatively, residual tumour phantom should be detectable. Inspired by the study of Pleijhuis et al., adding a contrast agent to the tumour phantom, enables imaging modalities such as radiography (X-ray), ultrasonography (US) and magnetic resonance imaging (MRI), to inspect the tumour phantom pre- and postoperatively ^{106,104}. Since the In-Body Systems department of Philips Research has a CT-scan available taking X-rays, firstly a good contrast agent should be found that is detectable by X-ray but does not interfere with the IMA requirements.

15.1 CT-scan

A CT-scan produces X-rays, which are high energy electromagnetic radiation with wavelengths ranging from 0.01 to 10 nm. High density material such as bone absorbs and scatters X-rays, whereas low-density materials such as air do not. As a result, X-rays passing through bone are blocked, therefore do not reach the film and appear as shades of white, whereas X-rays passing through air, reach the film and appear as shades of black ^{151,152,153}. Hence, by convention, low-density material appears darker and high-density material appear brighter on the X-ray images. Quantitatively, tissue density is represented by Hounsfield units (HU) or CT numbers, which range from -1000 to +1000. Air, water and high-density bone make up this range, namely they have a HU of respectively -1000, 0 and 1000. However, some newer CT scans have a range of up to 4000 HU ^{154,155}.

15.2 Barium sulphate

Barium sulphate is a stable, inexpensive and commonly used X-ray contrast material ¹⁵⁶. Similarly, to high-density bone, it absorbs and scatters X-rays, therefore appearing as shades of white on X-ray images. This is well illustrated in figure 46, which displays an X-ray image of a patient who swallowed a solution of barium sulphate for the examination of his intestines ¹⁵¹. Hence, adding barium sulphate to the agar tumour phantom makes it detectable on X-ray. As a result, it enables preoperative tumour localization and post-operative tumour residue inspection. However as earlier stated, it is a requisite that barium sulphate should not interfere with the IMA requirements. Hence in the following chapter the agar tumour phantom including barium sulphate, will be analysed with regard to its visual-, F/W-ratio-, mechanical-, electrically conductive- and thermo tolerance properties. However, first the right amount of barium sulphate should be found that enables accurate distinction on the CT scan, between the healthy- and tumour phantom.

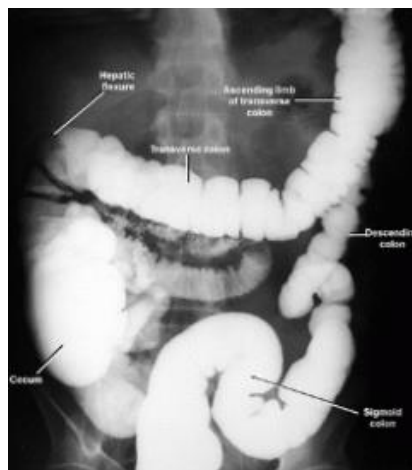


Figure 46: Barium sulphate solution swallowed by patient showing the intestines ¹⁷⁴.

16. BaSO₄ & X-ray Contrast

The goal of this study is to find the minimum required concentration of barium sulphate, to show a sufficient contrast on the X-ray images between the tumour and healthy phantom, while not interfering with requirement (8), namely keeping a minimal difference in visual properties between the healthy- and tumour phantom.

16.1 Materials and methods

Materials & equipment

Agar (Terrasana ¹¹³), extra pure barium sulphate (Hinmeijer, the Netherlands, 233.40 g/mol, CAS nr.: 7727-43-7 ¹⁵⁷), tap water and lard from the local butcher (Alain Bernard, Amsterdam) were used to make the barium sulphate phantoms. The IKA C-MAG HS7 control was used to heat up the water and lard and mix all the materials together. A Cone Beam CT (CBCT) system (Philips Healthcare, Best, the Netherlands), was used to scan the phantoms (fig. 47). Contrary to convention, this CT scan obtained X-ray images with high-density material appearing darker and low-density material appearing lighter.

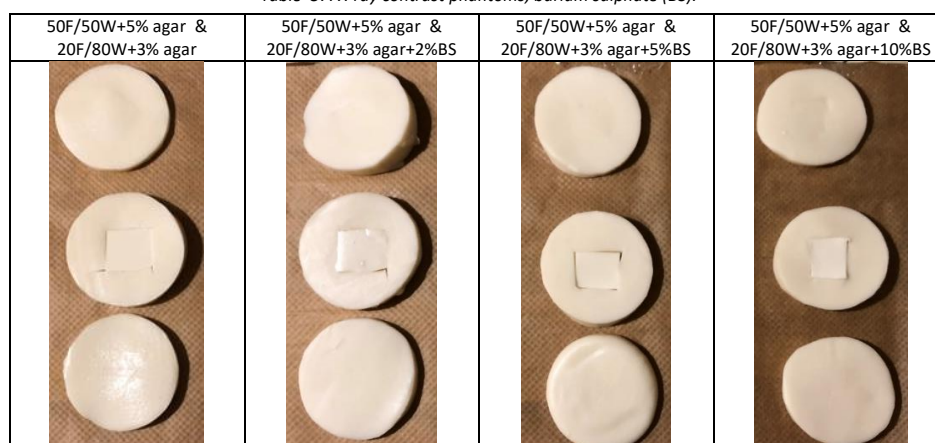


Figure 47: Cone Beam CT (CBCT) system at Philips Healthcare.

Setup and methods

Four healthy tissue phantoms (50F/50W-5%agar) were made according to the production method stated in table 22. Furthermore, four tumour phantoms (20F/80W-3%agar) with concentrations of 0,2,5 and 10% of barium sulphate by weight of water, were made according to the production method stated in paragraph 16.3. The healthy phantoms were cut into slices with thicknesses of approximately 10 mm, and the tumour phantoms were cut into squares with surfaces of approximately 20x20 mm and thicknesses of approximately 10 mm. Subsequently, the tumour squares were placed in between the healthy tissue phantoms, so the X-ray contrast could sufficiently be tested, see table 37. From these phantom combinations, several images were acquired by the CT system, which subsequently were compared to each other by qualitative visual inspection.

Table 37: X-ray contrast phantoms, barium sulphate (BS).



16.2 Production method

Concerning the barium sulphate tumour phantom, similar equipment was used as the production methods stated in table 22. The barium sulphate phantoms consisted of 200 mL fat and water and were made as followings; Lard was heated until melted (40 °C) and tap water was heated to 100°C. 3% of agar by weight of water was added to the water and mixed for 3 minutes at 800 rpm. Lard was slowly added to the agar/water mixture and mixed for 3 minutes at 800 rpm. Various percentages of barium sulphate were added to the agar/water/lard mixture and mixed for 10 minutes at 800 rpm. In case the total mixture seemed homogeneous, the mixture was weighted. If due to water evaporation, the total weight was still too low, it was corrected for by adding the right amount of water (100 °C) and mixed for 3 minutes at 800 rpm. The heater was turned off and the mixture was put into an ice bath. Mixing was continued until the mixture had a temperature of 35 °C. The mixture was then poured into glass cups and refrigerated (4°C) overnight to solidify. The following day these phantoms were taken out of the refrigerator and cups, to get to room temperature (3 hours).

16.3 Barium sulphate & Hounsfield unit

This sub-paragraph discusses the expected influence of barium sulphate on the X-ray contrast when adding BaSO₄ to the tumour phantom. In order to do so, the HU values of all phantom materials should be known. Since it was hard to find the HU values of agar and lard, the HU values of respectively fat and agarose were obtained, which have a similar density. Table 38 displays the obtained HU values of fat, agarose and BaSO₄. As can be seen, fat and agarose have low HU values, whereas barium sulphate has much higher HU values. Hence, it is expected that adding barium sulphate to the tumour phantom, results in a sufficient X-ray contrast between the tumour and healthy phantom. Additionally, similar to the study of Litt et al., it is expected that increasing barium sulphate's concentrations, linearly increases the CT attenuation¹⁵⁶.

Table 38: HU values of fat, agarose and BaSO₄.

Study	Material	Hounsfield units (HU)
Broder et al. ¹⁵⁸	Fat	-100 to -50
Litt et al. ¹⁵⁶	Agarose 0.25-6% wt/vol	20 to 35
	Barium sulphate 1-6% wt/vol	200 to 850

16.4 Results

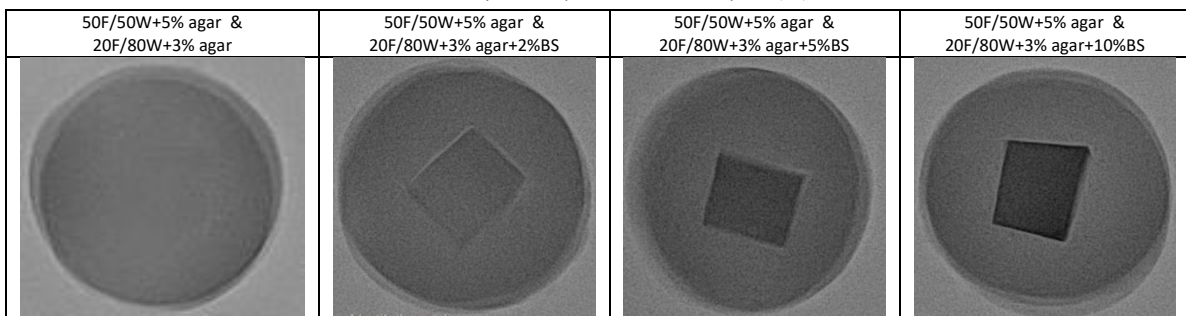
Table 39 illustrates pictures taken in the same room at the same time, from the most potential agar phantoms and the barium sulphate phantoms, before being cut into squares. Increasing the concentration of barium sulphate increases the whiteness of the phantoms. As a result, the 50F/50W+5%agar phantom is now visually most similar to the 20F/80W-3%agar+5%BS phantom.

Table 39: Visual properties of the most potential agar phantoms and the barium sulphate phantoms, barium sulphate (BS).



Table 40 shows the X-ray results of the healthy phantoms including square tumour phantoms with various barium sulphate concentrations. As expected, increasing the concentration of barium sulphate increases the darkness of the tumour phantoms. Furthermore, no difference in X-ray contrast can be seen between the healthy and tumour phantom where no barium sulphate is added. Finally, it can be observed that 5% of barium sulphate is the minimum amount of barium sulphate needed to show a sufficient contrast on the X-ray images between the tumour and healthy phantom.

Table 40: X-ray contrast phantoms, barium sulphate (BS).



16.5 Conclusion

The goal of this study was to find the minimum required concentration of barium sulphate, to show a sufficient contrast on the X-ray images between the tumour and healthy phantom, while not interfering with requirement (8), namely keeping a minimal difference in visual properties between the healthy- and tumour phantom.

Three phantoms (20F/80W+3%agar) with various concentrations of barium sulphate were made, namely 2,5 and 10% by weight of water, from which the 20F/80W+3%agar+5%BS phantom was the most promising. Firstly, because it was visually the most similar to the healthy tissue phantom (50F/50W+5%agar), therefore not interfering with requirement 8. Secondly, because it had the minimum amount of barium sulphate necessary to show a sufficient contrast on the X-ray images between the healthy and tumour phantom, therefore meeting the pre-and postoperative requirements 4 and 11.

However, one major study limitation is that solely tumour phantoms with a thickness of 10 mm were tested. Perhaps 5% of barium sulphate by weight of water does not show enough X-ray contrast with a tumour thickness much smaller than 10 mm. Furthermore, CT-scans have a spatial resolution of approximately 0.7 lines per mm, hence postoperatively, tumour phantom residue smaller than 1.43 mm, cannot be distinguished from the healthy phantom. Nevertheless, this thesis project solely functions as a proof of concept for the validation study. Hence for further research, tumours much smaller than 10 mm should be tested, to see whether 5% of barium sulphate still shows enough X-ray contrast. Furthermore, perhaps the validation study could use film-screen mammography, which also uses X-rays, but has a spatial resolution of 15 lines per mm, thus could detect phantom residue as small as 0.067 mm¹⁵⁹.

17. BaSO₄ & IMA Requirements

Last chapter showed that the minimum amount of barium sulphate, needed to show a sufficient contrast on the X-ray images between the tumour and healthy phantom, was 5% by weight of water. However, adding barium sulphate to the tumour phantom, should not interfere with the IMA requirements (5-10), namely the tumour and healthy tissue phantom should still have a significant difference in F/W-ratio, realistic mechanical-, electrically conductive- and thermo tolerance properties and minimal mechanical- and visual differences. Hence, the goal of this chapter is to determine the influence of barium sulphate on the F/W-ratio, mechanical-, electrically conductive- and thermo tolerance properties of agar tumour phantom (20F/80W), by doing qualitative and quantitative tests similar to research phase 2.

17.1 Compression Tests

The mechanical properties of the barium sulphate tumour phantom were tested by compression tests.

17.1.1 Materials and methods

The compression tests were performed at the same time as the compression tests of chapter 11. Hence, the exact same equipment and experiment setup were used, which is elaboratively discussed in paragraph 11.2. The barium sulphate tumour phantom (20F/80W-3%agar-5%BaSO₄) was made with the materials and production method stated in paragraph 16.2 and 16.3. Two samples were produced to make sure the results were consistent. Both samples had a thickness of 18 mm and a square surface of 1444mm², which is smaller than the compression surface, and therefore accounts for geometrical changes as the samples are compressed. On both samples, two measurements were performed resulting in a total of 4 measurements. Further information with regard to data analysis can be found in chapter 11.2. The mechanical properties of the barium sulphate tumour phantom were compared to the mechanical properties of the regular tumour phantom (20F/80W-3%agar) and the healthy tissue phantom (50F/50W-5%agar) reported in chapter 11.

17.1.2 Barium sulphate & Mechanical properties

This sub-paragraph discusses the expected influence of barium sulphate on the mechanical properties of the agar tumour phantom. Literature shows that barium sulphate mixed with various materials, increases the Young's Modulus^{160,161,162}. However, for low concentrations BaSO₄, small increases in Young's Moduli were seen. Hence, since this study solely uses 5% of BaSO₄ by weight of water, a neglectable increase in Young's Modulus is expected.

17.1.3 Results & Conclusion

The average stress-strain response of the tumour agar phantoms with and without barium sulphate and the derived Young's Moduli are respectively given in figure 48 and table 41. In chapter 11 the mechanical properties of the tumour phantom (20F/80W-3%agar) without BaSO₄ was elaboratively discussed. It was concluded that despite the study limitations, the regular tumour phantom was mechanically realistic and had a minimal difference in mechanical properties between the healthy- and tumour phantom, therefore meeting both mechanical requirements (6 & 7).

In line with literature, table 41 shows that 5% of barium sulphate added to the regular tumour phantom, slightly increased the derived Young's Modulus^{160,161,162}. However, these changes are sufficiently small, thereby the mechanical requirements do not require high mechanical accuracy. Hence, the agar tumour phantom in combination with 5% of barium sulphate, meets requirement 6 and 7. Namely, it is mechanically realistic and differs minimally in mechanical properties from the healthy tissue phantom.

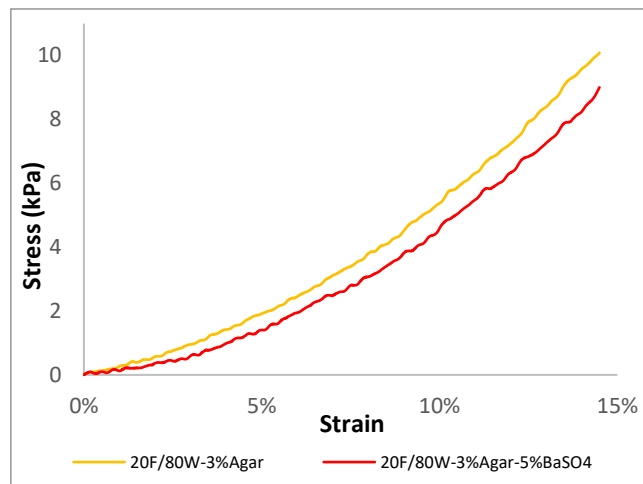


Figure 48: Average stress-strain response of agar phantoms.

Table 41: Young's Moduli of relevant studies and produced agar phantoms.

Young's Modulus (kPa) and SD				
Studies	Phantom- or tissue type	Strain rate:	Slope 1 – 1.2 stress (kPa)	Slope <20% strain
<u>Agar</u> Chen et al. ¹¹⁹ (2016) Data derived from fig. 2	Agar 1% w/w	6mm/min	-	80
	Agar 2% w/w		-	450
<u>Breast tissue</u> Matsumura et al. ⁹⁴ (2009) (zero pre-strain)	Normal fat tissue	1mm/min	17.3 ± 4.8	-
	Normal glandular tissue		15.4 ± 3.9	-
	DCIS		15.6 ± 2.0	-
	IDC		27.0 ± 9.2	-
<u>Breast tissue</u> Umamoto et al. ⁹⁵ (2014) (zero pre-strain)	Normal fat tissue	1mm/min	19.08 ± 4.99	-
	Normal glandular tissue		16.99 ± 4.92	-
	DCIS		16.15 ± 4.24	-
	IDC		30.5 ± 11.46	-
Results	Phantom type	Strain rate:	Slope 1 – 1.2 stress (kPa)	Slope 14 - 15% strain
<u>Agar</u>	50F/50W+5% agar by weight of water	6mm/min	38 ± 2	90 ± 19
	20F/80W+3% agar by weight of water		41 ± 5	100 ± 26
	20F/80W+3% agar + 5%BaSO4 by weight of water		42 ± 8	106 ± 14

17.2 DRS Tests

The optical properties and the derived F/W-ratio of the barium sulphate tumour phantom were tested by DRS tests.

17.2.1 Materials and methods

The DRS measurements were performed at the same time as the DRS measurements of chapter 12. Hence, the exact same equipment and experiment setup were used, which is elaboratively discussed in paragraph 12.2. The barium sulphate tumour phantom (20F/80W-3%agar-5%BaSO4) was made with the materials and production method stated in paragraph 16.2 and 16.3. Three samples were produced to make sure the results were consistent. On each sample, a total of 15 measurements were performed. Further information with regard to the measurements, data analysis, the derived parameters and its confidence intervals can be found in chapter 12. The optical properties of the 20F/80W-3%agar-5%BaSO4 phantom were compared to the optical properties of the regular tumour phantom (20F/80W-3%agar) and the healthy tissue phantom (50F/50W-5%agar) phantom reported in chapter 12.

Statistics

An independent one-tailed two-sampled t-test was performed, to see whether the F/W-ratio of the 50F/50W-5%agar phantom was significantly higher than the F/W-ratio from the 20F/80W-3%agar-5%BaSO4 phantom. It was assumed that the measured F/W-ratios were normally distributed. H0 states the highest and lowest F/W-ratio are equal. The significance level is $\alpha = 0.05$, hence H0 can be rejected if $p < 0.05$. In case p

= 0.05, we wrongfully reject H_0 in 5% of the cases. With regard to the scattering media, an independent two-tailed two-sampled t-test was performed, to see whether there was a significant difference between the 50F/50W-5%agar and 20F/80W-3%agar-5%BaSO₄ phantom. It was assumed that the measured scattering media were normally distributed. H_0 states the scattering media are equal and the significance level is $\alpha = 0.05$. Hence, H_0 can be rejected if $p < 0.05$. In case $p = 0.05$, we wrongfully reject H_0 in 5% of the cases

17.2.2 Barium sulphate & Optical properties

This sub-paragraph discusses the expected influence of barium sulphate on the optical properties of the agar tumour phantom. Barium sulphate is a common scatterer and is often used as a reference standard for reflectance, with an average reflectance of 92% between the range of 173 to 2500 nm^{163,164,165}. It has an average particle size of 1 μm , which is smaller than incoming NIR radiation, whereas fat has an average particle size of 20 μm or higher. Hence, it is expected that barium sulphate increases the scattering amplitude and Mie slope, and decreases the Mie-to-Rayleigh fraction of the agar tumour phantom^{166,167,156}. With regard to the absorption of barium sulphate, little information was found. Lindberg et al. stated that barium sulphate was a non-absorbing material. However, Hadi et al. who added BaSO₄ to PVA, found that barium sulphate did not shift, but solely increased the absorption of the PVA absorption peak (200 nm). Hence, barium sulphate did not change the chemical structure of the material but formed a new physical mixture by adding scattering centres^{167,168}. Based on these two studies, little can be said with regard to the expected absorption of barium sulphate. Perhaps agar, lard and barium sulphate interact totally different than the BaSO₄/PVA mixture, or perhaps barium sulphate indeed increases the absorption of the agar/lard phantom.

17.2.3 Results

In chapter 12, the DRS spectra characteristics as a result of differences in F/W-ratio are elaboratively discussed. In short, a high F/W-ratio phantom has sharp DRS valleys at 1211 and 930 nm, and an elevated DRS intensity between 1200 and 1400 nm, whereas a low F/W-ratio phantom has a small DRS valley at 970 nm and an overall low DRS intensity above 1400 nm.

Spectral shape & F/W-ratio

Figure 49 displays the normalized average DRS spectra of the 20F/80W phantoms, with and without barium sulphate. As can be seen, the barium sulphate phantom has a slightly larger DRS valley at the fat absorption peak (1211 nm) and a slightly lower DRS intensity at the water absorption area (above 1400 nm). As a result, the accuracy deteriorated. Namely, the estimated fat and water concentration of the barium sulphate phantom was higher than the phantom without barium sulphate (table 42). This is in line with Hadi et al. findings, namely that barium sulphate increases the absorption of the material it is mixed with¹⁶⁸. Nevertheless, the barium sulphate phantom showed great intra-sample homogeneity and inter-sample consistency. Furthermore, despite the inaccuracies, table 43 shows the obtained barium sulphate tumour phantom still has a realistic F/W-ratio of 0.70, which falls within the range of F/W-ratios (0.22 – 11.25) reported by breast studies in table 43.

However, more importantly, figure 50 displays the boxplot of the obtained F/W-ratios and shows that the null-hypothesis is rejected. More specifically, there is still a significant difference in F/W-ratio between the healthy phantom and barium sulphate tumour phantom. Namely, the healthy phantom, has a significant higher F/W-ratio ($M = 1.61$, $SD = 0.05$) than the barium sulphate tumour phantom ($M = 0.70$, $SD = 0.09$), $t(45) = 56.74$, $p = 8.2 \cdot 10^{-62}$. The highest F/W-ratio (50F/50W) simulates healthy breast tissue whereas the lowest F/W-ratio (20F/80W) simulates tumour breast tissue.

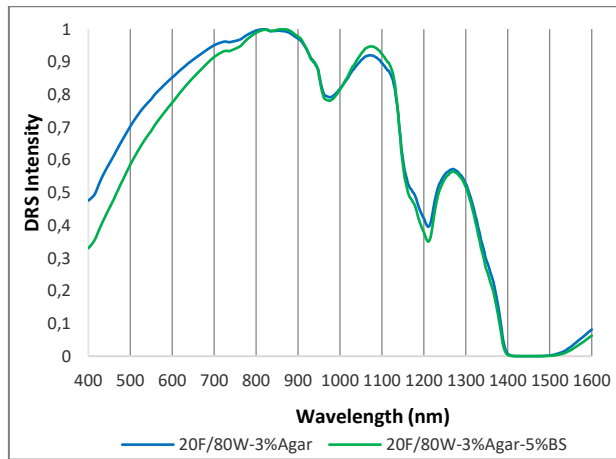


Figure 49: Average DRS spectrum of tumour agar phantom with and without BaSO4.

Table 42: Average estimated parameters with its standard deviations (SD).

Phantom type	Sample	Fat %	Water %	F/W-ratio	s800	b	fmie	
20F/80W + 3%Agar (Chapter 12)	Reference value	20%	80%	0.25	-	-	-	
	Inter-sample average ± SD (Consistency)	47.0 ± 3.4	76.3 ± 5.7	0.62 ± 0.08	15.8 ± 0.6	1.43 ± 0.04	0.99 ± 0.01	
	Δ with reference value (Accuracy)	27.0%	-3.7%	0.37	-	-	-	
20F/80W + 3%Agar + 5% BaSO4	Reference value	20%	80%	0.25	-	-	-	
	Intra-sample average ± SD (Homogeneity)	1	62.3 ± 1.8	97.7 ± 4.1	0.64 ± 0.04	18.3 ± 0.5	1.41 ± 0.08	0.92 ± 0.02
		2	59.8 ± 3.0	88.1 ± 3.6	0.68 ± 0.04	18.0 ± 0.8	1.46 ± 0.04	0.95 ± 0.02
		3	63.1 ± 4.7	81.0 ± 5.0	0.78 ± 0.10	18.7 ± 0.9	1.40 ± 0.10	0.92 ± 0.02
	Inter-sample average ± SD (Consistency)	61.7 ± 3.7	88.9 ± 8.1	0.70 ± 0.09	18.3 ± 0.8	1.42 ± 0.08	0.93 ± 0.03	
Δ with reference value (Accuracy)	41.7%	8.9%	0.45	-	-	-		

Table 43: F/W-ratio of healthy and tumour tissue & F/W-ratios of most agar phantoms, table constructed based on references cited in this table and based on the conducted DRS tests.

Study	Healthy tissue			Tumour tissue			
	Lipid (%) Mean	Water (%) Mean	F/W-ratio Mean	Lipid (%) Mean	Water (%) Mean	F/W-ratio Mean	
De Boer et al. ⁵⁶ (2016) in & ex vivo	-	-	7.5	-	-	0.8	
Nachabé ⁷² (2012) – Ch. 9, ex vivo	90 (AP)	8 (AP)	11.25	15 (DCIS)	50 (DCIS)	0.3	
	12 (GL)	55 (GL)	0.22				
Blackmore et al. ⁶⁰ (2015)	65.1	19.66	3.31	-	-	-	
Cerussi et al. ⁶³ (2001)	48.65	27.7	1.76	-	-	-	
O'Sullivan et al. ⁶⁸ (2013)	69.7	21.4	3.26	-	-	-	
Intes ⁶² (2005)	62.4	28.9	2.16	-	40.8	-	
Leproux et al. ⁷³ (2016)	-	-	-	62.54	47.67	1.31	
Cerussi et al. ⁷⁴ (2006)	66.1	18.7	3.53	58.5	25.9	2.26	
Wang et al. ⁷⁵ (2010)	69	15	4.6	45	26	1.73	
Agar	Reference values	50	50	1	20	80	0.25
	Obtained DRS values				Without BaSO4 47.0	76.3	0.62
	Obtained DRS values	87.6	54.6	1.61	With 5% BaSO4 61.7	88.9	0.70

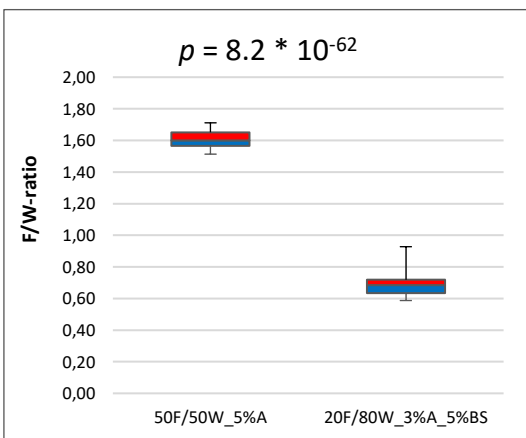


Figure 50: Boxplot of F/W-ratios of most potential agar phantoms.

Table 44: Average estimated parameters with its standard deviations (SD) and its p-value.

Parameter	20F/80W + 3%Agar + 5% BaSO4	50F/50W + 5%Agar	20F/80W + 3%Agar	50F/50W + 5%Agar
s800	18.3 ± 0.8	15.8 ± 0.3	15.8 ± 0.6	15.8 ± 0.3
p values	1.8 * 10 ⁻²⁷		0.48	
b	1.42 ± 0.08	1.43 ± 0.03	1.43 ± 0.04	1.43 ± 0.03
p values	0.49		0.66	
fmie	0.93 ± 0.03	1.00 ± 0.01	0.99 ± 0.01	1.00 ± 0.01
p values	5.8 * 10 ⁻²¹		0.62	

Scattering Media

As can be seen in table 44 and already elaboratively discussed in chapter 12, the 50F/50W phantom is not significantly different in scattering parameters from the 20F/80W phantom. However, with barium sulphate the 20F/80W phantom has a significantly higher scattering amplitude and significantly lower Mie-to-Rayleigh-fraction than the 50F/50W phantom. As discussed in paragraph 17.2, this was expected since barium sulphate is a scatterer and has an average particle size smaller than the wavelength of NIR incident radiation, most likely causing the increase in Rayleigh scattering, therefore the decrease in Mie-to-Rayleigh fraction. However, the Mie-slope did not change, which was somewhat unexpected, since as stated in paragraph 17.2.2, barium sulphate is a smaller scatterer than fat, therefore should have decreased the average scattering particle size of the 20F/80W phantom and increased its Mie-slope. However, the exact interaction between agar/lard and barium sulphate is unknown, therefore no conclusions on the scattering parameters can be drawn with full certainty. All in all, the barium sulphate tumour phantom still shows scattering parameter values similar to that of breast tissue^{56,70,76,72}.

17.2.4 Conclusion

The goal of this study was to determine the influence of barium sulphate on the optical properties and the derived F/W-ratio of the agar tumour phantom (20F/80W). Similarly, to the 20F/80W phantom, the 20F/80W with barium sulphate showed great homogeneity and -consistency in the fat and water concentration. However, both phantoms showed suboptimal accuracy. As stated in chapter 12, this was partially due to agar's influence on the fat absorption peak, causing fat overestimation. Yet, barium sulphate further deteriorated the accuracy of not only the fat- but also of the water concentration. Namely, both fat and water were further overestimated. However, these inaccuracies were also partially caused by the estimation error of DRS and its analytical model¹²⁷. Despite these inaccuracies, there was still a significant difference in F/W-ratio between the healthy phantom and barium sulphate tumour phantom, therefore meeting requirement 5.

17.3 Electrosurgical Tests

As explained in paragraph 1.1.3, the tissue effects as a result of electrosurgery are among other things related to the electrical conductivity and thermo tolerance properties of that specific material. Hence, the electrical conductivity and thermo tolerance properties of the barium sulphate tumour phantom will be tested by looking at the tissue effects as a result of electrosurgery.

17.3.1 Materials and methods

The electrosurgical tests were performed at the same time as the electrosurgical tests of chapter 13. Hence, the exact same equipment and experiment setup were used, which is elaboratively discussed in paragraph 13.2. One barium sulphate tumour sample (20F/80W-3%agar-5%BaSO₄) with a diameter of 12 cm and a thickness of approximately 18 mm, was made with the materials and production method stated in paragraph 16.2 and 16.3. Electrosurgery was applied on this phantom, from which the tissue effects were compared to tissue effects of the regular tumour phantom (20F/80W-3%agar), the healthy tissue phantom (50F/50W-5%agar) and pork tissue reported in chapter 13. The samples were compared to each other qualitatively, among other things by looking at the thermal spread and haptic feedback.

17.3.2 Barium sulphate & Tissue effects

This sub-paragraph discusses the expected influence of barium sulphate on the electrical conductivity and thermo tolerance properties, and therefore on the electrosurgical tissue effects of the agar tumour phantom. High electrical conductivity is accompanied by high heat production, whereas high thermo tolerance is accompanied by little thermal tissue effects for a given thermal dose. A material with a high thermo

tolerance, has a high melting point or high resistance to high temperatures, a low thermal conductivity or little thermal spread, and finally, a low specific heat or low required thermal dose to reach the thermal equilibrium, therefore minimizing the height of the reached temperatures near the electrosurgical cut ^{22,140,141}. No studies were found that determined the electrically conductive and thermo tolerance properties of BaSO₄. Solely the following was found, barium sulphate is a material with a high melting point (1580°C) and low specific heat of 114 (J/kg K) compared to the agar and lard (see table 35) ^{169,157}. Based on this information, it can be concluded that adding barium sulphate to the tumour phantom, increases the thermo tolerance, therefore decreases the amount of electrosurgical tissue effects. However, since this study solely uses 5% of BaSO₄ by weight of water, no significant differences in tissue effects are expected. Finally, above its melting point, barium sulphate decomposes emitting toxic fumes. However, since electrosurgery solely reaches temperatures up to 400°C, this should not be a problem ^{170,15}.

17.3.3 Results

Figure 51 displays the tissue effects of both tumour phantoms and the healthy phantom for the three different waveforms. In line with the mechanical property findings from chapter 17, the experienced haptic feedback of the barium sulphate phantom, felt similar to pork belly, thus realistic and similar to the regular tumour phantom (20F/80W-3%agar) and the healthy tissue phantom (20F/80W-3%agar). Noteworthy, it was possible to cut into the barium sulphate tumour phantom without using current but solely pushing the ESK downwards, whereas it was not possible to cut with the ESK into pork belly without using current. Nevertheless, the experienced haptic feedback was realistic, which is solely relevant for meeting requirement 6.

With regard to the tissue effects, similar to pork muscle tissue and the healthy and tumour phantoms, the barium sulphate tumour phantom showed for all waveforms, realistic tissue effects, namely local incisions with limited thermal spread. Hence, barium sulphate did not alter the electrosurgical tissue effects of the regular tumour phantom, which was expected since solely 5% of BaSO₄ by weight of water was added.



Figure 51: The most potential agar phantoms with and without BaSO₄. From left to right, tissue effects as a result of coagulation, blend cut and pure cut.

17.3.4 Conclusion

The goal of this study was to determine the influence of barium sulphate on the electrosurgical tissue effects of the agar tumour phantom (20F/80W). Similarly, to the 20F/80W phantom, the 20F/80W with barium sulphate, showed realistic tissue effects, namely local incisions without much thermal spread. Hence, 5% of barium sulphate by weight of water did not alter the electrosurgical tissue effects of the regular tumour phantom, therefore the 20F/80W-3%agar-5%BaSO₄ phantom automatically meets requirements 9 and 10.

18. Conclusion – Research Phase 3

The goal of this research phase was to further develop the most potential agar phantoms with regard to the pre- and postoperative margin assessment requirements (requirement 4 and 11), without interfering with the IMA requirements (5-10). It was found that adding 5% of barium sulphate to the tumour phantom, enables pre- and postoperative X-ray margin assessment, without interfering with the IMA requirements. Hence, in the next research phase we will continue to use the healthy agar phantom (50F/50W+5%agar) and the tumour agar phantom in combination with 5% of barium sulphate by weight of water (20F/80W+3%agar+5%BaSO₄).

Requirement 4: A contrast between tumour and healthy phantom tissue which is assessable preoperatively.

Requirement 11: A contrast between tumour and healthy phantom tissue which is assessable postoperatively.

The pre- and postoperative margin assessment requirements state that preoperatively, the tumour phantom location, size and border should be assessable, whereas postoperatively, residual tumour phantom should be detectable. With the help of literature, it was found that adding barium sulphate to tumour phantom, enables imaging modalities such as radiography (X-ray), to sufficiently assess the tumour phantom pre- and postoperatively. As a result, various concentrations of barium sulphate in combination with the tumour phantom, were tested qualitatively on its X-ray contrast. It was found that the minimum required concentration of barium sulphate, to show a sufficient contrast on the X-ray images between the tumour and healthy agar phantom, was 5% by weight of water. Hence, 5% of barium sulphate added to the tumour phantom, enables sufficient contrast between the tumour and healthy tissue phantom, therefore meeting requirement 4 and 11.

However, one major study limitation is that solely tumour phantoms with a thickness of 10 mm were tested. Perhaps 5% of barium sulphate by weight of water does not show enough X-ray contrast with a tumour thickness much smaller than 10 mm. Furthermore, this study used a CT-scan, which has a spatial resolution of approximately 0.7 lines per mm. Hence postoperatively, tumour phantom residue smaller than 1.43 mm, cannot be distinguished from the healthy phantom. Nevertheless, this thesis project solely functions as a proof of concept for the validation study. Hence for further research, tumours much smaller than 10 mm could be tested, to see whether 5% of barium sulphate still shows enough X-ray contrast. Furthermore, perhaps the validation study could use film-screen mammography, which also uses X-rays, but has a spatial resolution of 15 lines per mm, thus enables phantom residue detection as small as 0.067 mm¹⁵⁹.

IMA requirements (5-10).

Hence, 5% of barium sulphate added to the tumour phantom showed sufficient X-ray contrast. However, it is a requisite that it cannot interfere with the IMA requirements. As a result, the barium sulphate tumour phantom was extensively tested with regard to the IMA requirements. Visual inspection and compression tests showed that the tumour phantom with 5% of barium sulphate, was mechanically realistic and visually and mechanically very similar to the healthy phantom tissue. Furthermore, DRS tests showed that it significantly differed in F/W-ratio from the healthy phantom. Finally, with electrosurgery, realistic haptic feedback and -tissue effects were found. Hence, the agar tumour phantom in combination with 5% of barium sulphate, not only met the pre- and postoperative requirements, but also all the IMA requirements (5-10). Therefore, in the next research phase we will continue to use the healthy agar phantom (50F/50W+5%agar) and the tumour agar phantom in combination with 5% of barium sulphate by weight of water (20F/80W+3%agar+5%BaSO₄).

VI. RESEARCH PHASE 4

FINAL PHANTOM

The goal of this research phase is to successfully combine the healthy and tumour phantom into a breast-shaped phantom with a realistic size and shape, so that the validation study is as close to a real BCS procedure as possible (requirement 12). Furthermore, both the healthy and tumour phantom will be evaluated with regard to the general requirements (1-3), namely the reproducibility, homogeneity, durability, costs and ease of manufacturing of the phantom.

19. Final Phantom Production

In this chapter, the healthy and tumour phantom will be combined into a breast-shaped phantom with a realistic size and shape, so that the validation study is as close to a real BCS as possible.

19.1 Melting point

An agar/water mixture has a melting temperature of 85°C, whereas lard has a melting temperature of 38°C^{13,145}. Hence, since the tumour phantom has a lower lard- and a higher agar/water concentration than the healthy tissue phantom, it can be assumed that the tumour phantom has a higher melting point than the healthy tissue phantom. Inspired by Pleijhuis et al., this melting point difference will be used during the production process of the final phantom¹⁰⁴.

19.2 Materials & equipment

Agar (Terrasana¹¹³), lard from the local butcher (Alain Bernard, Amsterdam), tap water and extra pure barium sulphate (Hinmeijer, the Netherlands, 233.40 g/mol, CAS nr.: 7727-43-7¹⁵⁷) were used to make the final phantom. The IKA C-MAG HS7 control was used to heat up the water and lard, and mix all the materials together.

19.3 Production method

The final phantom had a total volume of 500 mL. First, the healthy and tumour tissue phantom were made separately, before being combined into a breast-shaped phantom with a tumour inclusion.

Tumour phantom

The tumour phantom consisted of 20% lard, 80% tap water and then 3% agar- and 5% barium sulphate by weight of water. Lard was heated until melted (40 °C) and tap water was heated to 100°C. 3% of agar by weight of water was added to the water and mixed for 3 minutes at 800 rpm. Lard was slowly added to the agar/water mixture and mixed for 3 minutes at 800 rpm. 5% of barium sulphate by weight of water was added to the mixture and mixed for 10 minutes at 800 rpm. In case the total mixture seemed homogeneous, the mixture was weighted. If due to water evaporation, the total weight was still too low, it was corrected for by adding the right amount of water (100 °C) and mixed for 3 minutes at 800 rpm. The heater was turned off and the mixture was put into an ice bath. Mixing was continued until the mixture had a temperature of 35 °C. The mixture was then poured into a glass cup and refrigerated (4°C) for 3 hours to solidify. Subsequently, the phantom was taken out of the cup and was cut into a cube, with an approximate dimension of 15x15x15 mm. Finally, the cubic tumour phantom was put back into the refrigerator.

Healthy phantom

The healthy phantom consisted of 50% lard, 50% tap water and then 5% agar by weight of water. Lard was heated until melted (40 °C) and tap water was heated to 100°C. 5% of agar by weight of water was added to the water and mixed for 3 minutes at 800 rpm. Lard was slowly added to the agar/water mixture and mixed for 3 minutes at 800 rpm. In case the total mixture seemed homogeneous, the mixture was weighted. If due to water evaporation, the total weight was still too low, it was corrected for by adding the right amount of water (100 °C) and mixed for 3 minutes at 800 rpm. The heater was turned off and the mixture was put into an ice bath. Mixing was continued until the mixture was still liquid and had a temperature of 45 °C.

Combining the phantoms

The healthy phantom mixture was poured in a custom-made breast-shaped mould (volume: 500 mL) to a height of 20 mm. After solidification for 3 hours at 4 °C, the cubic tumour phantom was positioned on the surface and temporarily fixed with a small needle (fig. 52). Next, the remaining of the healthy phantom mixture (45°C) was added to fill up the remaining mould volume, allowing the healthy phantom layers to melt together, whereas the tumour phantom did not melt, due to its higher melting temperature. The breast phantom was then refrigerated (4°C) for 3 hours to solidify, after which it was taken out of the refrigerator and gently removed from the mould (fig. 53). Finally, to prevent it from dehydration, the final phantom was stored in the refrigerator (4°C) in an airtight sealed box ¹²³.

X-ray

An X-ray image of the final phantom was taken by a Cone Beam CT system (Philips Healthcare, The Netherlands). Figure 54 illustrates the results and shows a clear distinction in contrast between the healthy- and tumour phantom tissue. Furthermore, the image illustrates the tumour phantom stays in shape, although warm healthy phantom liquid, with a temperature of 45 degrees is poured over the cubic tumour phantom.



Figure 52: Left: breast mold with a total volume of 500 mL, right: breast mold including healthy phantom tissue up to 20 mm with the cubic tumour phantom on top.



Figure 53: Final phantom with a total volume of 500 mL.

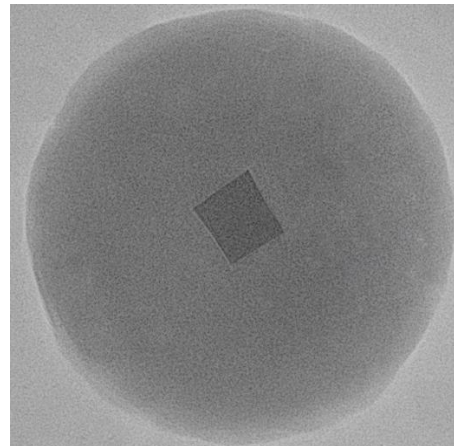


Figure 54: X-ray image of final phantom including a tumour. The tumour consists of 5% bariums sulphate by weight of water.

19.4 Conclusion

During this study, the healthy and tumour agar phantoms were successfully combined into a breast-shaped phantom with a realistic size and shape, allowing the validation study to be as close to a real BCS procedure as possible, therefore meeting requirement 12.

20. General requirements

In this chapter, the final phantom will be evaluated with regard to the general requirements (1-3), namely the reproducibility, homogeneity, durability, costs and ease of manufacturing.

20.1 Requirement 1: Easy to manufacture & inexpensive

The total material costs for producing one final phantom turned out to be approximately 3.5 euros. Even if with further research, more expensive purified agar from Sigma Aldrich will be used, the total price will not mount above 6 euros per phantom. With regard to the production process, in line with literature, the production of the agar phantoms in combination with water and lard, turned out to be considerably easy^{14,144}. Additionally, adding barium sulphate to the tumour phantom mixture did not complicate the production process, since no alterations in temperature or mixing order were required. However, combining the healthy and tumour phantom into the final phantom did add some delicate production steps. Nevertheless, overall, the production of the final phantom is considerably easy and cheap. Therefore, requirement 1 is met, enabling extensive phantom production and testing.



20.2 Requirement 2: Reproducible/consistent & homogeneous

Concerning the DRS tests from chapter 12 and 17, both healthy phantom and tumour barium sulphate phantom, showed great intra-sample homogeneity and inter-sample consistency with regard to the optical properties including the F/W-ratio. Hence requirement 2 is met, therefore with the validation study, changes in the derived data can only be attributed to the test setup or system¹³.

20.3 Requirement 3: Durable & stable/long-lasting

Ohmae et al. and Michaelsen et al., both produced water/lipid-based phantoms having optical stability and -durability, up to several weeks^{13,111}. Maddsen et al. found that under perfect conditions, agar phantoms can stay stable up to two and a half years¹⁷¹. Finally, Litt et al. combined barium sulphate and agarose showing great X-ray stability¹⁵⁶. Hence, literature shows promising results with regard to the durability and stability of the used phantom materials. However, due to time restrictions, this thesis project does not include quantitative tests concerning the durability and stability of the phantom properties such as the F/W-ratio. Yet, to give you an idea of the durability and stability of the phantom, qualitative tests were performed. More specifically, right after production, the phantoms were put into a sealed box in the refrigerator (4°C) and taken out every now and then, to see whether visual changes occurred, such as loss in homogeneity or the arisen of mold (table 45). The results show both healthy and tumour phantoms are homogeneous and mold-free until week two. However, after six weeks, both the healthy phantom and the tumour phantom without barium sulphate, show signs of mold, whereas the tumour phantom with barium sulphate, still seems mold-free. Probably this is because barium sulphate is an inorganic material, hence mixing it into the tumour phantom makes it harder for the phantom to grow moldy. Nevertheless, with the validation study, the final phantom will be cut. Hence, based on these results the durability and stability of at least 2 weeks seems sufficient enough to meet requirement 3, namely it enables the phantom to be stored for a sufficient amount of time before being used. Yet, these results are qualitative, therefore simply speculative. Hence, further research in the form of quantitative tests such as compression- and DRS tests are required to determine the durability and stability of the phantom properties. In case these results are disappointing, further phantom development could include preservatives such as sodium benzoate or natrium azide to improve the durability of the phantom^{14,104,136}.

Table 45: Visual inspection of durability and stability of healthy and tumour agar phantoms.

Time after production	Day 0	Week 2	Week 6
Phantom type			
(Healthy phantom) 50F/50W +5%agar			
(Tumour phantom) 20F/80W +3%agar			
(Tumour phantom) 20F/80W +3%agar +5%BaSO4			

20.4 Conclusion

In this chapter, the final phantom was evaluated with regard to the general requirements (1-3). The final phantom is inexpensive and easy to produce, enabling extensive phantom production and SESK testing. Furthermore, its properties are homogeneous and consistent, therefore with the validation study, changes in the derived data can only be attributed to the test setup or system. Finally, the phantom is durable enabling the phantom to be stored for a sufficient amount of time before being used.

VII. EVALUATION

The goal of this phase is to successfully evaluate the results and findings of the thesis project. Chapter 20 contains the overall discussion and recommendations for further research, whereas chapter 21 contains the final conclusion.

21. Discussion & Recommendations

This chapter contains the overall discussion of this master thesis and the recommendations for further research, based on the findings obtained during this thesis project.

21.1 Discussion

The goal of the discussion is to reflect upon the results and to determine the research contribution of this thesis project. Per research phase, the most important results will be summarized and compared to literature, furthermore the most important research limitations and -contributions will be discussed.

21.1.1 Research Phase 1 – Phantom Production

Various studies were capable of producing phantoms that sufficiently mimic either the F/W-ratio or mechanical properties of breast tissue^{14,103,111,123}. However, none of them developed a phantom combining these properties together. Hence, in research phase one, relevant studies were replicated from which a lot of useful information was extracted, namely what materials in combination with what production methods work best to produce homogeneous phantoms with F/W-ratios and mechanical properties similar to breast tissue. It turns out that agar or gelatin, in combination with water and lard, enable phantom production with realistic mechanical properties and F/W-ratios similar to human breast tissue (0.22 – 11.25)^{56,60,62,63,68,72,73,74,75}. The obtained F/W-ratios were 1.5 and 0.25 for the gelatin- and 1.0 and 0.25 for the agar phantoms. The highest F/W-ratio simulated healthy breast-, whereas the lowest F/W-ratio simulated tumour breast tissue.

Although these results are promising, not all studies were possible or feasible to replicate due to equipment unavailability, the fact that the used materials were often unspecified, and if they were specified, they were either not available or too expensive. As a result, inexpensive and easily accessible materials and equipment were used. For example, cheap impurified agar (Terrasana¹¹³) instead of expensive purified agar from Sigma Aldrich was used¹⁰³. Furthermore, Bush et al. dissolved agar into the water at 350°C, whereas the used heater “IKA C-MAG HS7 control”, although indicated differently, did not allow temperatures higher than 105°C¹⁴. These study limitations may have caused some production limitations, namely a limit in the obtainable F/W-ratios. For example, with agar, the maximum obtained F/W-ratio was 1 (50/50), whereas Ohmae et al. produced agar phantoms with F/W-ratios up to 80/20¹¹¹.

Research contribution research phase 1 – Phantom production

Nevertheless, both agar and gelatin phantoms still managed to obtain F/W-ratios and mechanical properties similar to real breast tissue. Hence, the first research contribution is as follows:

For both agar and gelatin, a sufficient production method has been found that enables lard and water to be mixed into a phantom, with both F/W-ratios and mechanical properties similar to human breast tissue.

21.1.2 Research Phase 2 – Testing most potential phantoms

In research phase 2, the most potential agar and gelatin phantoms, were extensively tested with regard to the IMA requirements, namely whether they had realistic mechanical, electrically conductive- and thermo tolerance properties, a significant difference in F/W-ratio and a minimal difference in visual- and mechanical properties between the healthy and tumour phantom. The most potential gelatin phantoms were the 40F/60W+30%gelatin- and the 20F/80W+20%gelatin phantom, and the most potential agar phantoms were the 50F/50W+5%agar- and the 20F/80W+3%agar phantom. The highest F/W-ratio simulated healthy breast-, whereas the lowest F/W-ratio simulated tumour breast tissue.

The visual properties were tested by visual inspection, the mechanical properties by compression tests, the F/W-ratio by DRS tests and the electrically conductive- and thermo tolerance properties by looking at the tissue effects with electrosurgery. It was found that the most potential agar phantoms met all IMA requirements, whereas the most potential gelatin phantoms did not, which is most likely due to its differences in thermo tolerance properties.

Requirement 5: A significant difference in F/W-ratio that simulates tumour and healthy breast tissue content.

DRS tests showed that both gelatin and agar emulsified lard and water sufficiently. Namely, the measured F/W-ratios of both F/W phantoms, showed great DRS homogeneity and -consistency. However, the accuracy was not optimal, the water concentration of the gelatin phantoms was slightly underestimated and the fat concentration of the agar phantoms was significantly overestimated. These inaccuracies were partially due to the estimation error of DRS and its analytical model¹²⁷. However, agar also played a role in these inaccuracies, more specifically it presumably influenced the fat absorption peak at 1211 nm which subsequently caused fat overestimation. This is somewhat unexpected since literature showed agar does not have any influence on the fat estimates of water/lipid-based phantoms^{103,111,14}. However, in contrast to literature, cheap impurified agar (Terrasana¹¹³) from the local food store, instead of expensive purified agar from Sigma Aldrich was used, which most likely caused the differences in result¹⁰³. However, due to the Corona virus, all testing facilities were closed, therefore no DRS tests and thus conclusions could be drawn with regard to the exact optical properties of the used agar and gelatin.

Despite these limitations, for both phantoms the obtained F/W-ratios, namely 2.0 and 0.34 for the gelatin- and 1.61 and 0.62 for the agar phantoms, are still realistic since they fall within the range of F/W-ratios (0.22 – 11.25) reported by breast studies in table 32^{56,60,62,63,68,72,73,74,75}. The highest F/W-ratio simulates healthy breast tissue whereas the lowest F/W-ratio simulates tumour breast tissue. However, more importantly, both gelatin and agar phantoms still showed a significant difference in F/W-ratio between the healthy- and tumour phantoms. Hence, both the gelatin and agar phantoms meet requirement 5, which enables us to sufficiently assess DRS with its capability in discriminating healthy from malignant breast tissue.

Requirement 6: Similar mechanical properties as real breast tissue (at room temperature).

Requirement 7: Minimal mechanical differences between tumour and healthy tissue.

Compression tests showed both gelatin and agar phantoms had good mechanical properties. The measured Young's Moduli were sufficiently similar to breast tissue, with the gelatin phantoms being the most similar to breast tissue and the agar phantoms being slightly stiffer than breast tissue. Furthermore, both the gelatin and agar phantoms showed a sufficiently small difference in mechanical properties between the healthy- and tumour phantoms. However, these results are solely based on two samples- and a total of four measurements per phantom type. Furthermore, due to equipment limitations, a slightly different experiment setup was used than in literature. More specifically, compared to Matsumura et al. and Umemoto et al., slightly different strain rates and strain ranges were used. Additionally, they compressed their breast samples locally, whereas I compressed the phantom samples over the whole surface^{94,95}. Nevertheless, in order to meet the mechanical requirements, the accuracy of the mechanical properties does not have to be that high, thus the results were promising enough. Hence, both gelatin and agar phantoms meet requirement 6 and 7, thus respectively enable realistic haptic feedback when using the ESK and eliminate the possibility of using intraoperative palpation, so that solely DRS with its capability in discriminating healthy from malignant tissue can be tested.

Requirement 8: Minimal visual differences between tumour and healthy tissue.

In research phase 1, visual inspection showed both gelatin and agar phantoms had a sufficiently small difference in colour or visual properties between the healthy- and tumour phantoms. Hence, both meet requirement 8 and therefore eliminate the possibility of using intraoperative visual inspection, so that solely DRS with its capability in discriminating healthy from malignant tissue can be tested.

Requirement 9: Similar electrically conductive properties as human breast tissue, at room temperature.

Requirement 10: Similar thermo tolerance properties as human breast tissue, at room temperature.

The tissue effects as a result of electrosurgery are among other things related to the electrical conductivity and thermo tolerance properties of that specific material. Hence, the electrosurgical tissue effects of gelatin and agar were tested and compared to that of pork tissue. The agar phantoms showed realistic tissue effects similar to pork muscle, namely local incisions without much thermal spread, whereas the gelatin phantoms showed unrealistic tissue effects, namely widespread melting accompanied by bubbles and incisions that melted together. Similar results were seen with pure agar and gelatin samples. Hence, the cause for the differences in result between the gelatin and agar phantoms, is probably due to a difference in thermo tolerance, namely a low melting point of pure gelatin (35 °C) and a high melting point of pure agar (85 °C). More specifically, the temperature in the vicinity of the electrosurgical cut, mounted up above the melting temperature of the gelatin phantoms, but not above the melting temperature of the agar phantoms. However, to make sure of this, further research should be done with regard to the exact melting temperatures and thermal distribution of the phantoms with electrosurgery. In case gelatine's low melting temperature is indeed the cause for widespread melting with electrosurgery, formaldehyde could be added, which increases the melting temperature of gelatine^{101,172}. Nevertheless, for now, solely the agar phantoms meet requirement 9 and 10, therefore enabling realistic tissue effects when using the electrosurgical knife.

For this thesis project, these qualitative results are promising enough to meet the concerning requirements. However, to determine the actual cause for the observed phantom tissue effects, not only on the melting point and thermal distribution, but also the electrical conductivity and other thermo tolerance properties (specific heat and thermal conductivity) should be determined. Hence, for further research it is recommended to measure and quantify the aforementioned phantom properties, to find out what exactly caused the observed tissue effects.

Research contribution research phase 2 – Most potential phantoms

Until now, no similar device to the SESK was developed, more importantly, no test phantom was produced that combined all the aforementioned properties, relevant for intraoperative tumour phantom resection with the SESK. Concerning the observed electrosurgical tissue effects, the second contribution is as follows:

Agar is whereas gelatin is not, a promising material for producing phantoms with electrosurgical tissue effects similar to human breasts.

21.1.3 Research Phase 3 – Contrast Agent

The goal of this research phase was to further develop the most potential agar phantoms with regard to the pre- and postoperative margin assessment requirements (requirement 4 and 11), without interfering with the IMA requirements (5-10). The most potential agar phantoms are the healthy (50F/50W+5%agar) and tumour (20F/80W+3%agar) agar phantom. It was found that adding 5% of barium sulphate to the tumour phantom, enables pre- and postoperative X-ray margin assessment, without interfering with the IMA requirements.

Requirement 4: A contrast between tumour and healthy phantom tissue which is assessable preoperatively.

Requirement 11: A contrast between tumour and healthy phantom tissue which is assessable postoperatively.

The pre- and postoperative margin assessment requirements state that preoperatively, the tumour phantom location, size and border should be assessable, whereas postoperatively, residual tumour phantom should be detectable. With the help of literature, it was found that adding barium sulphate to tumour phantom, would enable imaging modalities such as radiography (X-ray), to sufficiently assess the tumour phantom pre- and postoperatively. As a result, various concentrations of barium sulphate in combination with the tumour phantom were tested qualitatively on its X-ray contrast. It was found that the minimum required concentration of barium sulphate, to show a sufficient contrast on the X-ray images between the tumour and healthy agar phantom, was 5% by weight of water. Hence, 5% of barium sulphate added to the tumour phantom, enables sufficient contrast between the tumour and healthy tissue phantom, therefore meeting requirement 4 and 11.

However, one major study limitation is that solely tumour phantoms with a thickness of 10 mm were tested. Perhaps 5% of barium sulphate by weight of water does not show enough X-ray contrast with a tumour thickness much smaller than 10 mm. Hence for further research, tumours much smaller than 10 mm should be tested, to see whether 5% of barium sulphate still shows enough X-ray contrast. Furthermore, this study used a CT-scan, which has a spatial resolution of approximately 0.7 lines per mm. Hence postoperatively, tumour phantom residue smaller than 1.43 mm, cannot be distinguished from the healthy phantom. Perhaps for further research, the validation study should use film-screen mammography, which also uses X-rays, but has a spatial resolution of 15 lines per mm, thus enables phantom residue detection as small as 0.067 mm¹⁵⁹. Finally, with this study, the X-ray images were compared qualitatively, which is open for interpretation. Hence, for further research quantitative tests could be done that acquire the HU values of the obtained X-ray images, making the comparison between the images less subjective. Nevertheless, all in all, the results are promising enough since this thesis project solely functions as a proof of concept for the validation study.

IMA requirements (5-10).

5% of barium sulphate added to the tumour phantom showed sufficient X-ray contrast. However, it is a requisite that adding barium sulphate to the tumour phantom, cannot interfere with the earlier obtained IMA requirements. As a result, the barium sulphate tumour phantom was similar to the most potential agar and gelatin phantoms, tested on the visual properties by visual inspection, -mechanical properties by compression tests, -F/W-ratio by DRS tests and -electrically conductive- and thermo tolerance properties by looking at the electrosurgical tissue effects. Hence, the earlier discussed study limitations (21.1.2) also apply here. However, some additional study limitations popped up, which will be discussed here.

Visual inspection showed 5% of barium sulphate added to the tumour phantom, was visually even more similar to the healthy phantom tissue, than without BaSO₄, therefore meeting requirement 8. In line with literature, compression tests showed that the tumour phantom with 5% of barium sulphate, slightly increased the stiffness of the phantom^{160,161,162}. However, the stiffness was still realistic and sufficiently similar to the healthy phantom tissue, therefore meeting requirement 6 and 7. With regard to the DRS tests, in line with literature, barium sulphate increased the absorption of the materials it is mixed with, namely fat and water¹⁶⁸. However, due to the Corona virus, all testing facilities were closed, therefore no DRS tests and thus conclusions could be drawn with regard to the exact optical properties of pure barium sulphate. Nevertheless, great intra-sample homogeneity and -inter-sample consistency was found. Furthermore, a significant difference in F/W-ratio, between the healthy and barium sulphate tumour phantom was found. Hence, the results were promising enough to meet requirement 5. Finally, with electrosurgery, realistic haptic feedback and -tissue effects were found. Hence, 5% of barium sulphate added to the agar tumour phantom, not only provides enough X-ray contrast to meet the pre- and postoperative requirements, but also does not interfere with the previously obtained IMA requirements (5-10).

Research contributions research phase 3 – BaSO₄ Contrast Agent

Previous studies already showed that barium sulphate is a good contrast agent and increases the absorption and stiffness of the materials it is mixed with ^{156,160,161,162,168}. With regard to the electrosurgical tissue effects, little can be said, since the tumour phantom not only contains barium sulphate, but also agar, which as stated earlier, contributed a lot to the favourable electrosurgical tissue effects of the phantom. Hence, with regard to research phase 3, no significant research contribution could be found.

21.1.4 Research Phase 4 – Final Phantom

In the final research phase, a production method was found that successfully combines the healthy and tumour phantom into the final phantom, namely a breast-shaped phantom with a realistic size and shape. The final phantom turned out to be inexpensive and easy to produce while being, homogeneous, consistent and durable. As a result, the final phantom meets all phantom requirements, enabling extensive testing and further validation of the SESK.

Research contributions research phase 4 – Most potential phantoms

In the last research phase, the healthy and tumour phantom were combined into the final phantom, enabling the design of a study similar to BCS, therefore enabling extensive SESK testing and further validation of the SESK. Hence, the final research contribution is as follows:

A sufficient production method has been found that enables agar, lard, water and barium sulphate, to be mixed into a phantom, that enables validation of the SESK.

21.2 Recommendations

This section contains the recommendations for further research based on the findings obtained during this research project. Seven main topics are interesting for follow-up research.

21.2.1 Final Phantom Stability

Although the overall findings are promising, this thesis project solely functions as a proof of concept for the final phantom. To finalize whether the phantom could indeed be used for the validation study, further research should be done concerning the phantom F/W-ratio stability with electrosurgery.

F/W-ratio and electrosurgical cutting.

The results show the final phantom has similar to real breasts, a significant difference in F/W-ratio between the tumour and healthy phantom. Based on this F/W-ratio difference, the final phantom enables us to intraoperatively test DRS with its capability in discriminating healthy from tumour tissue. However, electrosurgery significantly alters the tissue composition ^{7,8}. Hence, perhaps with electrosurgery, the F/W-ratio will be altered. Obviously, this would obstruct the F/W-ratio reliability, making the phantom unsuitable for the validation study. Hence, further research should be done with regard to the final phantom F/W-ratio stability, as a result of electrosurgery.

21.2.2 X-ray

Contrast

Chapter 16 showed the minimum required concentration of BaSO₄ showing a sufficient X-ray contrast, was 5% by weight of water. However, as stated in paragraph 21.1.3, solely tumour phantoms with a thickness of 10 mm were tested. Since tumours can be much smaller than 10 mm, further research should be done to see whether 5% of barium sulphate, still shows enough X-ray contrast with tumours much smaller than 10 mm.

Spatial resolution

During this thesis project, a CT scan was used which has a spatial resolution of approximately 0.7 lines per mm. Hence postoperatively, tumour phantom residue smaller than 1.43 mm, cannot be distinguished from the healthy phantom. Hence with the validation study, it is recommended to use an X-ray system with a higher spatial resolution such as film-screen mammography. Namely, film screen mammography has a spatial resolution of 15 lines per mm, thus enables phantom residue detection as small as 0.067 mm, which would make the validation study more realistic ¹⁵⁹.

CT-number (HU-values)

In chapter 16, the X-ray images of the tumours including BaSO₄ were compared to each other qualitatively. Hence, to eliminate the evaluation subjectivity, further research should include quantitative tests that compare the HU values of the obtained X-ray images.

21.2.3 Validation study

If the final phantom indeed shows F/W-ratio stability after electrosurgery, and sufficient X-ray contrast for small tumours, the validation study can take place. Hence, further research should include the validation study, which tests whether the SESK is a better alternative for BCS than the ESK. More specifically, compared to the ESK, it has to be found whether or not, the SESK reduces the percentage of positive margins found post-operatively. See chapter 4 for a more elaborate explanation. Finally, similar to Pleijhuis et al., it is recommended to use realistic tumour inclusions with different shapes and sizes, which are placed at various depths ¹⁰⁶.

21.2.4 Electrical Conductivity and Thermo tolerance

The tissue effects as a result of electrosurgery are among other things related to the electrical conductivity and thermo tolerance properties of that specific material. Hence, during this thesis project, the electrosurgical tissue effects of gelatin and agar were tested and compared to that of pork tissue. It turned out that the agar-based phantoms showed realistic tissue effects, namely local incisions without much thermal spread, whereas the gelatin-based phantoms did not show realistic tissue effects, namely widespread melting accompanied by bubbles. Hence, it was concluded that agar does whereas gelatin does not meet the electrical conductivity and thermo tolerance properties (9 & 10). However, the electrical conductivity and thermo tolerance properties (melting point, specific heat and thermal conductivity) were not actually measured and quantified. Hence, further research should be done quantifying these phantom properties, to make sure what the actual cause is for the observed tissue effects.

21.2.5 Workflow and Work speed

With the validation study, surgeons will use the SESK to obtain DRS measurements of the phantom, while trying to dissect the tumour. However, the exact influence of DRS added to the ESK on the workflow and work speed is still unknown. Therefore, it is recommended that with the validation study, the following is analysed, namely the intraoperative interaction between DRS data processing and electrosurgical cutting of the surgeon. More specifically, compared to a traditional BCS procedure, alterations in the workflow or work speed, as a result of DRS added to the ESK, have to be analysed. C. van Gent provided a detailed overview of the complete surgical workflow of a traditional BCS, thus can be used as a reference ¹².

21.2.6 Ideal Phantom Materials

Although the final phantom shows great homogeneity and consistency concerning the fat and water concentration, the accuracy of the estimates was suboptimal. Namely, water was slightly whereas fat was significantly overestimated. This was likely due to agar's influence on the fat absorption peak (1211 nm), and barium sulphate's influence on the absorption of the materials it is mixed with, namely fat and water ¹⁶⁸.

Concerning agar, this is somewhat unexpected, since literature shows agar does not have any influence on the fat and water estimates ^{103,111,14}. However, in contrast to literature, cheap impurified agar (Terrasana ¹¹³) from the local food store, instead of expensive purified agar from Sigma Aldrich was used, which most likely caused the differences in results ¹⁰³. Nevertheless, though the current phantom meets all phantom requirements, perhaps, with further research F/W-ratio adjustments have to be made, making these inaccuracies impractical. Hence, for further research, it is recommended to use purified agar from Sigma Aldrich, to improve the accuracy of the fat and water estimates. Concerning barium sulphate, little is known with regard to the influence of barium sulphate on the NIR absorption. Solely one study was found which showed that barium sulphate influences the absorption of the materials it is mixed with ¹⁶⁸. Hence, further research should be done concerning the absorption of barium sulphate in the NIR region. In case the results are disappointing, perhaps other contrast agents such as Iodine could be used and tested ¹⁷³.

21.2.7 Durability & stability

In chapter 20, qualitative tests were done with regard to the durability and stability of the phantoms. In line with literature, the results showed both healthy and tumour phantoms are homogeneous and mold-free until week two ^{13,111,171,156}. This lifetime of 2 weeks is sufficient enough to meet the concerning durability and stability requirement. Namely, it enables the phantom to be stored for a sufficient amount of time before being used. However, these results are qualitative, therefore simply speculative. Further research in the form of quantitative tests such as compression- and DRS tests are required to determine the durability and stability of the phantom properties. In case these results are disappointing, further phantom development could include preservatives such as sodium benzoate or natrium azide to improve the durability of the phantom ^{14,104,136}.

22. Final Conclusion

Previous studies show that the SESK, which adds DRS to the traditional ESK, is a promising technique for BCS, namely it enables real-time tissue characterization while cutting. More specifically, it adds DRS to the traditional ESK, enabling intraoperative healthy from malignant tissue discrimination, therefore potentially reducing the re-excision rate with BCS procedures. However, the SESK cannot be used on patients yet since it has not been validated yet. Several studies suggest that phantoms are ideal for validation of systems including imaging systems like DRS. Hence, developing a phantom that mimics the properties of healthy and malignant breast tissue, would be ideal. This makes it possible to do extensive research and enables for validation of the SESK. At the moment there is not such a breast phantom yet, hence the objective of this master thesis is:

Develop a breast phantom that enables validation of the smart electrosurgical knife.

In order to see whether the objective is obtained, three research questions were formulated. The answers to these research questions will also determine whether the research objective is obtained.

Validation Study

1. What are the requirements of a study that enables validation of the smart-electrosurgical knife?

Inspired by the study of Pleijhuis et al., it was found that a study that enables validation of the SESK should be constructed as follows¹⁰⁴; surgeons have to conduct BCS with both the SESK and the traditional ESK on tissue-simulating phantoms including a tumour, and see whether surgeons who use the SESK, consistently obtain a higher percentage of negative margins than when using the traditional ESK. Only then the SESK is more promising than the traditional ESK, therefore validating its purpose.

Hence, in order to test and validate the SESK, the validation study should mimic a BCS, which includes pre-, intra- and postoperative margin assessment. Hence, the validation study should be constructed as follows; preoperatively, the tumour phantom size, border and location will be assessed, intraoperatively, tumour phantom resection will take place, with the help of the SESK(DRS) or ESK, but without any other IMA technique, and postoperatively, residual tumour inspection will take place, to compare the results of the experimental group (SESK) to the results of the control group (ESK). Since the validation study requirements are defined, it is now necessary to develop a breast phantom that enables such a validation study.

Phantom Requirements

2. What are the requirements of a phantom that enables such a validation study?

To sufficiently mimic a BCS, the phantom should have a similar size and shape as a human breast containing a tumour. With regard to pre- and postoperative margin assessment, the phantom should have a contrast between the tumour and healthy phantom, which enables size, border and location assessment of the phantom tumour upfront and residual tumour inspection after surgery. Intraoperatively, the phantom should have a significant difference in F/W-ratio between the tumour and healthy phantom. This enables us to assess DRS with its capability in discriminating healthy from malignant tissue. Furthermore, visually and mechanically, there should be a minimal difference between the tumour and healthy phantom, which eliminates the possibility of using the other IMA techniques, namely palpation and visual inspection. Finally, the phantom should have similar mechanical- electrically conductive and thermo tolerance properties as real breast tissue. This will result in realistic haptic feedback and tissue effects with electrosurgery.

Final Phantom

3. Is it possible to produce a phantom that meets the phantom requirements?

During this thesis project, various F/W-ratios of water and lard, in combination with various materials such as guar gum, agar, gelatin and barium sulphate, were produced and tested with regard to the aforementioned phantom requirements. It turned out that agar in combination with water, lard and the contrast agent barium sulphate, enables breast phantom production, that meets all phantom requirements. More specifically, the final phantom is a breast-shaped phantom with a realistic size and shape, consisting of healthy tissue with a tumour inclusion. The healthy tissue is composed of 50% lard, 50% water and then 5% agar by weight of water, whereas the tumour is composed of 20% lard, 80% water and then 3% agar- and 5% barium sulphate by weight of water. Since this phantom meets all phantom requirements, the thesis objective is reached, namely it enables the design of a study that subsequently enables extensive testing and further validation of the SESK.

References

1. Adank, M. W., Fleischer, J. C., Dankelman, J. & Hendriks, B. H. W. Real-time oncological guidance using diffuse reflectance spectroscopy in electrosurgery: the effect of coagulation on tissue discrimination. *J. Biomed. Opt.* **23**, (2018).
2. Bray, F. *et al.* Global cancer statistics 2018: GLOBOCAN estimates of incidence and mortality worldwide for 36 cancers in 185 countries. *CA. Cancer J. Clin.* **68**, 394–424 (2018).
3. Bleicher, R. J. *et al.* Breast conservation versus mastectomy for patients with T3 primary tumors (>5 cm): A review of 5685 medicare patients. *Cancer* **122**, 42–49 (2015).
4. de Boer, L. L. *et al.* Fat/water ratios measured with diffuse reflectance spectroscopy to detect breast tumor boundaries. *Breast Cancer Res. Treat.* **152**, 509–518 (2015).
5. Sharma, V. *et al.* Auto-fluorescence lifetime and light reflectance spectroscopy for breast cancer diagnosis: potential tools for intraoperative margin detection. *Biomed. Opt. Express* **3**, 1825 (2012).
6. St John, E. R. *et al.* Diagnostic Accuracy of Intraoperative Techniques for Margin Assessment in Breast Cancer Surgery. *Ann. Surg.* **265**, 300–310 (2016).
7. Adank, M. W. Evaluation of a smart electrosurgical knife – Reflectance Spectroscopy in breast conserving surgery .
8. Fleischer, J., Hendriks, H. W. & Dankelman, J. Integration of tissue-sensing into electrosurgical instruments. (2015).
9. Adank, M. W. Assessing the added value of diffuse reflectance spectroscopy in electrosurgery. (2016).
10. Mollerus, F. C. S. The integration of diffuse reflectance spectroscopy into the electrosurgical knife used during breast-conserving surgery - Establishing the most promising intraoperative margin assessment technique and the design considerations for this integration. 1–145
11. Mollerus, F. C. S. The integration of diffuse reflectance spectroscopy into the electrosurgical knife used during breast-conserving surgery - Determining and overcoming the challenge of tissue debris adhering to the ‘smart’ electrosurgical knife.
12. van Gent, C. M. Exploring methods to prevent tissue debris adhering to t he ‘ smart ’ electrosurgical knife.
13. Michaelsen, K. E. *et al.* Anthropomorphic breast phantoms with physiological water , lipid , and hemoglobin content for near-infrared spectral tomography water , lipid , and hemoglobin content for near-infrared spectral tomography. (2014). doi:10.1117/1.JBO.19.2.026012
14. Bush, E. C. *et al.* Fat-water phantoms for magnetic resonance imaging validation: A flexible and scalable protocol. *J. Vis. Exp.* **2018**, 1–9 (2018).
15. Carlander, J. *et al.* Comparison of experimental nerve injury caused by ultrasonically activated scalpel and electrosurgery. *Br. J. Surg.* **92**, 772–777 (2005).
16. Advincula, A. P. & Wang, K. The evolutionary state of electrosurgery: Where are we now? *Curr. Opin. Obstet. Gynecol.* **20**, 353–358 (2008).

17. Gallagher, K., Dhinsa, B. & Miles, J. Electrosurgery. 70–72 (2011). doi:10.1201/9781315162478
18. Mccauley, G. Understanding electrosurgery. (2010).
19. Bisinotto, F. M. B. *et al.* Burns related to electrosurgery – Report of two cases. *Brazilian J. Anesthesiol.* **67**, 527–534 (2017).
20. Carr-Locke, D. L. & Day, J. Principles of Electrosurgery. *Success. Train. Gastrointest. Endosc.* 125–134 (2011). doi:10.1002/9781444397772.ch11
21. Feldman, L. S., Fuchshuber, P. R. & Jones, D. B. *The SAGES Manual on the Fundamental Use of Surgical Energy (FUSE)*.
22. Dwehirst, M. W., Viglianti, B. L., Lora-Michiels, M., Hoopes, P. J. & Hanson, M. Thermal Dose Requirement for Tissue Effect. **16**, 338–348 (2014).
23. Grootendorst, M. R., Cariati, M., Kothari, A., Tuch, D. S. & Purushotham, A. Cerenkov luminescence imaging (CLI) for image-guided cancer surgery. *Clin. Transl. Imaging* **4**, 353–366 (2016).
24. Gent, C. M. Van. Colloquiem - Exploring methods to prevent tissue debris adhering to the smart electrosurgical knife. (2018).
25. Breast-conserving Surgery (Lumpectomy) | BCS Breast Surgery. Available at: <https://www.cancer.org/cancer/breast-cancer/treatment/surgery-for-breast-cancer/breast-conserving-surgery-lumpectomy.html>. (Accessed: 27th February 2019)
26. Breast-Conserving Surgery | Johns Hopkins Medicine Health Library. Available at: https://www.hopkinsmedicine.org/healthlibrary/test_procedures/gynecology/breast-conserving_surgery_92,p07789. (Accessed: 27th February 2019)
27. Hunt, K. K., Smith, B. D. & Mittendorf, E. A. The Controversy Regarding Margin Width in Breast Cancer: Enough is Enough. *Ann. Surg. Oncol.* **21**, 701–703 (2014).
28. Surgical Margins | Breastcancer.org. Available at: <https://www.breastcancer.org/symptoms/diagnosis/margins>. (Accessed: 6th March 2019)
29. Evers, D. J., Hendriks, B. H. W. & Ruers, T. J. M. Optical spectroscopy: current advances and future applications in cancer diagnostics and therapy. (2012). doi:10.2217/fon.12.15
30. Evers, D. J. *Optical sensing for tissue differentiation*. (2014).
31. Keersop, A. T. M. H. Van, Nachabe, R., Hendriks, B. H. W., Mueller, M. & Bydlon, T. PhotonicNeedle Spectral Analysis User manual. (2011).
32. Bydlon, T. M., Nachabé, R., Ramanujam, N., Sterenborg, H. J. C. M. & Hendriks, B. H. W. Chromophore based analyses of steady-state diffuse reflectance spectroscopy : current status and perspectives for clinical adoption. **24**, 9–24 (2015).
33. Taroni, P. *et al.* Breast tissue composition and its dependence on demographic risk factors for breast cancer: Non-invasive assessment by Time Domain diffuse optical spectroscopy. *PLoS One* **10**, 1–16 (2015).
34. Jacques, S. L. Optical properties of biological tissues : a review. (2013). doi:10.1088/0031-9155/58/14/5007
35. Evers, D. J. *et al.* Diffuse reflectance spectroscopy: Towards clinical application in breast cancer. *Breast Cancer Res. Treat.* **137**, 155–165 (2013).

36. Brown, J. Q., Vishwanath, K., Palmer, G. M. & Ramanujam, N. Advances in quantitative UV-visible spectroscopy for clinical and pre-clinical application in cancer. *Curr. Opin. Biotechnol.* **20**, 119–131 (2009).
37. Prabitha, V. G. *et al.* Detection of cervical lesions by multivariate analysis of diffuse reflectance spectra : a clinical study. 67–75 (2016). doi:10.1007/s10103-015-1829-z
38. BREAST ANATOMY AND PHYSIOLOGY - Ultrasound Registry Review. Available at: <https://ultrasoundregistryreview.com/BreastTrial4.html>. (Accessed: 17th April 2019)
39. Ismail Jatoi & Rody, A. *Management of Breast Diseases*. (2010).
40. Definition of breast lobe - NCI Dictionary of Cancer Terms - National Cancer Institute. Available at: <https://www.cancer.gov/publications/dictionaries/cancer-terms/def/breast-lobe>. (Accessed: 16th April 2019)
41. Overview of the Breast - Breast Cancer | Johns Hopkins Pathology. Available at: <https://pathology.jhu.edu/breast/basics/overview>. (Accessed: 3rd April 2019)
42. Chapter 12. Breast Disease | Williams Gynecology, 2e | AccessMedicine | McGraw-Hill Medical. Available at: <https://accessmedicine.mhmedical.com/content.aspx?bookid=399§ionid=41722300>. (Accessed: 18th April 2019)
43. Jesinger, R. A. Breast anatomy for the interventionalist. *Tech. Vasc. Interv. Radiol.* **17**, 3–9 (2014).
44. Hassiotou, F. & Geddes, D. Anatomy of the human mammary gland: Current status of knowledge. *Clin. Anat.* **26**, 29–48 (2013).
45. Ellis, H. Anatomy and physiology of the breast. *Surgery* **31**, 11–14 (2013).
46. Marshall. Anatomy & Physiology. *EggMeat Symp.* **3**, 1–12 (2011).
47. Patient education: Breast cancer guide to diagnosis and treatment (Beyond the Basics) - UpToDate. Available at: https://www.uptodate.com/contents/breast-cancer-guide-to-diagnosis-and-treatment-beyond-the-basics/print?source=related_link. (Accessed: 5th May 2019)
48. DeSantis, C. E., Ma, J., Goding Sauer, A., Newman, L. A. & Jemal, A. Breast cancer statistics, 2017, racial disparity in mortality by state. *CA. Cancer J. Clin.* **67**, 439–448 (2017).
49. Types of Breast Cancer | Different Breast Cancer Types. Available at: <https://www.cancer.org/cancer/breast-cancer/understanding-a-breast-cancer-diagnosis/types-of-breast-cancer.html>. (Accessed: 6th March 2019)
50. NCI Dictionary of Cancer Terms - National Cancer Institute. Available at: <https://www.cancer.gov/publications/dictionaries/cancer-terms/search?contains=false&q=BREAST+CANCER>. (Accessed: 6th March 2019)
51. Surgery, B. Breast Cancer Surgery Patient Handbook.
52. Types of Breast Cancer - Breast Cancer | Johns Hopkins Pathology. Available at: <https://pathology.jhu.edu/breast/my-results/types-of-breast-cancer/>. (Accessed: 15th April 2019)
53. Siziopikou, K. P. Ductal carcinoma in situ of the breast: Current concepts and future directions. *Arch. Pathol. Lab. Med.* **137**, 462–466 (2013).
54. Cutuli, B. *et al.* Lobular carcinoma in situ (LCIS) of the breast: Is long-term outcome similar to ductal

- carcinoma in situ (DCIS)? Analysis of 200 cases. *Radiat. Oncol.* **10**, 1–7 (2015).
55. Miller, K. D. *et al.* Cancer treatment and survivorship statistics, 2016. *CA. Cancer J. Clin.* **66**, 271–89 (2016).
 56. de Boer, L. L. *et al.* Using DRS during breast conserving surgery : identifying robust optical parameters and influence of inter-patient variation. **7**, 6141–6152 (2016).
 57. Wang, J. *et al.* In vivo quantitative imaging of normal and cancerous breast tissue using broadband diffuse optical tomography. (2010). doi:10.1118/1.3455702
 58. Shah, N. *et al.* Spatial variations in optical and physiological properties of healthy breast tissue. *J. Biomed. Opt.* **9**, 534 (2004).
 59. Berckel, P. van. Developing tissue mimicking breast phantoms for validating the smart electrosurgical knife. (2019).
 60. Blackmore, K. M., Knight, J. A., Walter, J. & Lilge, L. The Association between Breast Tissue Optical Content and Mammographic Density in Pre- and Post-Menopausal Women. 1–16 (2015). doi:10.1371/journal.pone.0115851
 61. Spinelli, L. *et al.* Bulk optical properties and tissue components in the female breast from multiwavelength time-resolved optical mammography. *J. Biomed. Opt.* **9**, 1137 (2004).
 62. Intes, X. Time-domain optical mammography SoftScan: Initial results. *Acad. Radiol.* **12**, 934–947 (2005).
 63. Cerussi, A. E. *et al.* Sources of absorption and scattering contrast for near-infrared optical mammography. *Acad. Radiol.* **8**, 211–218 (2001).
 64. Shah, N. *et al.* Noninvasive functional optical spectroscopy of human breast tissue. *Proc. Natl. Acad. Sci.* **98**, 4420–4425 (2001).
 65. Poplack, S. P. *et al.* Electromagnetic Breast Imaging: Average Tissue Property Values in Women with Negative Clinical Findings. *Radiology* **231**, 571–580 (2004).
 66. Durduran, T. *et al.* Bulk optical properties of healthy female breast tissue. (2002).
 67. Cerussi, A. E. *et al.* Spectroscopy enhances the information content of optical mammography. *J. Biomed. Opt.* **7**, 60 (2002).
 68. O’Sullivan, T. D. *et al.* Optical imaging correlates with magnetic resonance imaging breast density and reveals composition changes during neoadjuvant chemotherapy. *Breast Cancer Res.* **15**, 1–15 (2013).
 69. Bydlon, T. M. Intra-operative Assessment of Breast Tumor Margins Using Diffuse Reflectance Spectroscopy by. 1–173 (2012).
 70. Grosenick, D. *et al.* Review of optical breast imaging and spectroscopy. **21**, (2016).
 71. Spinelli, L., Torricelli, A., Pifferi, A. & Taroni, P. Characterization of female breast lesions from multi-wavelength time-resolved optical mammography. (2005). doi:10.1088/0031-9155/50/11/004
 72. Nachabé, R. Diagnosis with near infrared spectroscopy during minimally invasive procedures. *J. Biomed. Opt.* (2012).
 73. Leproux, A. *et al.* Differential diagnosis of breast masses in South Korean premenopausal women using diffuse optical spectroscopic imaging Differential diagnosis of breast masses in South Korean

- premenopausal women using diffuse optical spectroscopic imaging. **21**, (2016).
74. Cerussi, A. *et al.* In vivo absorption , scattering , and physiologic properties of 58 malignant breast tumors determined by broadband diffuse optical spectroscopy. **11**, 1–16 (2006).
 75. Wang, J., Pogue, B. W., Jiang, S. & Paulsen, K. D. Near-infrared tomography of breast cancer hemoglobin, water, lipid, and scattering using combined frequency domain and cw measurement. *Opt. Lett.* **35**, 82 (2010).
 76. Zhu, C., Palmer, G. M., Breslin, T. M., Harter, J. & Ramanujam, N. Diagnosis of breast cancer using fluorescence and diffuse reflectance spectroscopy: a Monte-Carlo-model-based approach. *J. Biomed. Opt.* **13**, 034015 (2008).
 77. Grosenick, D. *et al.* Time-domain scanning optical mammography: II. Optical properties and tissue parameters of 87 carcinomas. (2005). doi:10.1088/0031-9155/50/11/002
 78. Fang, Q. *et al.* Combined Optical and X-ray Tomosynthesis Breast Imaging. **258**, 89–97 (2011).
 79. Quarto, G. *et al.* Optical discrimination between malignant and benign breast lesions. **953814**, (2015).
 80. Anderson, P. G., Kainerstorfer, J. M. & Sassaroli, A. Broadband Optical Mammography : Chromophore Concentration and Hemoglobin Saturation Contrast in Breast Cancer. 1–23 (2015). doi:10.1371/journal.pone.0117322
 81. Choe, R., Konecky, S. D. & Corlu, A. Differentiation of benign and malignant breast tumors by in-vivo parallel-plate diffuse optical tomography. **14**, 1–18 (2009).
 82. Zhang, Y. *et al.* Visible and near-infrared spectroscopy for distinguishing malignant tumor tissue from benign tumor and normal breast tissues in vitro . *J. Biomed. Opt.* **18**, 077003 (2013).
 83. Zhu, Q. *et al.* Early-Stage Invasive Breast Cancers: Potential Role of Optical Tomography with US Localization in Assisting Diagnosis. **256**, (2010).
 84. Lamouche, G. *et al.* Review of tissue simulating phantoms with controllable optical, mechanical and structural properties for use in optical coherence tomography. *Biomed. Opt. Express* **3**, 1381 (2012).
 85. Gefen, A. & Dilmoney, B. Mechanics of the normal woman’s breast. *Technol. Health Care* **15**, 259–71 (2007).
 86. Encyclopaedia-Britannica. Young’s Modulus.
 87. Ramião, N. G. *et al.* Biomechanical properties of breast tissue, a state-of-the-art review. *Biomech. Model. Mechanobiol.* **15**, 1307–1323 (2016).
 88. Krouskop, T. A., Wheeler, T. M., Kallel, F., Garra, B. S. & Hall, T. Elastic Moduli of Breast and Prostate Tissues Under Compression. **274**, 260–274 (1998).
 89. Wellman, P. S., Howe, R. D., Dalton, E. & Kern, K. A. Breast Tissue Stiffness in Compression is Correlated to Histological Diagnosis. 1–15 (1999).
 90. Samani, a, Bishop, J., Yaffe, M. J. & Plewes, D. B. Biomechanical 3-D finite element modeling of the human breast using MRI data - Medical Imaging, IEEE Transactions on. *IEEE Trans. Med. Imaging* **20**, 271–279 (2001).
 91. Samani, A., Zubovits, J. & Plewes, D. Elastic moduli of normal and pathological human breast tissues: An inversion-technique-based investigation of 169 samples. *Phys. Med. Biol.* **52**, 1565–1576 (2007).

92. Samani, A. & Plewes, D. An inverse problem solution for measuring the elastic modulus of intact ex vivo breast tissue tumours. *Phys. Med. Biol.* **52**, 1247–1260 (2007).
93. Sarvazyan, A. P. *et al.* Biophysical Bases of Elasticity Imaging. in 223–240 (Springer, Boston, MA, 1995). doi:10.1007/978-1-4615-1943-0_23
94. Matsumura, T., Umemoto, T. & Fujihara, Y. Measurement of Elastic Property of Breast Tissue for Elasticity Imaging. 1451–1454 (2009).
95. Umemoto, T. *et al.* Ex vivo and in vivo assessment of the non-linearity of elasticity properties of breast tissues for quantitative strain elastography. *Ultrasound Med. Biol.* **40**, 1755–1768 (2014).
96. Resistance and Resistors. Available at: <https://courses.lumenlearning.com/boundless-physics/chapter/resistance-and-resistors/>. (Accessed: 6th June 2019)
97. Resistivity and Electrical Conductivity Basic Electronics Tutorials. Available at: <https://www.electronics-tutorials.ws/resistor/resistivity.html>. (Accessed: 6th June 2019)
98. Tiang, S. S., Sadoon, M., Zanoon, T. F., Ain, M. F. & Abdullah, M. Z. Radar Sensing Featuring Biconical Antenna and Enhanced Delay and Sum Algorithm for Early Stage Breast Cancer Detection. (2013).
99. Xiao, X. & Kikkawa, T. Study on the Breast Cancer Detection by UWB Microwave Imaging. 8–11 (2008).
100. Jones, D. B. Safe energy use in the operating room. **52**, 447–468 (2015).
101. Pogue, B. W. & Patterson, M. S. Review of tissue simulating phantoms for optical spectroscopy, imaging and dosimetry. **11**, 1–16 (2006).
102. Li, P., Yang, Z. & Jiang, S. Tissue mimicking materials in image-guided needle-based interventions: A review. *Mater. Sci. Eng. C* **93**, 1116–1131 (2018).
103. Quarto, G. *et al.* Comparison of organic phantom recipes and characterization by time-resolved diffuse optical spectroscopy. *Diffus. Opt. Imaging IV* **8799**, 879905 (2013).
104. Pleijhuis, R. G. *et al.* Near-infrared fluorescence (NIRF) imaging in breast-conserving surgery: Assessing intraoperative techniques in tissue-simulating breast phantoms. *Eur. J. Surg. Oncol.* **37**, 32–39 (2011).
105. Zhu, B. & Sevick-Muraca, E. M. A review of performance of near-infrared fluorescence imaging devices used in clinical studies. *Br. J. Radiol.* **88**, (2015).
106. Pleijhuis, R. G. *et al.* Obtaining adequate surgical margins in breast-conserving therapy for patients with early-stage breast cancer: Current modalities and future directions. *Ann. Surg. Oncol.* **16**, 2717–2730 (2009).
107. Pan, H. *et al.* Intraoperative Ultrasound Guidance Is Associated with Clear Lumpectomy Margins for Breast Cancer: A Systematic Review and Meta-Analysis. *PLoS One* **8**, 1–8 (2013).
108. Shipp, D. W. *et al.* Intra-operative spectroscopic assessment of surgical margins during breast conserving surgery. *Breast Cancer Res.* **20**, 1–14 (2018).
109. What is Incremental Development? | Agile Alliance. Available at: [https://www.agilealliance.org/glossary/incremental-development/#q=\(infinite~false~filters~\(postType~\(~/page~/post~/aa_book~/aa_event_session~/aa_experience_report~/aa_glossary~/aa_research_paper~/aa_video\)~tags~\(~/incremental*20development\)\)~searchTerm~/~sort~false~sortDirection~/asc~page~1\)](https://www.agilealliance.org/glossary/incremental-development/#q=(infinite~false~filters~(postType~(~/page~/post~/aa_book~/aa_event_session~/aa_experience_report~/aa_glossary~/aa_research_paper~/aa_video)~tags~(~/incremental*20development))~searchTerm~/~sort~false~sortDirection~/asc~page~1)). (Accessed: 16th February 2020)

110. All about the Iterative Design Process | Smartsheet. Available at: <https://www.smartsheet.com/iterative-process-guide>. (Accessed: 16th February 2020)
111. Ohmae, E. *et al.* Stable tissue-simulating phantoms with various water and lipid contents for diffuse optical spectroscopy. *Biomed. Opt. Express* **9**, 5792 (2018).
112. Original Superfoods Guargum Poeder 100 Gram - Unlimited Health. Available at: <https://unlimitedhealth.nl/nl/original-superfoods-guargum-poeder-100-gram>. (Accessed: 18th April 2020)
113. Assortiment | TerraSana Natuurvoeding. Available at: <http://www.terrasana.nl/nl/producten/groep/798/artcode/270.2060/>. (Accessed: 18th April 2020)
114. 8002-43-5 ▪ Lecithin, from Soybean ▪ 120-00832 ▪ 124-00835[Detail Information] | Laboratory Chemicals-FUJIFILM Wako Pure Chemical Corporation. Available at: <https://labchem-wako.fujifilm.com/asia/product/detail/W01W0112-0083.html>. (Accessed: 21st February 2020)
115. EL11 | Chempri.com. Available at: <https://www.chempri.com/nl/product-en/el11>. (Accessed: 21st February 2020)
116. EL 33 | Chempri.com. Available at: <https://www.chempri.com/nl/product-en/el-33>. (Accessed: 21st February 2020)
117. Zarai, Z., Balti, R., Sila, A., Ben Ali, Y. & Gargouri, Y. Helix aspersa gelatin as an emulsifier and emulsion stabilizer: Functional properties and effects on pancreatic lipolysis. *Food Funct.* **7**, 326–336 (2016).
118. Gomez-Guillen, M. C., Gimenez, B., Lopez-Caballero, M. E. & Montero, M. P. Functional and bioactive properties of collagen and gelatin from alternative sources: A review. *Food Hydrocoll.* **25**, 1813–1827 (2011).
119. Chen, A. I., Balter, M. L., Chen, M. I., Gross, D. & Maguire, T. J. Multilayered tissue mimicking skin and vessel phantoms with tunable mechanical , optical , and acoustic properties. (2016).
120. Functional properties | GELITA. Available at: <https://www.gelita.com/en/functions/functional-properties>. (Accessed: 7th March 2020)
121. Gelatine 250 bloom - Natural Spices. Available at: <https://www.naturalspices.eu/gelatine-250-bloom.html>. (Accessed: 18th April 2020)
122. Tris Buffered Saline BioUltra, tablet (for 500 mL), pH 7.6 | Sigma-Aldrich. Available at: <https://www.sigmaaldrich.com/catalog/product/sigma/94158?lang=en®ion=NL>. (Accessed: 18th April 2020)
123. Manickam, K., Reddy, R. & Seshadri, S. Characterization of biomechanical properties of agar based tissue mimicking phantoms for ultrasound stiffness imaging techniques. *J. Mech. Behav. Biomed. Mater.* **35**, 132–143 (2014).
124. Matsumura, T. *et al.* Measurement of elastic property of breast tissue for elasticity imaging. *Proc. - IEEE Ultrason. Symp.* 1451–1454 (2009). doi:10.1109/ULTSYM.2009.5442044
125. Farrell, T. J. & Patterson, M. S. A diffusion theory model of spatially resolved, steady-state diffuse reflectance for the noninvasive determination of tissue optical properties in vivo. (1992).
126. Nachabé, R., Hendriks, B. H. W., Voort, M. Van Der, Adrien, E. & Sterenborg, H. J. C. M. Estimation of biological chromophores using diffuse optical spectroscopy : benefit of extending the UV-VIS

wavelength range to include 1000 to 1600 nm. **18**, 879–888 (2010).

127. Nachabé, R., Hendriks, B. H. W., Desjardins, A. E., van der Voort, M. & van der Mark, M. B. Estimation of lipid and water concentrations in scattering media with diffuse optical spectroscopy from 900 to 1600 nm. **15**, 1–10 (2010).
128. Cook, J. R., Bouchard, R. R. & Emelianov, S. Y. Tissue-mimicking phantoms for photoacoustic and ultrasonic imaging. **2**, 2243–2254 (2011).
129. Dabbagh, A., Abdullah, B. J. J., Ramasindarum, C. & Abu Kasim, N. H. Tissue-mimicking gel phantoms for thermal therapy studies. *Ultrason. Imaging* **36**, 291–316 (2014).
130. Cubeddu, R., Pifferi, A., Taroni, P., Torricelli, A. & Valentini, G. A solid tissue phantom for photon migration studies Rinaldo. (1997).
131. Gabriel, C. Compilation of the Dielectric properties of body tissues at RF and Microwave Frequencies. (1995).
132. Halter, R. J. *et al.* experience. **30**, 1–23 (2010).
133. Suk, H. O. *et al.* Electrical conductivity images of biological tissue phantoms in MREIT. *Physiol. Meas.* **26**, (2005).
134. Marchal, C., Nadi, M., Tosser, A. J., Roussey, C. & Gaulard, M. L. Dielectric properties of gelatine phantoms used for simulations of biological tissues between 10 and 50. **5**, (1989).
135. Kandadai, M. A., Raymond, J. L. & Shaw, G. J. Comparison of electrical conductivities of various brain phantom gels: Developing a 'brain gel model'. *Mater. Sci. Eng. C* **32**, 2664–2667 (2012).
136. Kato, H., Hiraoka, M. & Ishida, T. An agar phantom for hyperthermia. *Med. Phys.* **13**, 396–398 (1986).
137. Ishida, T. & Kato, H. Muscle Equivalent Agar Phantoms for 13.56 MHz RF-induced Hyperthermia. (1980).
138. Yuan, Y. *et al.* A heterogeneous human tissue mimicking phantom for RF heating and MRI thermal monitoring verification. **57**, 2021–2037 (2010).
139. Shirsat, N., Lyng, J. G., Brunton, N. P. & McKenna, B. Ohmic processing: Electrical conductivities of pork cuts. *Meat Sci.* **67**, 507–514 (2004).
140. Henriques Jr., F. C. & Moritz, A. R. Studies of Thermal Injury. *Am. J. Pathol.* 530–549 (1946).
141. Liu, J. & Yang, R. Tuning the thermal conductivity of polymers with mechanical strains. 1–9 (2010). doi:10.1103/PhysRevB.81.174122
142. Zuluaga-Gomez, J., Zerhouni, N., Al Masry, Z., Devalland, C. & Varnier, C. A survey of breast cancer screening techniques: thermography and electrical impedance tomography. *J. Med. Eng. Technol.* **43**, 305–322 (2019).
143. Krokida, M. K., Panagiotou, N. M., Maroulis, Z. B. & Saravacos, G. D. Thermal conductivity: Literature data compilation for foodstuffs. *Int. J. Food Prop.* **4**, 111–137 (2001).
144. Menikou, G. & Damianou, C. Acoustic and thermal characterization of agar based phantoms used for evaluating focused ultrasound exposures. 1–14 (2017). doi:10.1186/s40349-017-0093-z
145. Porto, R. S. AgarGel : Agar-Agar : Properties and Specifications. Available at: <http://www.agargel.com.br/agar-tec-en.html>. (Accessed: 1st July 2019)

146. Holt, R. G. & Roy, R. A. Original Contribution CROSS-CORRELATION. *Medicine (Baltimore)*. **26**, 1525–1537 (2001).
147. Huang, J., Holt, R. G., Cleveland, R. O. & Roy, R. A. focused ultrasound heating in flow-through tissue phantoms. **116**, 2451–2458 (2014).
148. Will, J., Lovatt, S. J. & Amos, N. D. Additional Thermal Conductivity Values of Foods Measured by a Guarded Hot Plate f " p. **37**, (1998).
149. ASHRAE. THERMAL PROPERTIES OF FOODS. (2006).
150. Tucker, R. D. Monopolar and Bipolar Electrosurgery and Associated Problems. 149–177 (2003).
151. Rubesin, S. E. Upper gastrointestinal tract. *Radiol. Secrets Plus Third Ed.* 101–118 (2010). doi:10.1016/b978-0-12-802900-8.00011-7
152. Broder, J. & Preston, R. *Imaging the Head and Brain. Diagnostic Imaging for the Emergency Physician* (Elsevier, 2011). doi:10.1016/B978-1-4160-6113-7.10001-8
153. The Electromagnetic Spectrum | Boundless Physics. Available at: <https://courses.lumenlearning.com/boundless-physics/chapter/the-electromagnetic-spectrum/>. (Accessed: 4th April 2020)
154. Emadi, N., Safi, Y., Akbarzadeh Bagheban, A. & Asgary, S. Comparison of CT-number and gray scale value of different dental materials and hard tissues in CT and CBCT. *Iran. Endod. J.* **9**, 283–286 (2014).
155. CT number | definition of CT number by Medical dictionary. Available at: <https://medical-dictionary.thefreedictionary.com/CT+number>. (Accessed: 5th April 2020)
156. Litt, H. I. & Brody, A. S. BaSO₄-loaded agarose: A construction material for multimodality imaging phantoms. *Acad. Radiol.* **8**, 377–383 (2001).
157. Bariumsulfaat kopen. Available at: <https://www.hinmeijer.nl/product/118904/bariumsulfaat-99->. (Accessed: 9th April 2020)
158. Broder, J. *Imaging of Nontraumatic Abdominal Conditions. Diagnostic Imaging for the Emergency Physician* (Elsevier, 2011). doi:10.1016/B978-1-4160-6113-7.10009-2
159. Huda, W. & Brad Abrahams, R. X-ray-based medical imaging and resolution. *Am. J. Roentgenol.* **204**, W393–W397 (2015).
160. Ibrahim, R., Soeudy, E. & Kamal, A. M. INFLUENCE OF BARIUM SULFATE ON THE PHYSICAL , MECHANICAL , TRIBOLOGICAL PROPERTIES AND DYNAMIC BEHAVIOR OF A BRAKE LINING. (2010).
161. Wang, K., Wu, J., Ye, L. & Zeng, H. Mechanical properties and toughening mechanisms of polypropylene / barium sulfate composites. **34**, 1199–1205 (2006).
162. Ang, H. Y. *et al.* Radiopaque Fully Degradable Nanocomposites for Coronary Stents. 1–14 (2018). doi:10.1038/s41598-018-35663-2
163. Grum, F. & Luckey, G. W. Optical Sphere Paint and a Working Standard of Reflectance. *Appl. Opt.* **7**, 2289 (1968).
164. Radiologyinfo.org. Contrast Materials. (2018).
165. Light Scattering Grade Barium Sulfate. Available at: <https://www.prnewswire.com/news-releases/light-scattering-grade-barium-sulfate-248191361.html>. (Accessed: 5th April 2020)

166. Zhang, Y. *et al.* Distribution of fat droplets/particles and protein film components in batters of lean and back fat produced under controlled shear conditions. *CYTA - J. Food* **11**, 352–358 (2013).
167. Lindberg, J. D., Douglass, R. E. & Garvey, D. M. Absorption-coefficient-determination method for particulate materials. (1994).
168. Hadi, A. G. *et al.* Study the Effect of Barium Sulphate on Optical Properties of Polyvinyl Alcohol (PVA). **1**, 52–55 (2013).
169. Demo 26: Conductivity of Solutions. Available at: <https://chemistry.ucsd.edu/undergraduate/teaching-labs/demos/demo26.html>. (Accessed: 9th April 2020)
170. U.S. National Library of Medicine. Barium Sulfate.
171. Madsen, E. L., Frank, G. R. & Dong, F. Liquid or solid ultrasonically tissue-mimicking materials with very low scatter. *Ultrasound Med. Biol.* **24**, 535–542 (1998).
172. Hall, T. J., Bilgen, M., Insana, M. F. & Krouskop, T. A. Phantoms Materials for Elastography. **44**, (1997).
173. X-ray - Mayo Clinic. Available at: <https://www.mayoclinic.org/tests-procedures/x-ray/about/pac-20395303>.
174. Barium sulphate in medicine | Medicine Today. Available at: <http://medblog.medlink-uk.net/jackbrownmed/2017/05/01/barium-sulphate-in-medicine/>. (Accessed: 4th April 2020)

APPENDIX A: Parameter Confidence intervals

Table 46: Average estimated parameters and corresponding average confidence intervals of the most potential phantoms, barium sulphate (BS).

Phantom type	Fat/(Fat + Water)	Fat + Water	s800	b	fmie
60F/40W-30%Gelatin	66.4 ± 0.5	80.1 ± 4.4	19.9 ± 1.8	0.44 ± 0.16	0.96 ± 0.02
20F/80W-20%Gelatin	25.4 ± 1.0	94.1 ± 3.0	14.6 ± 0.6	0.56 ± 0.19	0.94 ± 0.02
50F/50W-5%Agar	61.6 ± 0.5	142.3 ± 2.4	15.8 ± 0.4	1.43 ± 0.11	1.00 ± 0.03
20F/80W-3%Agar	38.2 ± 0.8	123.3 ± 2.3	15.8 ± 0.4	1.43 ± 0.11	0.99 ± 0.03
20F/80W-3%Agar-5%BS	41.1 ± 1.0	150.7 ± 3.7	18.3 ± 0.5	1.42 ± 0.19	0.93 ± 0.06

APPENDIX B: Scientific Paper

An Agar-based Breast Phantom to Test and Validate the Smart Electrosurgical Knife

P.G.T. van Berckel¹, B.H.W. Hendriks^{1,2}, J. Dankelman¹

¹ Delft University of Technology, Biomechanical Engineering Department, Delft, The Netherlands

² Philips Research, In-Body Systems Department, Eindhoven, The Netherlands

Abstract — Previous studies show that the smart electrosurgical knife, which adds diffuse reflectance spectroscopy to the traditional electrosurgical knife, is a promising technique for breast-conserving surgery. Based on the fat/water-ratio, it enables healthy from malignant tissue discrimination while cutting, therefore potentially reducing the re-excision rate with breast-conserving surgery procedures. However, the smart electrosurgical knife cannot be used on patients yet since it has not been validated yet. Phantoms are ideal for validation of systems including imaging systems like diffuse reflectance spectroscopy. Hence, the goal of this study was to develop a breast phantom that enables validation of the smart electrosurgical knife. A breast phantom with a realistic size and shape, consisting of healthy tissue with a tumour inclusion was created. The phantom was made of agar in combination with lard, water and barium sulphate. Similarly, to a real breast conserving surgery procedure, the breast phantom enables pre-, intra- and postoperative margin assessment. More specifically, the phantom shows sufficient X-ray contrast between the tumour and healthy tissue, which enables size, border, and location assessment of the phantom tumour upfront and residual tumour inspection after surgery. The phantom shows a significant difference in fat/water-ratio between the tumour and healthy tissue, which enables us to assess diffuse reflectance spectroscopy with its capability in discriminating healthy from malignant tissue intraoperatively. Visually and mechanically, there is a minimal difference between the tumour and healthy phantom, which eliminates the possibility of using other intraoperative margin assessment techniques such as palpation and visual inspection. Finally, the phantom shows realistic tissue effects and haptic feedback when using the electrosurgical knife. Hence, the phantom enables the design of a study that subsequently enables extensive testing and further validation of the smart electrosurgical knife.

I. INTRODUCTION

Breast cancer is the most commonly diagnosed cancer in females worldwide and affects one in eight women during their lifetime ¹. It is estimated that in 2018, worldwide 2 million new cases and 626679 deaths occurred due to breast cancer ². Breast-conserving surgery (BCS) is the standard surgical treatment for early-stage breast cancer ³. It involves removing the tumour with a minimal margin of healthy tissue, leaving as much normal breast tissue as possible and is used in combination with radiotherapy, which eliminates residual cancer cells in the breast. However, recognition of the tumour during BCS is difficult. As a result, in 10-60% of the cases positive margins are found post-operatively by histopathologic evaluation and require re-excisions to obtain negative margins ⁴. Re-excisions have several negative consequences, among other things delayed receipt of adjuvant therapy, impaired cosmetic outcome, worsened psychosexual function and added medical expenses ^{5,6}. Over the last decade, the In-Body Systems department of Philips Research together with the Delft University of Technology have conducted research to find a standard margin assessment technique to overcome this problem. The research studies of J. Fleischer, M. Adank, F. Mollerus and C. van Gent have shown that diffuse reflectance spectroscopy (DRS), is a promising technique for intraoperative margin

assessment (IMA) ^{7,8,9,10,11,12}. In their studies they used the smart electrosurgical knife (SESK), which adds DRS to the traditional electrosurgical knife (ESK) and enables real-time tissue characterization while cutting. More specifically, they showed that based on the fat/water-ratio, DRS is a promising technique for discriminating between healthy and tumour tissue intraoperatively.

A. Problem statement

However, their research studies were conducted under controlled experimental conditions on ex vivo animal tissue specimens that do not necessarily represent the in vivo status of human breast tissue. Substantial changes occur immediately post-mortem compared to in vivo, few samples and datasets were taken, thereby the non-uniformity of breast tissue both in an individual patient and between patients is not represented by their samples. Hence, their findings solely serve as a reference value. Further validation of the SESK is therefore still needed.

B. Goal

Several studies suggest that phantoms are ideal for validation of systems including imaging systems like DRS ^{13,14}. Hence, developing a breast phantom that mimics the properties of healthy and malignant breast tissue will be ideal. This makes it possible to do extensive research that allows for further validation of the SESK,

which brings research on the SESK one step closer to a successful launch in the medical industry¹³. At the moment there is not such a breast phantom yet, hence the goal of this study is to develop a breast phantom that enables validation of the smart electrosurgical knife.

II. PHANTOM REQUIREMENTS

Inspired by the study of Pleijhuis et al., it was found that a study that enables validation of the SESK should be constructed as follows¹⁰⁴; surgeons have to conduct BCS with both the SESK and the traditional ESK on breast tissue-simulating phantoms including a tumour, and see whether surgeons who use the SESK, consistently obtain a higher percentage of negative margins than when using the traditional ESK. Only then the SESK is more promising than the traditional ESK, therefore validating its purpose.

Hence, in order to test and validate the SESK, the validation study should mimic a BCS procedure on a breast phantom, which includes pre-, intra- and postoperative margin assessment. Concerning pre- and postoperative margin assessment, the phantom should have a contrast between the tumour and healthy tissue, which enables size, border and location assessment of the tumour tissue upfront and residual tumour inspection after surgery. Intraoperatively, the phantom should have a significant difference in fat/water-ratio between the tumour and healthy tissue. This enables us to assess DRS with its capability in discriminating healthy from malignant tissue. Furthermore, visually and mechanically, there should be a minimal difference between the tumour and healthy tissue, which eliminates the possibility of using other IMA techniques such as palpation and visual inspection. Finally, the phantom should have a realistic size and shape, should show realistic tissue effects and give realistic haptic feedback to the surgeon with electrosurgery.

III. MATERIALS AND METHODS

A. Phantom production

A.1. Materials & Equipment

Lard (Alain Bernard, Amsterdam) and tap water were used to mimic the fat and water content of human breast tissue^{13,103}. To mix lard and water into realistic fat/water-ratios and enable phantom production with realistic mechanical properties, regular cheap agar (Terrasana¹¹³) was used as an emulsifier and coagulant^{14,103,111,119}. Finally, extra pure barium sulphate (Hinmeijer, the Netherlands, 233.40 g/mol, CAS nr.: 7727-43-7¹⁵⁷) was used in the tumour, which enables pre- and postoperative tumour inspection with the X-ray¹⁵⁶. The IKA C-MAG HS7 control was used to heat up the water and lard, and mix all the materials together.

A.1. Production method

Several samples of the healthy and tumour phantom were produced so they could be tested with regard to their electrosurgical tissue effects, fat/water-ratio,

mechanical- and visual properties. These samples had a total volume of fat and water of 200 mL.

The **healthy phantom** samples consisted of 50% lard, 50% tap water and then 5% agar by weight of water. Lard was heated until melted (40 °C) and tap water was heated to 100°C. 5% of agar by weight of water was added to the water and mixed for 3 minutes at 800 rpm. Lard was slowly added to the agar/water mixture and mixed for 3 minutes at 800 rpm. In case the total mixture seemed homogeneous, the mixture was weighted. If due to water evaporation, the total weight was still too low, it was corrected for by adding the right amount of water (100 °C) and mixed for 3 minutes at 800 rpm. The heater was turned off and the mixture was put into an ice bath. Mixing was continued until the mixture had a temperature of 45 °C. The mixture was then poured into glass cups and refrigerated (4°C) for 3 hours to solidify. The following day the healthy phantom was taken out of the refrigerator and cups to get to room temperature (3 hours).

Tumour phantom samples were produced with and without barium sulphate, to see what barium sulphate's influence was on the electrosurgical tissue effects, fat/water-ratio, X-ray contrast, mechanical- and visual properties. The regular tumour phantom consisted of 20% lard, 80% tap water and then 3% agar by weight of water, whereas the barium sulphate tumour phantom consisted of an additional 5% barium sulphate by weight of water. Lard was heated until melted (40 °C) and tap water was heated to 100°C. 3% of agar by weight of water was added to the water and mixed for 3 minutes at 800 rpm. Lard was slowly added to the agar/water mixture and mixed for 3 minutes at 800 rpm. Concerning the barium sulphate tumour phantom, an additional 5% of barium sulphate by weight of water was added to the mixture and mixed for 10 minutes at 800 rpm. In case the total mixture seemed homogeneous, the mixture was weighted. If due to water evaporation, the total weight was still too low, it was corrected for by adding the right amount of water (100 °C) and mixed for 3 minutes at 800 rpm. The heater was turned off and the mixture was put into an ice bath. Mixing was continued until the mixture had a temperature of 45 °C. The mixture was then poured into a glass cup and refrigerated (4°C) for 3 hours to solidify. The following day the tumour phantom was taken out of the refrigerator and cups to get to room temperature (3 hours).

After these phantoms were extensively tested, a **breast shaped phantom** with a tumour inclusion and a total volume of 500 mL was made. A healthy phantom mixture (45 °C) was poured into a custom-made breast shaped mould to a height of 20 mm. After solidification for 3 hours at 4 °C, a barium sulphate tumour phantom with an approximate dimension of 15x15x15 mm was positioned on the surface and temporarily fixed with a small needle (fig. 1). Next, the remaining of the healthy phantom mixture (45°C) was added to fill up the remaining mould

volume, allowing the healthy phantom layers to melt together, whereas the barium sulphate tumour phantom did not melt, due to its higher melting temperature. Namely, the barium sulphate tumour phantom had a lower lard- and a higher agar/water concentration than the healthy phantom, which was the cause for its overall higher melting point^{13,145}. Finally, the breast phantom was refrigerated (4°C) for 3 hours to solidify, after which it was taken out of the refrigerator and gently removed from the mould (fig. 1).



Figure 1: Left: breast mold including healthy phantom tissue up to 20 mm with the cubic tumour phantom on top, Right: The breast shaped phantom with a total volume of 500 mL.

B. DRS tests – fat/water-ratio

The fat/water-ratio of the healthy and tumour phantoms were tested by doing DRS measurements. The homogeneity, accuracy and consistency of the phantoms were evaluated. Furthermore, a statistical analysis was performed, to see whether there is a significant difference in fat/water-ratio between the healthy- (highest fat/water-ratio) and barium sulphate tumour phantom (lowest fat/water-ratio).

B.1. Equipment

An optical system, which consists of a spectroscopic system and a fibre-optic-probe, was used to obtain DRS spectra of the most potential phantoms. A white tungsten broadband light (Avantes, Apeldoorn, the Netherlands) was emitted by the spectroscopic system, through the illuminating fibre of the probe and onto the measured phantom. Within the phantom, the light undergoes multiple scattering and absorption and is diffusely reflected back onto the collecting fibres of the probe. The penetration depth of the light, depends on the absorption and reduced scattering coefficient of the phantom and is approximately half the distance between the illuminating- and collecting fibres⁷². The fibre distance between the illuminating fibre and collecting fibres (VIS & NIR) was 1.8 mm, hence the penetration depth was approximately 0.9mm. The collecting fibres transmit the light to the fibre splitter which divides the light into two wavelength components, namely the visual- and the NIR range. The spectroscopic system consisted of two spectrometers that process the light in the visual-(400-1000 nm, Mayapro 2000, Ocean Optics, Dunedin, USA) and the NIR range (900-1650 nm, NIRQuest 512, Ocean Optics, Dunedin, USA). The whole system was controlled by a custom-made, Labview Software user interface (National Instruments, Austin, Texas, USA). With the help of the PNSas software, which is a program developed by

Philips, the measured spectra were fit and the optical characteristics were derived¹¹.

B.2. Phantom measurements

DRS measurements were performed while the probe was in full contact with the phantom (figure 2). All measurements were performed at room temperature. For each measurement, an integration time of 0.5 seconds was used. For the healthy-, tumour- and barium sulphate tumour phantom, 3 samples were created, and each sample was measured at five different measurements locations. On each measurement location three DRS measurements were performed, amounting up to a total of 15 measurements per sample and 45 measurements per phantom type.

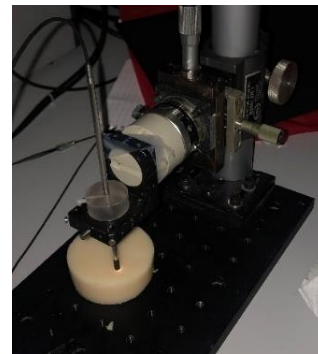


Figure 2: Measurements in full contact between the probe and sample.

B.3. Data analysis

The measurements were analysed by using PNSas software, which is a program based on Farrell's model and the diffusion theory, to fit and stitch the measured spectra together and translate the measured spectra into optical parameter estimates. In prior publications, this model has been discussed in detail, including a validation of the performance^{31,125,126,127}. The known absorption- and scattering coefficients present in the phantoms, were used by the PNSas software, to translate the spectra into relevant parameters. These parameters included the fat fraction [$Fat / (Fat + Water)$] and the total volume of fat and water ($Fat + Water$). Confidence intervals of each parameter were calculated to determine the significance of the fitted values⁴.

From these optical parameters, the fat percentage was derived by multiplying the fat fraction with the total volume of fat and water. Subsequently, the water percentage was derived by subtracting the fat fraction from the total volume of fat and water. Thereafter, the fat/water-ratio was calculated by dividing the fat by the water concentration. In this way, any over-estimation of the individual parameters due to being at the boundary of the diffusion approximation was minimized⁴. To test the fat/water-ratio accuracy, consistency and homogeneity of each phantom, the following was done; the accuracy per phantom type was tested by comparing its measured- to its reference values, the consistency was tested by looking at the inter-sample variations and the homogeneity by looking at the intra-sample variations.

B.4. Statistics

An independent one-tailed two-sampled t-test was performed to see whether the healthy phantom had a significant higher fat/water-ratio than the barium sulphate tumour phantom. It was assumed that the measured fat/water-ratios were normally distributed. H_0 states the highest and lowest fat/water-ratio are equal. The significance level is $\alpha = 0.05$, hence H_0 can be rejected if $p < 0.05$. In case $p = 0.05$, we wrongfully reject H_0 in 5% of the cases.

C. Compression tests – mechanical properties

As stated in the phantom requirements, the mechanical properties of the breast phantom should be realistic and differ minimally between the healthy and barium sulphate tumour phantom. The mechanical properties were tested by doing compression tests.

C.1. Equipment

The equipment used in this study was all located at the Minimally Invasive Surgery and Interventional Techniques (MISIT) lab at 3mE. A uniaxial compression test was used to measure the Young's Modulus of the phantoms. A linear stage was used PRO-115 (Aerotech, USA/UK) to exert force on the phantoms via a square object with a surface area of 1600 mm². Between the square surface and the linear stage, a 22N Force Sensor, LSB200 (FUTEK, USA) was mounted to measure the force.

C.2. Phantom measurements

For the healthy-, tumour- and barium sulphate tumour phantom, 2 samples were created. All samples had a thickness of 18 mm and a square surface of 1444mm², which is smaller than the compression surface, and therefore accounts for geometrical changes as the samples are compressed. A zero-pre-strain compression and a low strain rate of 6mm/min were used. Manickam et al. stated that agar has a brittle nature and has a yield point that could be reached above 15% strain. Hence, to enable two measurements per sample, a maximum strain of around 15% was applied¹²³. On each sample, two measurements were performed resulting in a total of 4 measurements per phantom type. All tests were carried out at room temperature. Figure 3 shows the experiment setup.

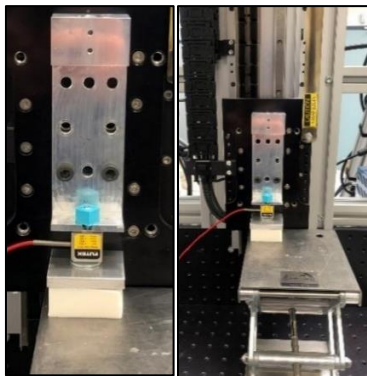


Figure 3: Experiment setup with linear stage, force sensor and sample.

B.3. Data analysis

The raw data from these tests consisted of a measured output voltage and position of the linear stage. By calibrating the force sensor, the measured output voltage was converted to a measured force. The position and measured force were used to calculate the stress and strain from these phantoms. To eliminate the effect of noise, a moving average was used from which subsequently, a stress-strain curve with a clear line was derived. Finally, the Young's Modulus was derived from the slope of the stress-strain curve using Excel.

D. Electrosurgical tests

The electrosurgical phantom tissue effects were evaluated qualitatively by visual inspection.

D.1. Equipment

The electrosurgical circuit was composed of a sample, electrosurgical generator (Force FX, Valleylab, Boulder, United States), a monopolar electrosurgical knife (Weide) and a dispersive pad. The current flows from the electrosurgical generator through the knife to the sample. The sample serves as the conductive element and acts as a resistor within this circuit. The resistance, converts the electrical energy into thermal energy, causing heat production and tissue destruction. The current leaves the sample at the dispersive pad and returns to the electrosurgical generator.

D.2. Phantom measurements

For the healthy-, tumour- and barium sulphate tumour phantom, one sample was created. They had a 12 cm diameter and a thickness of approximately 18 mm. The phantom tissue effects were compared to the tissue effects of pork tissue instead of human tissue, since pork tissue is cheap and easy to obtain and does not have ethical restrictions for experiments, whereas human tissue does. Pork belly muscle tissue from the Albert Heijn was used and had a thickness of approximately 10 mm. All samples were cut at room temperature. On each sample 30 seconds of pure cut, blend cut, and coagulation was performed, while the ESK was held slightly away from the sample. For all three waveforms, a power setting of 50 Watt was used, which is a commonly used setting for monopolar electro surgery¹⁶. First, the pork samples were tested, followed by the phantom samples. The samples were compared to each other qualitatively, by looking at the electrosurgical tissue effects.

E. X-ray tests

An X-ray image of the breast phantom with the barium sulphate tumour inclusion was taken and qualitatively analysed by visual inspection. According to Litt et al., even small concentrations of barium sulphate significantly increase the X-ray attenuation. It was therefore expected that 5% of bariums sulphate by weight of water shows sufficient X-ray contrast between the healthy- and barium sulphate tumour tissue¹⁵⁶.

E.1. Equipment

A Cone Beam CT (CBCT) system (Philips Healthcare, Best, the Netherlands), was used to scan the breast phantom. On the X-ray images, high-density material appeared darker and low-density material appeared lighter.

IV. RESULTS & DISCUSSION

A. Visual properties

Figure 4 illustrates pictures taken in the same room at the same time, from the healthy- and barium sulphate tumour phantom. The healthy phantom is visually indistinguishable from the barium sulphate tumour phantom, therefore eliminating the possibility of using visual inspection intraoperatively.



Figure 4: Visual properties of the healthy- (left) and barium sulphate tumour phantom (right), barium sulphate (BS).

B. DRS tests – fat/water-ratio

A.1 Confidence intervals

In order to determine the significance of the fitted values, confidence intervals for each parameter were calculated by the PNSas software and given in table 1. All confidence intervals are very small; hence the estimated fitted parameter values are reliable and can therefore be used.

Table 1: Average estimated parameters and corresponding average confidence intervals of the phantoms, barium sulphate (BS).

Phantom type	Fat/(Fat + Water)	Fat + Water
50F/50W-5%Agar	61.6 ± 0.5	142.3 ± 2.4
20F/80W-3%Agar	38.2 ± 0.8	123.3 ± 2.3
20F/80W-3%Agar-5%BS	41.1 ± 1.0	150.7 ± 3.7

A.2 Fat/water-ratio

In table 2, the average estimated fat and water concentrations and its standard deviations are given. With standard deviations smaller than 8% of the average value, all phantoms show great intra-sample homogeneity and within a phantom type, great inter-sample consistency. However, inaccurate results are shown with regard to the fat and water concentration. The fat concentrations were significantly overestimated with 37.6% (87.6% - 50%) for the healthy phantom, 27% (47% - 20%) for the tumour phantom and 41.7% (61.7% - 20%) for the barium sulphate tumour phantom.

Since, the healthy and tumour phantom solely consist of lard, water and agar, agar most likely influenced the overestimation of the fat concentration.

This is somewhat unexpected since literature shows agar does not have any influence on fat/water-ratio estimates of water/lipid-based phantoms. However, in contrast to literature, cheap impurified agar from the local food store, instead expensive purified agar was used, which might have led to the unexpected results^{14,103,111}.

As can be seen in table 2, barium sulphate further deteriorated the accuracy of the tumour phantom. The estimated fat and water concentration of the barium sulphate tumour phantom was higher than the tumour phantom without barium sulphate. This is in line with Hadi et al. findings, namely that barium sulphate increases the absorption of the material it is mixed with¹⁶⁸.

Despite these inaccuracies, table 3 shows all phantoms still have realistic fat/water-ratios that fall within the range of fat/water-ratios (0.22 – 11.25) reported by breast studies in table 3. However, more importantly, figure 5 displays the boxplot of the obtained fat/water-ratios and shows that the null-hypothesis is rejected. More specifically, there is a significant difference in fat/water-ratio between the healthy phantom and barium sulphate tumour phantom. Namely, the healthy phantom, has a significant higher fat/water-ratio ($M = 1.61$, $SD = 0.05$) than the barium sulphate tumour phantom ($M = 0.70$, $SD = 0.09$), $t(45) = 56.74$, $p = 8.2 \times 10^{-62}$, therefore meeting the concerning fat/water-ratio requirement.

Table 2: Average estimated parameters with its standard deviations (SD).

Phantom	Sample		Fat %	Water %
	Reference value		50%	50%
50F/50W + 5%Agar	Intra-sample average ± SD	1	85.4 ± 2.3	52.9 ± 0.8
	(Homogeneity)	2	86.5 ± 2.4	54.1 ± 2.6
		3	91.0 ± 3.7	56.9 ± 2.0
	Inter-sample average ± SD (Consistency)		87.6 ± 2.8	54.6 ± 2.6
	Δ with reference value (Accuracy)		37.6%	4.6%
20F/80W + 3%Agar	Reference value		20%	80%
	Intra-sample average ± SD	1	44.6 ± 3.3	81.0 ± 4.0
	(Homogeneity)	2	49.3 ± 2.2	74.9 ± 3.6
		3	47.2 ± 2.7	72.8 ± 5.7
	Inter-sample average ± SD (Consistency)		47.0 ± 3.4	76.3 ± 5.7
Δ with reference value (Accuracy)		27.0%	-3.7%	
20F/80W + 3%Agar + 5% BaSO4	Reference value		20%	80%
	Intra-sample average ± SD	1	62.3 ± 1.8	97.7 ± 4.1
	(Homogeneity)	2	59.8 ± 3.0	88.1 ± 3.6
		3	63.1 ± 4.7	81.0 ± 5.0
	Inter-sample average ± SD (Consistency)		61.7 ± 3.7	88.9 ± 8.1
Δ with reference value (Accuracy)		41.7%	8.9%	

Table 3: Average fat/water-ratio of healthy and tumour tissue, table constructed based on references cited in this table and based on the conducted DRS tests.

Study	Healthy tissue			Tumour tissue			
	Lipid (%)	Water (%)	F/W-ratio	Lipid (%)	Water (%)	F/W-ratio	
	Mean	Mean	Mean	Mean	Mean	Mean	
De Boer et al. ⁵⁶ (2016) in & ex vivo	-	-	7.5	-	-	0.8	
Nachabé ⁷² (2012) Ch. 9, ex vivo	90 (AP) 12 (GL)	8 (AP) 55 (GL)	11.25 0.22	15 (DCIS)	50 (DCIS)	0.3	
Blackmore et al. ⁶⁰ (2015)	65.1	19.66	3.31	-	-	-	
Cerussi et al. ⁶³ (2001)	48.65	27.7	1.76	-	-	-	
O'Sullivan et al. ⁶⁸ (2013)	69.7	21.4	3.26	-	-	-	
Intes ⁶² (2005)	62.4	28.9	2.16	-	40.8	-	
Leproux et al. ⁷³ (2016)	-	-	-	62.54	47.67	1.31	
Cerussi et al. ⁷⁴ (2006)	66.1	18.7	3.53	58.5	25.9	2.26	
Wang et al. ⁷⁵ (2010)	69	15	4.6	45	26	1.73	
Agar	Reference values	50	50	1	20	80	0.25
	Obtained DRS values				Without BaSO4		
					47.0	76.3	0.62
	Obtained DRS values	87.6	54.6	1.61	With 5% BaSO4		
				61.7	88.9	0.70	

fat/water-ratio (F/W-ratio).

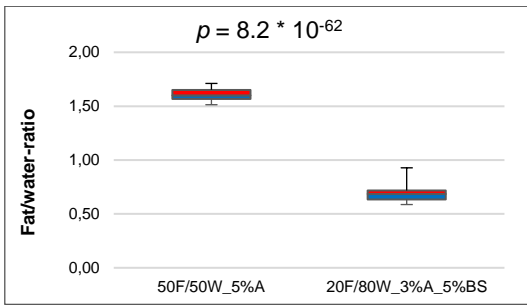


Figure 5: Boxplot of fat/water-ratios of healthy and bariums sulphate tumour phantom, agar (A), barium sulphate (BS).

C. Compression tests – mechanical properties

The average Young's Moduli are given in table 4. In line with literature, barium sulphate slightly increased the Young's Modulus of the tumour phantom ^{160,161,162}. Nevertheless, the measured Young's Modulus of the barium sulphate tumour phantom was still sufficiently similar to that of the healthy phantom, therefore eliminating the possibility of using haptic feedback as an IMA technique. Furthermore, compared to the breast tissue studies of Matsumura et al. and Umemoto et al., all phantoms showed Young's Moduli sufficiently similar to breast tissue, therefore enabling realistic haptic feedback with electrosurgery ^{95,124}.

Table 4: Young's Moduli of beast studies and phantoms, barium sulphate (BS).

Young's Modulus (kPa) and SD		
Study		Slope 1 – 1.2 kPa
Matsumura et al. ⁹⁴ (2009) (zero pre-strain)	Fat tissue	17.3 ± 4.8
	Glandular tissue	15.4 ± 3.9
	DCIS	15.6 ± 2.0
	IDC	27.0 ± 9.2
Umemoto et al. ⁹⁵ (2014) (zero pre-strain)	Fat tissue	19.08 ± 4.99
	Glandular tissue	16.99 ± 4.92
	DCIS	16.15 ± 4.24
	IDC	30.5 ± 11.46
Results per phantom type		Slope 1 – 1.2 kPa
Healthy phantom		38 ± 2
Tumour phantom		41 ± 5
Tumour phantom + BS		42 ± 8

Electrosurgical tests

Figure 6 and 7 display the electrosurgical tissue effects of pork muscle tissue and the healthy-, tumour- and barium sulphate tumour phantom. Similar to pork muscle tissue, the phantoms showed for all waveforms realistic tissue effects, namely local incisions with little thermal spread. This was somewhat expected, since agar in combination with lard has similar electrical conductivity, thermal conductivity and specific heat as human breast tissue, which are properties that are directly related to the electrosurgical tissue effects of a specific material, see table 5 ^{16,140}.

Table 5: Electrically conductive, thermal conductive and specific heat properties of human breast tissue and phantom materials, breast (B), tumour (T), gland (G), fat (F).

Study	Tissue or material	T (°C)	Conductivity (S/m)		Thermal conductivity (W/m K)	Specific heat (J/Kg K)
			50 Hz	500 Hz		
Zuluaga et al. ¹⁴²	B-G	37 °C	-	-	0.48	3770
	B-T		-	-	0.48	3852
	B-F		-	-	0.21	2674
Halter et al. ¹³²	B-T-in vivo	37 °C	-	0.05	-	-
	B-T-ex vivo		-	0.1	-	-
Krokida et al. ¹⁴³	Agar	30 °C	-	-	0.62	-
		21 °C	-	-	0.65	3300
Huang et al. ¹⁴⁷	Agar	-	-	-	0.59	3700
Kandadai et al. ¹³⁵		22 °C	-	0.08	-	-
Will et al. ¹⁴⁸	Pork fat	-1.87 °C	-	-	0.21	-
ASHRAE ¹⁴⁹		0 °C > x	-	-	0.22	2170
Shirsat et al. ¹³⁹		20 °C	0.04	-	-	-



Figure 6: From left to right: the healthy-, tumour- and barium sulphate tumour phantom. Per phantom type, tissue effects from left to right: coagulation, blend cut and pure cut.



Figure 7: From left to right: coagulated, blend and cut pork muscle tissue.

D. X-ray contrast

An X-ray image of the breast phantom with a tumour inclusion is illustrated in figure 8. As expected, 5% of barium sulphate by weight of water added to the tumour phantom, shows sufficient X-ray contrast between the healthy- and barium sulphate tumour phantom ¹⁵⁶.

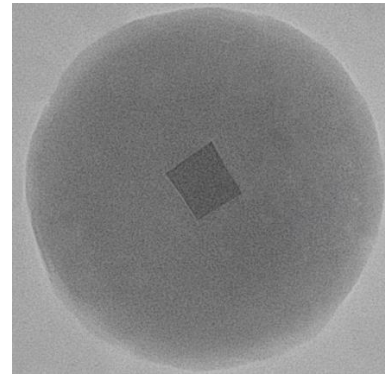


Figure 8: X-ray image of breast phantom with a tumour inclusion. The tumour consists among other things of 5% bariums sulphate by weight of water.

V. DISCUSSION

A. DRS tests – fat/water-ratio

DRS tests showed that the measured fat/water-ratios of all phantoms, showed great homogeneity and consistency. However, the accuracy was not optimal, the fat concentrations of all phantoms were significantly overestimated, and the water concentration of the barium sulphate tumour phantom was slightly overestimated. These inaccuracies were partially due to the estimation error of DRS and its analytical model ¹²⁷.

Yet, agar also played a role in these inaccuracies, namely agar caused significant fat overestimation, which was somewhat unexpected since literature shows agar does not have any influence on the fat estimates of water/lipid-based phantoms ^{103,111,14}. However, in contrast to literature, cheap impurified agar (Terrasana ¹¹³) from the local food store, instead of expensive purified agar from Sigma Aldrich was

used, which most likely caused the differences in result¹⁰³. Additionally, barium sulphate further deteriorated the fat and water content estimates, which is in line with Hadi et al. findings¹⁶⁸. However, to draw conclusions with full certainty regarding the influence of agar and barium sulphate on the fat and water absorption of the phantoms, further DRS tests should be done involving different concentrations of agar and barium sulphate added to the phantoms. Despite these limitations, all phantoms showed realistic fat/water-ratios. Furthermore, a significant difference in fat/water-ratio was found between the healthy- and barium sulphate tumour phantom. As a result, the concerning fat/water-ratio requirement was met, which enables us to sufficiently assess DRS with its capability in discriminating healthy from malignant breast tissue.

B. Compression tests – mechanical properties

In this study, the Young's Moduli of the phantoms were compared to that of breast tissue from the studies of Matsumura et al. and Umemoto et al.^{95,124}. However, they used a strain rate of 1mm/min and measured the Young's Moduli of breast tissue locally, whereas in this study, a slightly higher strain rate of 6 mm/min was used and the Young's Moduli of the phantoms were measured over the whole surface of the phantoms. Furthermore, the results of this study are solely based on two samples and a total of four measurements per phantom type. Nevertheless, for this study, the mechanical properties of the phantoms do not have to be extremely accurate to meet the concerning mechanical requirements. Hence, the results are sufficient enough, namely the phantoms showed Young's Moduli sufficiently similar to breast tissue with a satisfactory small difference between the healthy and barium sulphate tumour phantom. As a result, realistic haptic feedback with electrosurgery is enabled and the possibility of using haptic feedback as an IMA technique is eliminated.

C. Electrosurgical tests

The phantoms showed for all waveforms realistic tissue effects, namely local incisions with little thermal spread. These qualitative results are promising enough to meet the concerning electrosurgical requirement. However, to determine the actual cause for the observed phantom tissue effects, it is recommended that further research among other things measures and quantifies the melting point, electrical conductivity, thermal conductivity, and specific heat of the phantoms, and also determines its thermal distribution with electrosurgery^{16,140}.

D. X-ray contrast

It was found that adding 5% of barium sulphate by weight of water to tumour phantom, showed sufficient X-ray contrast between the healthy and barium sulphate tumour phantom. This enables imaging modalities such as radiography (X-ray), to sufficiently assess the barium sulphate tumour phantom pre- and postoperatively.

However, the barium sulphate tumour phantom had a thickness of 15 mm. Perhaps 5% of barium sulphate by weight of water does not show enough X-ray contrast with a tumour thickness much smaller than 15 mm. Hence for further research, tumours much smaller than 15 mm should be tested, to see whether 5% of barium sulphate still shows enough X-ray contrast. Furthermore, this study used a CT-scan, which has a spatial resolution of approximately 0.7 lines per mm. Hence postoperatively, tumour phantom residue smaller than 1.43 mm, cannot be distinguished from the healthy phantom. Hence for further research, the validation study could use film-screen mammography, which also uses X-rays, but has a spatial resolution of 15 lines per mm, thus enables phantom residue detection as small as 0.067 mm¹⁵⁹. Finally, with this study, X-ray images were qualitatively analysed, which is open for interpretation. Hence for further research, quantitative tests could be done that acquire the quantified HU values of the obtained X-ray images. Nevertheless, the results are promising enough since this study solely functions as a proof of concept for the validation study.

VI. CONCLUSION

Previous studies show that the smart electrosurgical knife, which adds diffuse reflectance spectroscopy to the traditional electrosurgical knife, is a promising technique for breast-conserving surgery. Based on the fat/water-ratio, it enables healthy from malignant tissue discrimination while cutting, therefore potentially reducing the re-excision rate with breast-conserving surgery procedures. However, the smart electrosurgical knife cannot be used on patients yet since it has not been validated yet.

With this study, a breast phantom was created, which enables the design of a study that subsequently enables extensive testing and further validation of the smart electrosurgical knife. The breast phantom consists of agar in combination with lard, water, and barium sulphate. Similarly, to a real breast conserving surgery procedure, the breast phantom enables pre-, intra- and postoperative margin assessment. More specifically, the phantom shows sufficient X-ray contrast between the tumour and healthy tissue, which enables size, border, and location assessment of the phantom tumour upfront and residual tumour inspection after surgery. The phantom shows a significant difference in fat/water-ratio between the tumour and healthy tissue, which enables us to assess diffuse reflectance spectroscopy with its capability in discriminating healthy from malignant tissue intraoperatively. Visually and mechanically, there is a minimal difference between the tumour and healthy phantom, which eliminates the possibility of using other intraoperative margin assessment techniques such as palpation and visual inspection. Finally, the phantom shows realistic tissue effects and haptic feedback when using the electrosurgical knife.